VILNIUS UNIVERSITY

Evelina Gaidamauskaitė

COMPUTATIONAL MODELING OF COMPLEX REACTIONS KINETICS IN
BIOSENSORS

Doctoral dissertation
Physical sciences, informatics (09P)

Vilnius, 2011

The work was performed in 2006-2011 at the Vilnius University.

Scientific supervisor:

prof. dr. Romas Baronas (Vilnius University, physical sciences, informatics - 09P)

VILNIAUS UNIVERSITETAS

Evelina Gaidamauskaitė

KOMPIUTERINIS DAUGIAPAKOPIŲ REAKCIJŲ KINETIKOS
BIOJUTIKLIUOSE MODELIAVIMAS

Daktaro disertacija
Fiziniai mokslai, informatika (09P)

Vilnius, 2011

Disertacija rengta 2006-2011 metais Vilniaus universitete.

Mokslinis vadovas:

prof. dr. Romas Baronas (Vilniaus universitetas, fiziniai mokslai, informatika - 09P)

Acknowledgements

Let me express my gratitude to the people who have helped me in many ways. My first words of gratitude are due to my supervisor, prof. Romas Baronas, for introducing me to the problem of numerical modeling of biosensors, for academic guidance and for the invaluable patience over these last years. It is an honor for me to thank prof. Juozas Kulys from the Institute of Biochemistry for challenging discussions.

I have also received a lot of care and support from my family. Among them, special thanks to my brothers Ervinas Gaidamauskas for profound support on Biochemistry, Erikas Gaidamauskas for the help throughout the process, and Eduardas Gaidamauskas for challenging me to fulfill my potential. I heartily thank my parents, Dalia and Sergejus. They raised me, taught me, and supported me. And of course to Aleksandras, thanks for the incredible amount of patience you had with me in the last months.

<div align="right">

Evelina Gaidamauskaitė
Vilnius
26th September 2011

</div>

Table of Contents

Notation and Acronyms

a_i	boundary of the i-th layer
A	geometrical surface of the electrode
A	absorbance
A_∞	steady state absorbance
A_R	steady state absorbance calculated at the moment T_R
Bi	Biot number
B_S	dimensionless sensitivity of the biosensor
cmpI	compound I
C	concentration of C
d	thickness of the enzyme layer
D	diffusion coefficient
D_Q	diffusion coefficient of substance Q
E	enzyme
ES	enzyme-substrate complex
E_{ox}	oxidized form of enzyme
E_{red}	reduced form of enzyme
E	concentration of the enzyme
E_r	relative error
$E_{ox,i}$	concentration of the oxidized enzyme in the i-th layer
$E_{red,i}$	concentration of the reduced enzyme in the i-th layer
E_0	initial concentration of the enzyme
ES	concentration of the enzyme-substrate complex
F	Faraday constant
$F(t)$	measured fluorescence
F_I	intensity of fluorescence
$Fe(CN)_6^{3-}$	hexacyanoferrate(III) (ferricyanide)
$Fe(CN)_6^{4-}$	hexacyanoferrate(II) (ferrocyanide)

h	mesh size in the x direction
H^+	hydrogen ion
H_2O	water
H_2O_2	hydrogen peroxide
H_b	concentration of the hydrogen peroxide in the diffusion layer
H_e	concentration of the hydrogen peroxide in the enzyme layer
H_0	hydrogen peroxide concentration in the bulk solution
I	electric current
I_0	intensity of excitation light
I_R	steady state current calculated at the moment T_R
I_{0R}	steady state current before the addition of the mediator
I_S	synergistic current
I_∞	steady state current
j	diffusion flux density
J	density of the current
J_g	density of the steady state current (at $S_0 \gg K_M$)
J_l	density of the steady state current (at $S_0 \ll K_M$)
J_p	density of the steady state current
J_R	density of the steady state current calculated at the moment T_R
k_i	i-th reaction rate constant
K_M	Michaelis constant
l_{ef}	effective thickness of the enzyme layer and Nernst layer
Laccase(ox)	oxidized form of laccase
Laccase(red)	reduced form of laccase
M	number of mesh intervals on the t-axis
M_{ox}	oxidized mediator
M_{red}	reduced mediator
n_e	number of electrons involved in charge transfer
N	number of mesh intervals on the x-axis
O	oxygen (O_2)
O_i	oxygen concentration in the i-th layer
O_0	initial concentration of the oxygen
P	product
P_i	i-th product
P	concentration of the product

P_b	concentration of the product in the diffusion layer
P_e	concentration of the product in the enzyme layer
$P_{i,j}$	concentration of the i-th product in the j-th layer
RDF	resource description framework
S	substrate
S$_i$	i-th substrate
S	concentration of the substrate
S_b	concentration of the substrate in the diffusion layer
S_e	concentration of the substrate in the enzyme layer
$S_{i,j}$	concentration of the i-th substrate in the j-th layer
S_0	concentration of substrate in the bulk solution
$S_{i,0}$	concentration of i-th substrate in the bulk solution
SBML	Systems Biology Markup Language
SBGN	Systems Biology Graphical Notation
t	time axis coordinate
T	duration of the process analysis
T_R	moment the steady state was reached
T_E	computation time required to achieve relative error limit
$u(x,t)$	unknown function of the continuous arguments
u_i^j	unknown function of the discrete arguments
v	reaction rate
V_{max}	maximum reaction rate
x	space axis coordinate
XML	Extensible Markup Language

Greek letters

α	arbitrary number
δ	thickness of the diffusion layer
ϵ	limits of the relative error
ε	relative difference of the current density
ε_P	molar extinction coefficient of the product
σ^2	Damköhler number
Σ	ratio of the substrate and hydrogen peroxide concentrations
τ	mesh size in the t direction

φ	quantum yield of fluorophore
$\Omega_{h\tau}$	rectangular uniform mesh

Subscripts

i	index of mesh intervals on the x-axis

Superscripts

$\bar{}$	average value
$*$	time function
0	initial concentration
j	index of mesh intervals on the t-axis

Introduction

Fast and accurate information is crucial to making right decisions and taking appropriate actions. Humans perceive information by the biological sensor system, including our five senses of sight, hearing, taste, smell and feeling. However, our senses alone are often insufficient in many cases. Therefore, additional auxiliary equipment is constantly being developed, such as sensors, biosensors, biological fuel cells and reactors. In this thesis we shall focus on the design and development of multi-step biosensors.

In the context of this thesis, the term biosensor is used to refer to sensors using biomolecules as selective recognition elements [17, 124, 139, 152]. Biosensors are analytical devices made up of a combination of a biological entity, usually an enzyme, that recognizes a specific analyte (substrate) and the transducer that translates the biorecognition event into a signal (see Fig. 1). The strength of the signal is usually proportional to the concentration of the target analyte.
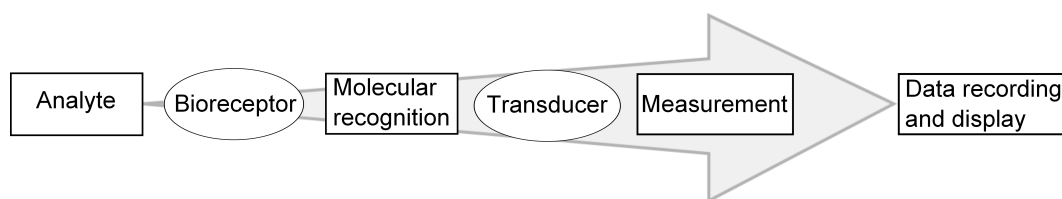
Figure 1: Biosensing process.

According to IUPAC definition:

Biosensor is an integrated receptor-transducer device, which is capable of providing selective quantitative or semi-quantitative analytical information using a biological recognition element [137].

1

Biosensors are constructed to be relatively cheap, sensitive and reliable devices, widely used in clinical diagnostics, drug discovery, food analysis, environmental and industrial monitoring and some other purposes [97, 118, 143, 152, 156].

Rapidly expanding area of the applications require a new types of biosensors. In order to create these biosensors the corresponding experimental studies are necessary. However, these investigations generally are very expensive, primarily due to the high cost of the reagents, especially enzymes. Computational experiments could very well replace physical ones. The computational modeling of biosensors is based on the solution of the nonlinear partial differential equations [17]. These equations involve linear diffusion term as well as nonlinear reaction rate of biocatalytical transformation of substrate. The analytical solutions are only available in the extreme cases of substrate concentrations [125]. In general case, one of the numerical techniques from a variety of methods must be employed. In this research we focus on the finite difference numerical schemes. In order to assure optimal scheme the comparative research must be performed.

Most of the computational researches are based on single step reaction approximation. Modern biosensors are composed of several different enzymes or the single enzyme carrying out different reactions simultaneously. Moreover, even more complicated situations arise when cross-reaction of the substrates and the products occurs (see Chapter 4). Therefore, the multi-step character of a reaction scheme must be considered and modeled accordingly. In this thesis such reaction (synergistic) scheme is studied in great details.

For each individual reaction system a unique mathematical model is usually developed [17]. However, this process is cumbersome and error-prone. The deterministic nature of model creation allows the automated models to be built. The resulting software will facilitate the process of design and production of new biosensors for life science research. The applicability in and the high demand for research, industry and medical care of various biosensors is witnessed today and is fairly expected to grow even more in the near future [127].

Research Object

Models of biosensors and the simulation techniques are the research objects of this thesis. The main focus is upon mathematical and computational modeling of multi-step biosensors. The research object also includes the applicability of various finite difference schemes and automated construction of computational models.

Research Methodology

New mathematical models were formulated applying kinetic approach for the description of the chemical and diffusional processes. The corresponding reaction-diffusion equations represent a parabolic type nonlinear partial differential equations. A number of the most common finite difference techniques for the solution of the problem was used. For the development of the new software program that automates computer modeling of biosensors the SBML description and JAVA programming languages were used. Properties of the multi-step biosensors were investigated by the computer simulations.

Statement of the Problem and Tasks

The problem that was addressed in this study was to develop a method for automated numerical simulation of multi-step biosensors.

The problem statement of this study can be further divided into the following tasks:

1. Development of mathematical models for the practical multi-step biosensors: optical peroxidase-based and amperometric laccase-based biosensors.

2. Comparison of common finite difference schemes for the numerical solution of reaction-diffusion equations. Identification of the most suitable scheme for the simulation in terms of accuracy of the solution, computation time needed to solve the problem and ease of use of the technique.

3. Development of a general tool for the computational modeling of multi-step biosensors.

4. Investigation of the influence of the model parameters on the optical biosensor response.

5. Simulation the synergetic effect of the simultaneous substrates conversion in the laccase-based biosensor by using the developed tool.

Scientific Novelty and Results

1. Original mathematical models were developed for absorbance and fluorescent peroxidase-based biosensors.

2. A novel regeneration boundary condition was introduced for the mathematical model of laccase-based biosensor.

3. The comparison of the common finite difference schemes shows that the fastest schemes to achieve the required relative error are implicit and Hopscotch schemes. For the problems where accuracy is not a significant factor but the speed is, the simplest explicit scheme should be used.

4. Flexible model for computational modeling of different practical multi-step biosensors was developed.

5. The modeling of laccase biosensor explained and confirmed the synergistic effect.

Practical Significance

The mathematical models derived in this dissertation can be applied for the detailed investigation, engineering and control of action of the multi-step biosensors. They can also be easily generalized for other practically relevant biosensors. The introduced method of the construction and analysis of the multi-step biosensors' models forms a basis for the further future researches.

The new tool presented in this work is an interactive and user-friendly software program for the computational modeling of the multi-step biosensors. This computational tool can facilitate the work of biochemists and bioengineers doing the biosensor analysis. The performed computational experiments confirmed the adequacy and applicability of our methods for systems as complex as the synergistic laccase-based and optical perozidase-based biosensors.

The results of this thesis contributed to the goals of the following projects: "Development of bioelectrocatalysis for synthesis and analysis (BIOSA)" funded by a grant (No. PBT-04/2010) from the Research Council of Lithuania and "Developing computational techniques, algorithms and tools for efficient simulation and optimization of biosensors of complex geometry" funded by the European Social Fund under Measure VP1-3.1-ŠMM-07-K "Support to Research of Scientists and Other Researchers (Global Grant)".

Statements Promoted to Defend

1. The best accuracy among the common finite difference schemes for solving reaction-diffusion problem with Michaelis-Menten kinetics is achieved using implicit calculation and Hopscotch approaches. For the problems where the accuracy is not a significant factor but the speed is, the simplest explicit scheme should be used.

2. The multi-step character of chemical processes in complex biosensors can be specified extending SBML language. The developed tool can be applied for the computational modeling of the various multi-step biosensors.

3. Computational modeling of the laccase-based biosensor explained and confirmed the experimentally observed synergetic effect of mediator on the biosensor response.

4. The developed mathematical model of a peroxidase-based optical biosensor can be successfully used to investigate the kinetic peculiarities of the biosensor response. The biosensor response is highly stable at the relatively thick external diffusion layer, which has little effect on the response at high enzyme concentrations.

Reliability of the Results

To ensure the reliability of the results some of the numerical tests were compared with the experimental data. The results were of a little variation taking into account uncertainty in the parameter estimates. A good agreement with the latest published models was also obtained. The most contemporary mathematical techniques and software currently used by the biosensor modelers were employed.

Approval and Contribution of the Results

The main results of this thesis were published in five articles [1A, 2A, 3A, 4A, 5A]. Three of them ([1A, 2A, 4A]) in journals included in the ISI (the Institute for Scientific Information) Journal List. In addition, results were presented in the six reviewed conference proceedings ([6A, 7A, 8A, 9A, 10A, 11A]). Eleven contributed talks were given at various conferences:

1. E. Gaidamauskaitė, R. Baronas. Influence of Spontaneous Convection on Amperometric Biosensor Response. *23rd Nordic Seminar on Computational Mechanics*, 21-22 October, 2010, KTH, Royal Institute of Technology, Stockholm, Sweden.

2. E. Gaidamauskaitė, R. Baronas. A Computational Investigation of the Optical Biosensor by a Dimensionless Model. *Kompiuterininkų dienos - 2009*, 25 - 26 September, 2009, KTU, Kaunas, Lithuania.

3. E. Gaidamauskaitė, R. Baronas. Numerical Modelling of Peroxidase-based Optical Biosensor. *14th International Conference on Mathematical Modelling and Analysis MMA 2009*, 27 - 30 May, 2009, Daugavpils, Latvia.

4. E. Gaidamauskaitė, R. Baronas. Computer Modelling of Biosensor with Product Inhibition. *5th European Congress on Computational Methods in Applied Sciences and Engineering ECCOMAS 2008*, 30 June - 4 July, 2008, Venice, Italy.

5. R. Baronas, E. Gaidamauskaitė. A Reduced Model of Peroxidase-based Optical Biosensor. *13th International Conference on Mathematical Modelling and Analysis MMA 2008*, 4 - 7 June, 2008, Tartu (Kääriku), Estonia.

6. E. Gaidamauskaitė, R. Baronas. Modelling a Peroxidase-based Fluorescent Biosensor. *22nd European Conference on Modelling and Simulation ECMS 2008*, 3 - 6 June, 2008, University of Cyprus, Nicosia, Cyprus.

7. E. Gaidamauskaitė, R. Baronas. Computational Modelling of Rotating Disc Enzyme Electrode. *20th Nordic Seminar on Computational Mechanics*, 23-24 November, 2007, Chalmers University, Göteborg, Sweden.

8. E. Gaidamauskaitė. The Development of Computer Models for Biosensors. *XIII International Scientific IT Conference, Kompiuterininkų dienos - 2007*, 13-15 Semptember, 2007, Panevėžys, Lithuania.

9. E. Gaidamauskaitė. The Development of Computer Models for the Biosensors. *PhD Summer School "Formal Methods for System Analysis in Informatics"*, 13-19 May, 2007, Druskininkai, Lithuania.

10. E. Gaidamauskaitė, R. Baronas. Automatizuotas biojutiklių kompiuterinių modelių sudarymas (The development of computer models for amperometric biosensors). *Informacinės technologijos 2007*, 31 January - 1 February, 2007, KTU, Kaunas, Lithuania.

11. E. Gaidamauskaitė, R. Baronas. Baigtinių skirtumų metodo taikymas bio-jutiklio veiksmui modeliuoti. *Informacinės technologijos 2006*, 25-26 January, 2006, KTU, Kaunas, Lithuania.

Structure of the Thesis

The thesis is organized as follows. Chapter 1 discusses common biosensor types, defines a framework for the mathematical handling of the problem, overviews the literature and tools of computer modeling. Chapter 2 presents mathematical models of multi-step biosensors: a peroxide-based optical biosensor and a synergistic laccase-based biosensor. An automated solver is proposed in Chapter 3. Several types of finite difference schemes are compared and verified against known analytical solutions. In Chapter 4 we continue with the results of computational modeling of multi-step biosensors. We focus on analyzing the dimensionless sensitivity of the biosensor. Finally, in last Chapter 5, we conclude on our results and answer the research questions.

Chapter 1

Theoretical Framework

The precursor of today's biosensors was first presented in the early sixties. The concept of enzymatic electrochemical monitoring of glucose was established by Clark and Lyons [38] and soon modified by Updike *et al.* [140]. Enzyme-based glucose sensors work on the principle of detection of hydrogen peroxide (H_2O_2) formed by the oxidation of glucose (eq. 1.1). The H_2O_2 is electrochemically oxidized under an applied potential of 0.7 V, and the current measured is related to the concentration of glucose in the system (eq. 1.2).

$$\text{Glucose} + O_2 \xrightarrow{\text{Glucose oxidase}} \text{Gluconic acid} + H_2O_2, \qquad (1.1)$$

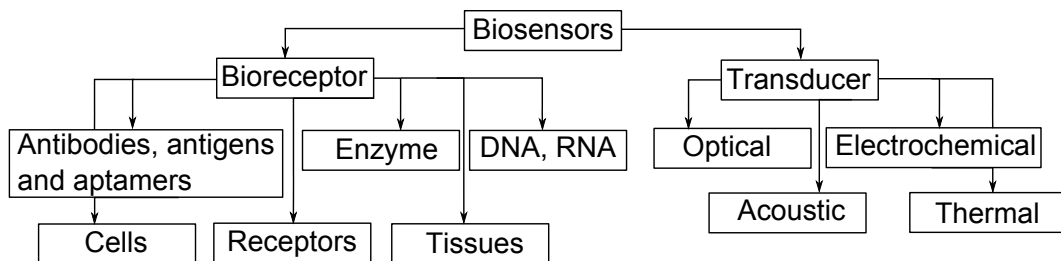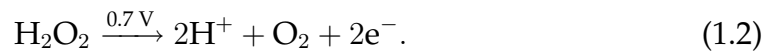$$H_2O_2 \xrightarrow{0.7\,\text{V}} 2H^+ + O_2 + 2e^-. \qquad (1.2)$$

Figure 1.1: Biosensor classification schemes.

This biosensor represents a class of electrochemical sensors. Nowadays, biosensors comprise a huge variety of different devices. Contemporary biosensors are generally classified according to the biological material (see Fig.1.1). They can also be classified based upon the transduction methods they employ. These types are discussed in greater detail below.

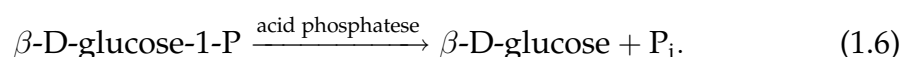# 1.1 Classification of Biosensors According to Bioreceptor System

With respect to the bioreceptor that recognizes the target analyte, biosensors can be classified into (1) affinity sensors, when non-covalent interactions like antibody-antigen reactions or DNA strand hybridization are involved, and (2) catalytic or enzyme sensors, when the target analyte is the enzyme substrate, or it can be detected by measuring the signal produced by one substrate or product of the enzymatic reaction involving the analyte [22].

Biomolecules such as enzymes, antibodies, antigens, nucleic acids, membranes, receptors, organelles and microorganisms as well as animal and plant cells or tissues have been used as biological sensing elements [89]. The enzyme, antibody and DNA/RNA biosensors will be discussed in more detail as their specificity for the natural substrates makes them the first candidates to be incorporated as the biorecognition element.

1.1.1 Enzyme biosensors

Enzymes catalyze reactions with a high degree of specificity, and the products of these reactions (or of reactants consumed) are detected directly if electroactive, colored or luminescent, or by using optical transducers. Though it would be desirable to directly detect changes in the enzyme substrate or in one reaction product, most of the analytes are not natural substrates of the enzymes carrying out these conversions. Therefore, the coupled enzymatic reactions are

used following the one where analyte participates, to finally produce a species detectable optically or electrochemically. The design below has been proposed by Conrath to detect inorganic phosphate [39]. The coupled reaction are shown in equations (1.3) to (1.6). They ultimately produce hydrogen peroxide, the species that is electrochemically transformed at the electrode to generate an amperometric signal.

$$\text{maltose} + \text{P}_\text{i} \xrightarrow{\text{maltose phosphorylase}} \alpha\text{-D-glucose} + \beta\text{-D-glucose-1-P}, \qquad (1.3)$$

$$\alpha\text{-D-glucose} \xrightarrow{\text{mutarotase}} \beta\text{-D-glucose}, \qquad (1.4)$$

$$\beta\text{-D-glucose} \xrightarrow{\text{glucose oxidase}} \text{glucuronic acid} + \text{H}_2\text{O}_2, \qquad (1.5)$$

$$\beta\text{-D-glucose-1-P} \xrightarrow{\text{acid phosphatese}} \beta\text{-D-glucose} + \text{P}_\text{i}. \qquad (1.6)$$
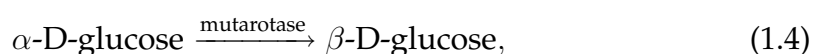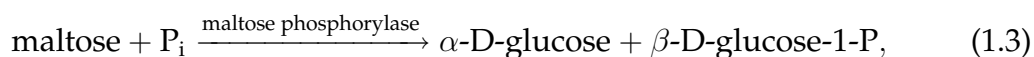
In this interesting example, the signal is not only amplified by the extra amount of substrate rendered by the acid phosphatase using a "side product", but also by recycling the analyte.

1.1.2 Antibody-antigen biosensors

Biosensor technology makes use of specific interactions between an antibody and an antigen. When the analyte of interest is an antigen it is possible to use the complementary antibodies as capturing molecules in the bioreceptor system [106, 148]. Antibodies reactive exclusively with their corresponding antigens, confer a remarkable specificity of the device.

Figure 1.2A depicts the competitive immunosensor format, where the target analyte competes with the labelled antigen for the biorecognition sites of the antibody attached to the electrode. Then the system is rinsed and the substrate labeled with redox enzyme is added. The resulting product is transformed at the electrode, leading to a detectable current. In this competitive assay, the signal diminishes as the analyte concentration increases.
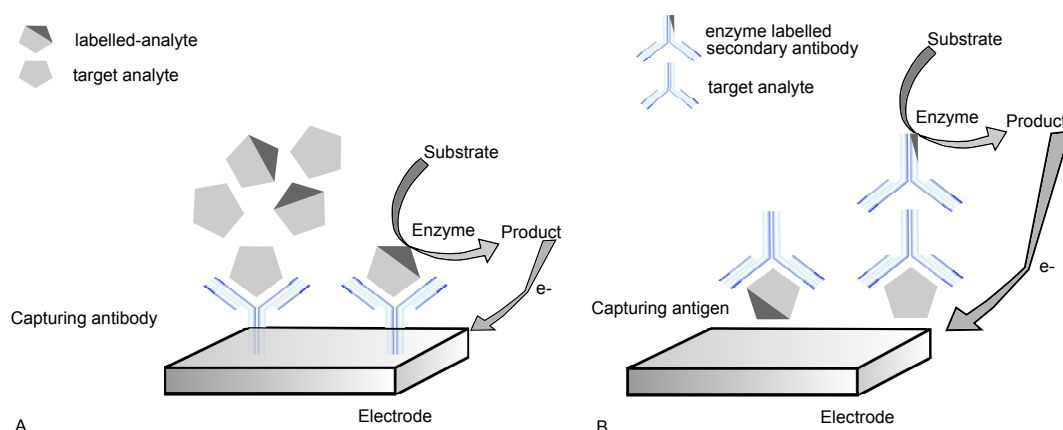
Figure 1.2: The working principle of the antibody-antigen biosensors (adopted from [22]). (A) A competitive immunoassay format to detect an antigen. (B) An indirect immunoassay format to detect a specific antibody.

When the analyte is an antibody, which is usually the case when diagnosing an infection, another immunological assay scheme can be performed, similar to that used to detect antigens [115]. This method specificity relies on the selective molecular recognition of the antibodies generated by the infected patients toward specific antigens, appropriately immobilized on an electrode. The assay is followed by a second reaction where the specific antibody reacts further with secondary antibody conjugated with an enzyme label, used to reveal up to which extent the first immunological reaction took place. When the substrate of the enzyme covalently coupled to the secondary antibody is added, the resulting current is measured indicating the presence of the analyte in the sample. In this case, one expects the signal to increase with the analyte concentration. Figure 1.2B illustrates the working principle of an indirect immunoassay format with amperometric detection.

Recently, aptamers have also been used as analyte-capturing species [96, 119, 151]. Aptamers are artificial specific oligonucleotides, DNA or RNA, with the ability to bind to non-nucleic acid target molecules, such as peptides, proteins, drugs, organic and inorganic molecules or even whole cells, with high affinity and specificity [22]. Numerous clinically related aptamer-based biosensors have been designed, as for example, an aptasensor for cocaine [6].

1.1.3 DNA/RNA biosensors

DNA and RNA strands are excellent candidates to be used as recognizing elements, due to the specific base-pairing interactions between complementary sequences [47, 123]. In a typical configuration of DNA- or RNA-based biosensors, a single-stranded nucleic acid sequence is anchored within the recognition layer, where the base-pairing interactions recruit the target analyte to the surface (Fig. 1.3).
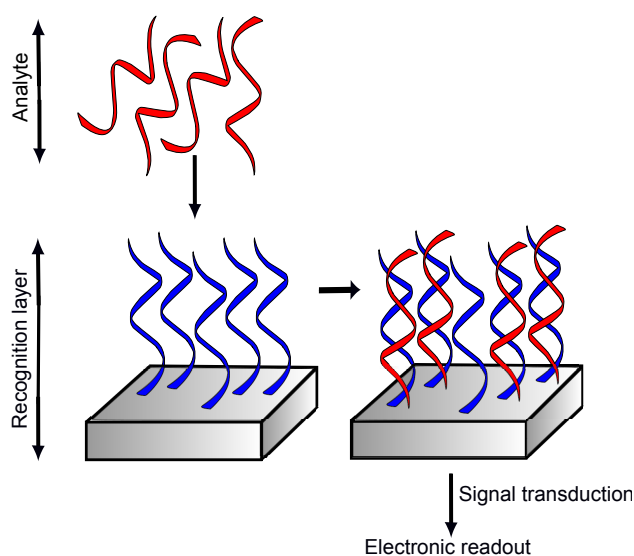
Figure 1.3: The general design of the DNA- or RNA-based biosensors (adopted from [47]).

There are a number of strategies to detect hybridization (optical, mechanical or electrochemical). The simplest strategy to detect nucleic acid hybridization relies on monitoring the direct oxidation/reduction of nucleotide bases (guanine). Another strategy to monitor DNA or RNA hybridization employs labelled-complementary DNA or RNA strands. Labels may include enzymes or electroactive molecules. Clinical applications using DNA- or RNA-based biosensors include devices useful to determine the markers of pathogenic bacteria [91], virus DNA such as that of SARS virus [1].

1.2 Classification of Biosensors According to Trasducer

Biosensors are also classified according to the parameter that is measured by the physicochemical transducer of the biological event. Thus, classically biosensors are grouped into optical, electrochemical, acoustic, thermal ones [145]. Special emphasis will be placed on the description of electrochemical and optical transducing principles.

1.2.1 Electrochemical enzyme biosensors

Electrochemical biosensors are ideally suited to analyze the content of a biological sample due to the direct transformation of a biological event to an electronic signal [60, 147]. Electrochemical sensors have some remarkable advantages, such as low-cost, portability and simplicity of use, over the conventional analytical methods [149]. Other notable advantages of electrochemical biosensors are their robustness, compactness, good detection limits, even with small analyte volumes, and ability to be used in turbid analyte samples with optically absorbing or fluorescing interfering compounds. On the other hand, electrochemical sensors have some limitations: electrochemically active substances in the sample, poor stability, and complicated electron transfer. Electrochemical biosensors are based on potentiometric, amperometric and impedimetric transducers [111].

Potentiometric sensors rely on the measurement of potential difference between the reference electrode and the working electrode without polarizing the electrochemical cell, that is, zero or no significant current flows between the electrodes. The working electrode acquires a variable potential depending on the concentration of a certain analyte in solution. For potentiometric measurements, the relationship between the concentration and the potential is governed by the Nernst equation [60, 111, 122, 149, 157]. Currently, semiconductor based especially ISFETs (ion-sensitive field effect transistors) and LAPS (light addressable potentiometric sensor) transducers are more common [111].

14

Amperometric biosensors are quite sensitive and more suited for commercialization than the potentiometric ones [60, 93, 148]. Amperometry is a method of electrochemical analysis in which the signal of interest is a current that is directly proportional to the concentration of the analyte. Generally, the current is measured at a constant potential and this is referred to as amperometry. If a current is measured during controlled variations of the potential, this is referred to as voltammetry. As certain chemical compounds are oxidized or reduced (redox reactions) at inert metal electrodes, electrons are transferred from the analyte to the working electrode or vice versa. Electrochemical sensing, besides the working (or redox) electrode, usually requires a reference electrode and a counter or auxiliary electrode. Voltage is applied between the reference and the working electrodes, and current flows between the working and the auxiliary electrodes. Due to the different electron transfer process, there are three so-called "generations" of biosensors [147, 149]. First generation biosensors are based on the natural enzyme substrates or products (mostly oxygen). Second generation biosensors involve artificial redox mediators (mostly dye molecules) between the reaction and the transducer [62]. The other approach is based on the direct electron transfer of proteins (third generation biosensors).

Impedimetric biosensors are less frequent compared to potentiometric and amperometric biosensors [111]. Impedimetric biosensors follow either impedance or its components resistance and capacitance. The inverse value of resistance is called conductance and for this reason some investigators name such systems as conductometric. Impedance biosensors include two electrodes with applied alternating voltage. An example of such a system could be an enzymatic reaction producing ionic compounds. The released ions are able to provide a significant increase of impedance and, thus, a measurable signal. The main disadvantage of impedance biosensors are false positive results due to electrolytes from the samples. Recent progress in the application of electrochemical sensors to analysis of clinical chemicals, food samples and environmental samples is reviewed in [108, 116, 149].

1.2.2   Optical enzyme biosensors

This subsection describes sensors and systems where the information is obtained by the measurement of photons (rather than electrons as in the case of electrochemical biosensors). Optical biosensors are known to be suitable for biomedical research, healthcare, pharmaceuticals, environmental monitoring, homeland security [28, 139]. They are irresponsive to electromagnetic interference, and can employed for multiplexed detection within a single device.

Optical biosensors can be used with many different types of spectroscopies (e.g., absorption, fluorescence, phosphorescence, Raman, refraction, dispersion spectrometry) to estimate different spectrochemical properties of target analytes [145]. The properties that are measured by optical biosensors include:

- amplitude,

- energy,

- polarization,

- decay time,

- phase.

Amplitude change derived from absorption, reflection, or other transmission loss mechanisms produces changes in the intensity of the impinging light [113]. The change of energy (or frequency) of the electromagnetic radiation might provide information about changes in the local environment surrounding the analyte, its molecular vibrations (e.g. Raman spectrometry), or the formation of new energy levels. The interaction of a free molecule with a fixed surface can often be measured with polarization detection. When a target molecule is bound to a fixed surface of optical biosensor, the emitted light remains polarized. However, the polarization of emitted light from a free molecule in solution is usually random. The decay time of fluorescence or phosphorescence can also be used to gather information about local molecular environment of target analytes. The refractive index may change when the analyte binds to a surface. Therefore, the phase of the emitted radiation is altered and this property can be exploited to quantify the amount of analyte.

Moreover, optical biosensors can be classified according to the detection protocols: fluorescence-based detection and label-free detection [51]. In fluorescence-based detection, either target molecules or biorecognition molecules are labeled with fluorescent tags, such as dyes. The intensity of the fluorescence emitted indicates the presence of the target molecules and the interaction strength between target and biorecognition molecules. An extra step is required for the biomolecule to be covalently labeled and this might interfere with the function of a biomolecule. As the number of optical labels on each molecule cannot be precisely controlled, the fluorescence signal bias may arise and hinder quantitative analysis. On the other hand, fluorescence-based detection is extremely sensitive, with the detection limit down to a single molecule and enables the analytical wavelengths to be shifted to almost any desired value [104]. Currently, the luminescent nanoparticles are often used as fluorophores. In contrast, in label-free detection, target molecules are not labeled or altered. The intrinsic optical property of the biomolecule as a result of its interaction with the target analyte is exploited. Although, such sensors are not numerous because their sensitivity is usually low, this type of detection is relatively easy and cheap to perform. In the label-free optical detection, there exist a number of detection methods, including the measurement of refractive index change induced by molecular interactions, optical absorption detection, and Raman spectroscopic detection [51, 113, 145].

Although biosensing devices employ a variety of recognition elements, predominantly used detection technique is based on enzymes. Therefore, a short description of the enzyme kinetics is introduced.

1.3   Enzyme Kinetics

The essential characteristic of enzyme action is catalysis [26, 49, 65, 90, 103, 135, 138, 141]. An enzyme enhances the rate of the reaction it influences. The catalysts is not consumed as a result of the reaction, nor does it alter the equilibrium constant [17, 23].

Michaelis and Menten proposed that enzymes take part in reactions as shown

in the following equation,

$$E + S \underset{k_2}{\overset{k_1}{\rightleftarrows}} ES \underset{k_4}{\overset{k_3}{\rightleftarrows}} E + P, \qquad (1.7)$$

where E stands for enzyme, S for substrate, P for products and ES for the enzyme-substrate complex [31, 102]. In this two-step reaction the enzyme combines with substrate to form the complex, which can either dissociate again into unchanged substrate and enzyme or go on to the second step and form the products and unchanged enzyme. The reverse of the second step would lead to the synthesis of ES from enzyme and products, but this process can generally be ignored unless the products are allowed to accumulate. On that assumption we can say that the initial rate of formation of the product will be given by the rate equation

$$v = k_3 ES, \qquad (1.8)$$

where v is equal to the rate of product formation and ES is the concentration of the enzyme-substrate complex. It is impossible to measure ES directly. However, it is clear that the total concentration of enzyme, E, will be the sum of the concentration of the complex, ES, and of the the free enzyme. Assuming also that the total substrate concentration, S, is much greater than E, we can then ignore the amount of S which is present in the ES complex. For the steady state overall process, the rate of formation of the enzyme-substrate complex will equal its rate of breakdown. This can be expressed in a steady-state equation,

$$\frac{(E - ES)S}{ES} = \frac{k_2 + k_3}{k_1} = K_M, \qquad (1.9)$$

where K_M is the Michaelis constant, which is equal to the substrate concentration necessary to develop one-half the maximum rate. Rearranging (1.9) equation and substituting it for the rate equation (1.8) gives

$$v = k_3 \frac{E \times S}{K_M + S}. \qquad (1.10)$$

The rate of the reaction will reach a maximum when the substrate concentration will be high enough so that all the enzyme will be in the form of enzyme-

substrate complex,

$$V_{max} = k_3 E. \tag{1.11}$$

The expression for the rate of the reaction is called Michaelis-Menten equation:

$$\mathbf{v} = \frac{V_{max}S}{K_M + S}. \tag{1.12}$$

The equation (1.12) describes the quantative relationship between reaction rate and substrate concentration, as illustrated in the Figure 1.4.
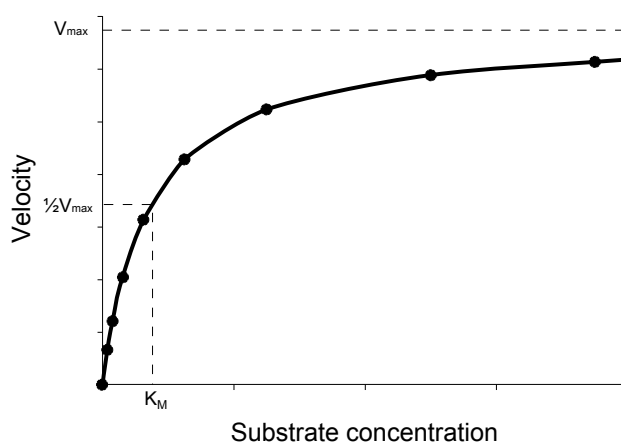

Figure 1.4: Relationship between substrate concentration and the velocity of an enzyme-catalyzed reaction. As the substrate concentration is increased, the velocity of the reaction approaches a maximum value.

1.4 Diffusion Equation

The conventional reaction mechanism in electrochemistry involves two steps: (i) enzyme reaction and (ii) diffusion of the reagents. Reactions are said to be diffusion-controlled when the diffusion steps take much longer than the reaction steps.

The diffusion processes are described by Fick's laws [44, 50, 61]. They were formulated in 1855 by A. Fick based on the analogy with heat conduction processes [53]. Fick's laws describe the diffusion phenomenologically without

claiming that it derives from basic microscopic concepts and corresponds to the free systems of weakly-interacting particles. It is, however, indicative of the importance of Fick's description that all subsequent developments have in no way affected the validity of his method.

Fick's first law describes the diffusion in a steady-state condition. According to this law diffusion flux density j is proportional to the concentration (C) gradient:

$$j = -D\frac{\partial C}{\partial x}. \tag{1.13}$$

This equation is written for the case of one-dimensional system and proportionality constant D is the material-dependent diffusion coefficient. Fick's second law is the basis of most diffusion measurements and describes diffusion in a non-steady-state condition when the concentration changes with time, but particles are neither created nor destroyed,

$$\frac{\partial C}{\partial t} = D\frac{\partial^2 C}{\partial x^2}. \tag{1.14}$$

The second Fick's law (1.14) can be derived from the first Fick's law taking into account the particle balance relationship:

$$\frac{\partial C}{\partial t} = -\frac{\partial j}{\partial x}. \tag{1.15}$$

Assuming the diffusion coefficient to be a space-independent we receive the diffusion equation (1.13). The influence of the space dependence of diffusion coefficient on the biosensor response was investigated in recent work [6A]. Partial differential equations generally can be divided into three categories: parabolic, elliptic and hyperbolic (see Fig. 1.5). Some examples of such classes include diffusion, poisson and wave equations [86, 120, 142]. The focus of this work will be on the nonlinear parabolic partial differential equations as they describe physical processes in the biosensors.
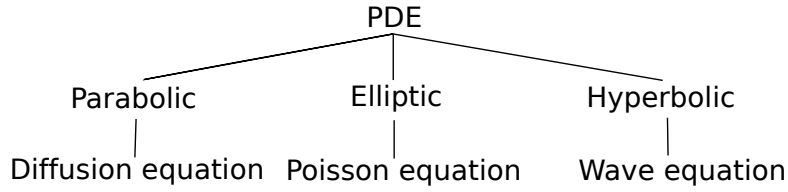
Figure 1.5: Classification of partial differential equations (PDEs).

1.5 Reaction - Diffusion Equation

The standard scheme of classical (amperometric, optical) biosensors usually consist of a continuous alternating diffusion and enzyme layers. The action of these biosensors can be described combining previously introduced reaction and diffusion members. Together they form a non-linear differential equation for the substrate and product concentrations,

$$\frac{\partial C}{\partial t} = D\frac{\partial^2 C}{\partial x^2} + \frac{V_{max}S}{K_M + S}, \tag{1.16}$$

here C corresponds to the concentration of the substrate (S) or the product (P). The latter equation can be relatively easy generalized for the complex geometry biosensors taking into account additional spatial coordinates. However, a one-dimensional approximation can be applied for the majority of biosensor models. Therefore, a one-dimensional approximation was also used in this thesis. To solve partial differential equations, initial and boundary conditions (Dirichlet and/or Neuman) must be defined.

The general analytical solution for the nonlinear differential equations cannot be obtained. The following solutions are available only in extreme cases, when the non-linear equation can be linearized. The linearization of the reactions - diffusion kinetic equation can be performed for the extreme values of the substrate concentration - high or low in comparison with the Michaelis - Menten constant K_M. For the low-concentration case ($S_0 \ll K_M$), the enzymatic reaction rate is directly proportional to the substrate concentration,

$$\frac{V_{max}S}{K_M + S} \approx \frac{V_{max}}{K_M}S, \quad \text{when } S \ll K_M. \tag{1.17}$$

In the high-concentration case ($K_M \ll S_0$), the diffusion process becomes more kinetically dominant, and the enzymatic reaction rate is,

$$\frac{V_{max} S}{K_M + S} \approx V_{max}, \quad \text{when } S \gg K_M. \tag{1.18}$$

Exact solutions are helpful in testing models and assessing accuracy of the solution.

A more detailed description on the previous applications of the reaction-diffusion equations for the modeling of the biosensor action can be found in monographs and review articles [17, 125].

1.6 Numerical Approaches of Enzyme Kinetics Modeling

1.6.1 Finite difference method

Analytical solutions of reaction-diffusion equations are limited to simplified cases of concentrations and geometry. Problems that incorporate more realistic settings can only be solved by numerical methods. One of the most widely used numerical techniques is the Finite Difference method [17, 86, 120, 142].

Let us consider a rectangular uniform mesh of intersecting lines in space and time ($0 \leq x \leq d, 0 \leq t \leq T$),

$$\Omega_{h\tau} = \{(x_i, t_j) : x_i = ih; t_j = j\tau; hN = d; \tau M = T; i = 0, ..., N; j = 0, ..., M\}. \tag{1.19}$$

We define the constants h and τ to be the mesh sizes in the x and t directions, respectively (see Fig. 1.6). The functions of the continuous arguments $u(x,t)$ are replaced by the functions of the discrete arguments u_i^j at mesh points.

Derivatives in the partial differential equation are approximated by linear combinations of function values at mesh points. The definition of a function's first

derivative $u'(x)$ is used to approximate derivatives,

$$u'(x) = \lim_{h \to 0} \frac{u(x + h) - u(x)}{h}. \tag{1.20}$$

The numerical solution drops the limit, approximating the derivative with a finite change of u over a finite h,

$$u'(x) \approx \frac{u(x + h) - u(x)}{h}. \tag{1.21}$$

To estimate the accuracy of this approximation let us consider Taylor Series expansion to find $u(x + h)$, assuming all necessary derivatives exist:

$$u(x + h) = u(x) + hu'(x) + \frac{1}{2}h^2 u''(x) + \frac{1}{3!}h^3 u'''(x) + \dots . \tag{1.22}$$

If we re-arrange equation (1.22) to solve for $u'(x)$, we get

$$u'(x) = \frac{u(x + h) - u(x)}{h} - \frac{1}{2}hu''(x) - \frac{1}{3!}h^2 u'''(x) - \dots . \tag{1.23}$$

Ignoring the remainder term in equation (1.23) we obtain approximation (1.21). Hence, the error introduced by using finite differences is $O(h)$.

Similarly, to approximate the second derivative we use the formula:

$$u''(x) \approx \frac{u(x - h) - 2u(x) + u(x + h)}{h^2}. \tag{1.24}$$

The approximation error obtained from the Taylor expansions for the second derivative is $O(h^2)$ [17].

1.6.1.1 The explicit difference scheme

There are many finite difference schemes that can be considered to solve PDEs. The simplest and most straightforward technique is Explicit Difference scheme [17, 32, 120].
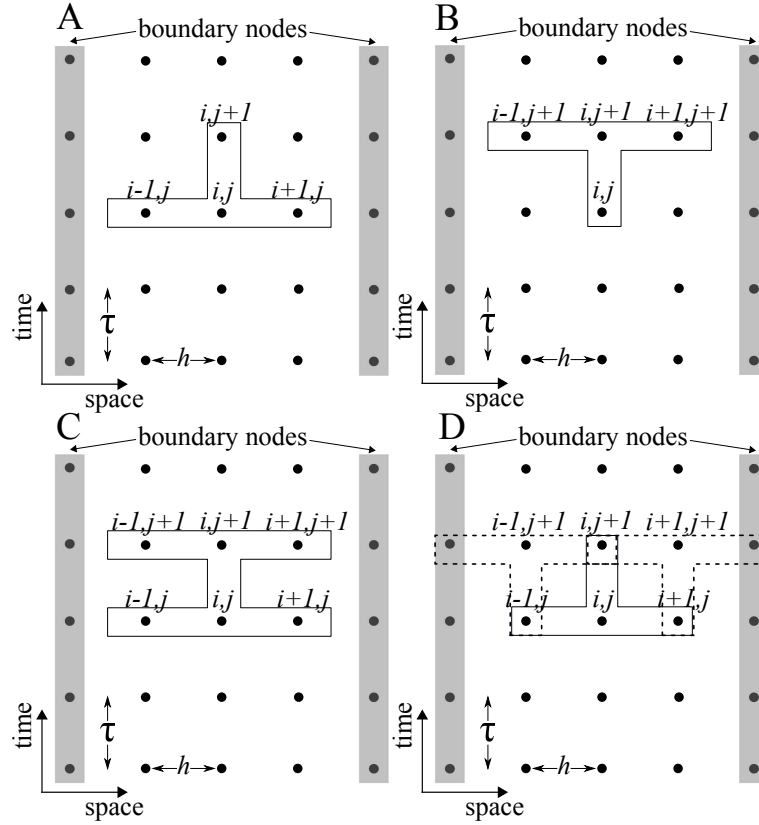
Figure 1.6: Finite difference schemes. (A) Explicit finite difference scheme. (B) Implicit finite difference scheme. (C) Crank-Nicolson finite difference scheme. (D) Hopscotch finite difference scheme.

Definition 1.6.1. The method is called *explicit* if it gives value of the solution on the upper layer explicitly in terms of values at lower layer, otherwise it is called *implicit*. □

We will demonstrate explicit scheme on diffusion problem (1.14). The diffusion equation can be approximated by this difference equation,

$$\frac{u_i^{j+1} - u_i^j}{\tau} = D \frac{u_{i+1}^j - 2u_i^j + u_{i-1}^j}{h^2}. \tag{1.25}$$

The equation (1.25) involves three mesh points on t_j layer and one mesh point on t_{j+1} layer as shown in Fig. 1.6A. The major advantages of explicit finite difference scheme are it's simplicity and low computational cost. However,

the main flaw is that this scheme is conditionally stable, the required condition being,

$$D\frac{\tau}{h^2} \le \frac{1}{2}. \tag{1.26}$$

Oscillation will occur if this condition is not satisfied.

Definition 1.6.2. The scheme is called *stable* if it does not magnify initial errors that arise during the course of the calculation. $\square$

1.6.1.2 The implicit difference scheme

In an implicit difference scheme (1.6B), the spatial derivative term $\partial^2 C/\partial x^2$ in equation (1.14) is evaluated at the new time step [17, 32, 120],

$$\frac{u_i^{j+1} - u_i^j}{\tau} = D\frac{u_{i+1}^{j+1} - 2u_i^{j+1} + u_{i-1}^{j+1}}{h^2}. \tag{1.27}$$

As a result, we have to solve a linear system of equations at each time level.

The very important feature of implicit finite difference scheme is that there are no restrictions on the ratio of mesh steps. The implicit method is second order accurate in space, but only first order accurate in time (i.e., $O(h^2 + \tau)$).

The diffusion problem is tridiagonal, that is, all the elements of the coefficient matrix of the system of equations is zero except for the three central diagonals. Such problems may be efficiently solved with the tridiagonal matrix algorithm (see Section 1.6.2).

1.6.1.3 The Crank-Nicolson Difference scheme

Another implicit, therefore unconditionally stable, scheme is Crank-Nicolson [17, 43, 120]. The Crank-Nicolson method is based on average in time of explicit

and implicit schemes (Fig. 1.6C),

$$\frac{u_i^{j+1} - u_i^j}{\tau} = \frac{D}{2} \left(\frac{u_{i+1}^{j+1} - 2u_i^{j+1} + u_{i-1}^{j+1}}{h^2} + \frac{u_{i+1}^j - 2u_i^j + u_{i-1}^j}{h^2} \right). \tag{1.28}$$

Crank-Nicolson scheme is second order accurate both in space and in time (i.e., $O(h^2 + \tau^2)$).

1.6.1.4 The Hopscotch Difference scheme

The Hopscotch scheme consists of two phases [48, 120]. In the first phase the odd-numbered mesh point are calculated explicitly by the scheme (1.25) as represented in Fig. 1.6D by a solid line. For the second phase at the same time layer the even mesh points are calculated implicitly (Fig. 1.6D, dotted line) by equation (1.27). Subsequent computation of time layers continues alternating the calculation order of the odd and even points.

Hopscotch scheme is fully explicit yet unconditionally stable.

1.6.2 Tridiagonal matrix algorithm

An approximation of one dimensional in space reaction-diffusion equation by implicit finite difference scheme results in a tridiagonal matrix. The tridiagonal system is written as:

$$\begin{vmatrix} b_1 & c_1 & 0 & 0 & \dots & 0 \\ a_2 & b_2 & c_2 & 0 & \dots & 0 \\ 0 & a_3 & b_3 & c_3 & \dots & 0 \\ . & . & & & \dots & . \\ . & . & & & \dots & . \\ . & . & & & \dots & c_{n-1} \\ 0 & 0 & 0 & 0 & a_n & b_n \end{vmatrix} \begin{vmatrix} x_1 \\ x_2 \\ . \\ . \\ . \\ x_{n-1} \\ x_n \end{vmatrix} = \begin{vmatrix} d_1 \\ d_2 \\ . \\ . \\ . \\ d_{n-1} \\ d_n \end{vmatrix} \tag{1.29}$$

The solution for the x_i in this matrix system is due to Llewellyn Thomas and is known as the Tridiagonal Matrix Algorithm (TDMA) [2, 36, 86, 142]. The method is based on an application of Gaussian elimination and consist of two phases: a forward elimination and a backward substitution. The method begins by forming coefficients p_i, q_i and u_i as follows ($i = 1, ..., n$):

$$p_i = a_i q_{i-1} + b_i, \qquad (1.30)$$

$$q_i = -c_i/p_i, \qquad (1.31)$$

$$u_i = (d_i - a_i u_{i-1}/p_i). \qquad (1.32)$$

The initial values being $q_0 = 0$ and $u_0 = 0$.

In the backward substitution phase the values of x_i can be calculated from the following equation:

$$x_k = q_k x_{k+1} + u_k, \quad k = n - 1, ..., 1, \quad x_n = u_n. \qquad (1.33)$$

The tridiagonal matrix algorithm is only applicable to matrices that are diagonally dominant, i.e.,

$$|b_i| \geq |a_i| + |c_i|, \quad i = 1, ..., n. \qquad (1.34)$$

This condition is satisfied for the finite difference approximation of one-dimensional reaction-diffusion equations.

The algorithm requires $O(n)$ operations instead of $O(n^3)$ required by Gaussian elimination [64]. Although it is more computationally intensive than the work required for an explicit solver, the time step can be increased significantly.

1.7 Computational Modeling of Biosensors

A range of software packages are available for biochemical modeling [75]. Due to this variety of tools many input data formats are utilized hindering exchange of the computational models. To address this problem a few standardized languages for representing and exchanging models between simulation tools were proposed [67, 134].

1.7.1 Model representation

Nowadays, the Systems Biology Markup Language (SBML) is considered a standard representation format for quantitative and qualitative biochemical models [54, 70]. SBML is an XML based language for representing models of biological processes. Adopting SBML format enables straightforwardly describe a biological process by means of compartments, species, reactions, parameters, unit definitions and rules. The editions of SBML are called *levels*, where each level extends the set of features of the language [54, 70]. All of the constructs of lower level can be mapped to the higher level. The distinct SBML levels are supposed to coexist. There are currently three levels of SBML defined.

In 2001 Caltech team issued a specification for SBML Level 1, which described fundamental features that are common to all biochemical network models [66].

The main conceptual elements in SBML are the interacting chemical substances (*Species*), how these substances participate in reactions (*Reaction*) and the reaction environment (*Compartment*). A *compartment* is an area of a particular type and finite size. There is one required attribute for a compartment element, *id*, to give it a unique identifier by which other parts of an SBML model definition can refer to it. A compartment can also have an optional *size* attribute representing a length of a compartment (if the compartment is one-dimensional). A model may contain multiple compartments.

The *species* element has two required attributes: *id* and *compartment*. Species must be defined once for every compartment where they are present.

```
<?xml version="1.0" encoding="UTF-8"?>
<sbml level="2" version="4" xmlns="http://www.sbml.org/sbml/level2/version4">
    <model id="EnzymaticReaction">
        <listOfCompartments>
            <compartment id="enzymelayer" size="1e-4"/>
        </listOfCompartments>
        <listOfSpecies>
            <species compartment="enzymelayer" id="ES" initialConcentration="0" name="ES"/>
            <species compartment="enzymelayer" id="P" initialConcentration="0" name="P"/>
            <species compartment="enzymelayer" id="S" initialConcentration="1e-20" name="S"/>
            <species compartment="enzymelayer" id="E" initialConcentration="5e-21" name="E"/>
        </listOfSpecies>
        <listOfReactions>
            <reaction id="veq1">
                <listOfReactants>
                    <speciesReference species="E"/>
                    <speciesReference species="S"/>
                </listOfReactants>
                <listOfProducts>
                    <speciesReference species="ES"/>
                </listOfProducts>
            </reaction>
            <reaction id="veq2">
                <listOfReactants>
                    <speciesReference species="ES"/>
                </listOfReactants>
                <listOfProducts>
                    <speciesReference species="E"/>
                    <speciesReference species="P"/>
                </listOfProducts>
            </reaction>
        </listOfReactions>
    </model>
</sbml>
```

Figure 1.7: SBML Level 2 model, describing the enzyme kinetics.

Reactions are defined using lists of participating reactants and products, along with optional parameters. Just as with other objects in SBML, there is a mandatory attribute *id*.

The *parameter* element is used in SBML to associate a name with a value, so that the name can be used in mathematical formulas in place of the value. The *parameter* element has one required attribute, *id*. The optional attribute *value* is of type double and defines the numerical value assigned to the parameter.

In addition, user can specify more detailed features to the objects of an SBML model, place restrictions on them and link SBML descriptions to complementary information about the objects in databases.

It took 6 years to finalize the next level of SBML from 2002 to 2008 [68]. The main changes introduced by that edition was MathML usage for mathematical

expressions, support for metadata and named function definitions. A simple example of a model of enzyme kinetics (1.7) in SBML Level 2 is given in Figure 1.7.

The current SBML Level 3 was published in 2010 with a number of significant changes in syntax and constructs [69]. The models defined in SBML Level 3 have modular structure. The core set of features are based largely on SBML Level 2. The extension packages, like "Layout", "Hierarchical Model Composition" and "Spatial Processes", can be layered on top of the Core. Currently, only the Core specification was issued and various packages are being developed for SBML Level 3.

SBML is not intended to be read by users or written by hand. The content of it can be viewed by reporting tool SBML2Latex which overviews an SBML file [46].

To facilitate the development of new tools and to integrate the existing tools specialized library libSBML is available [29]. It provides an application programming interface (API) for reading, writing and manipulating data in SBML format. Moreover, the packages for working with SBML in Mathematica and MATLAB, respectively MathSBML and SBMLToolbox are available [73, 129].

CellML is another open standard based on the XML to represent biological structures and processes [58, 63]. A CellML model is described as a network of *components* related to one another. *Components* may contain units definitions, variables, mathematical expressions, metadata and reactions. However, it should be noted, that the use of the reaction element is currently discouraged as there are ongoing discussions regarding removal of reactions from the future CellML specifications.

1.7.2 Model generation

XML editing requires knowledge of XML technology and it can be quite cumbersome [24]. This is a drawback, especially for a user who needs to specify complex biochemical reactions [35, 98]. Instead, software tools that provide higher-level interfaces to reading, writing, and manipulating XML should be

used. Moreover, there has been an initiative to develop and standardize a human-readable graphical representations for applications in systems biology. Such an effort, named Systems Biology Graphical Notation (SBGN), was developed by a community of biochemists, modelers and computer scientists [76, 87]. SBGN proposes three complementary types of diagrams: process diagram, entity relationship diagram and activity flow diagram, that can be used as three alternative descriptions of the same biological system. For instance, the model of enzyme kinetics (1.7), expressed in SBML in Fig. 1.7, can be presented diagrammatically using SBGN process diagram (see Fig. 1.8). There is a num-
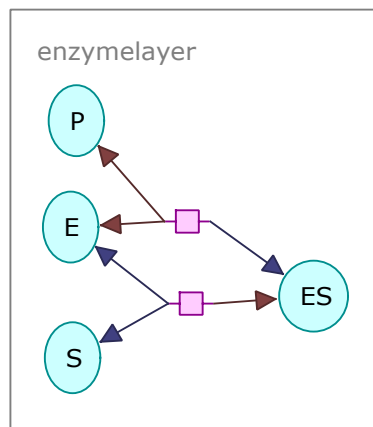

Figure 1.8: SBGN process diagram describing a simple enzyme-catalyzed reaction.

ber of software packages that provide support to SBML and SBGN [87, 131]. Most of these tools can read in, create, visualize and export a model expressed in SBML. Freely available (open source), platform independent applications like BioUML, CellDesigner, Cellware and others allow to simulate a model by constructing a system of ordinary differential equations and solving them numerically [45, 56, 78].

Nevertheless, the actual structure and reaction schemes applied in biosensor are not supported fully. Biosensors as the specific technical devices with electrical or optical signal transduction are not completely covered by SBML that is primarily designed for the cell-biological processes. In addition, the simulators mentioned above are based on solving ordinary differential equations without diffusion.

1.8 Conclusions

Contemporary biosensors present a huge variety of different appliances. They are generally classified according to the biological material or by the transduction methods they employ. The standard description of the biosensor action is based on the reaction-diffusion equations. The diffusion process is governed by the Fick's second law and for the description of the reaction kinetics a Michaelis-Menten approach is applied. It is impossible to find a general analytical solutions for the reaction-diffusion equations. In order to enable a computational modeling of the biosensor action a numerical methods usually are applied. A number of computational tools are available for the practical modeling of the reaction-diffusion kinetics. However, these tools are not suitable for the general investigation of the any possible biosensor. Numerical schemes presented in these packages are also not optimized for the large-scale calculations. Moreover, Michaelis-Menten approach can not be applied for the description of the multi-step reactions.

Chapter 2

Mathematical Models of Multi-Step Biosensors

A number of characteristics are important in the development of actual biosensors [42, 124, 139, 152]. To improve the productivity as well as the efficiency of the biosensor design, a model of the biosensor should be built [3, 132]. Mathematical models have been widely used to study and optimise analytical characteristics of the biosensors [11, 14, 17, 21, 71, 72, 79, 100, 126]. A wide range of contemporary biosensors involve a multi-step chemical reactions [124, 139, 152]. Reaction kinetics in such devices can be mathematically described only by the full mass transport rate equations. This chapter presents a mathematical models of the two multi-step biosensors: peroxidase-based optical and laccase-based synergistic biosensors [1A, 4A].

2.1 Peroxidase-based Optical Biosensor

Optical biosensors are known to be suitable for environment, clinical and industrial purposes [152]. Those devices allow real-time analysis of molecular interactions without labelling requirements [88]. Optical biosensors have been used to study interactions involving a wide range of interacting partners, from

drugs and viruses to peptides, proteins, oligonucleotides, carbohydrates, and lipids [109, 110, 121, 133, 153].

The understanding of the kinetic peculiarities of biosensors is of crucial importance for their design. To improve the productivity as well as the efficiency of biosensors design and to optimize the biosensors configuration a model of real biosensors should be build [41, 52]. Starting from seventies various mathematical models of biosensors have been developed and used to study and optimise analytical characteristics of electrochemical biosensors [8, 9, 12, 13, 15, 16, 19, 79, 80, 94, 95, 100, 112, 126, 155]. A comprehensive study of the mathematical modeling of amperometric biosensors is given in [125]. Mathematical modeling in the design of optical biosensors has been applied in individual cases only [101, 117].

2.1.1   Modeling biosensor

The biosensor comprises an enzyme layer immobilized on the reflective surface, laser and detector. Laser is used as the emitted light source. Also, the diffusion layer where the flux of the analyte takes place is also considered (see Fig. 2.1).
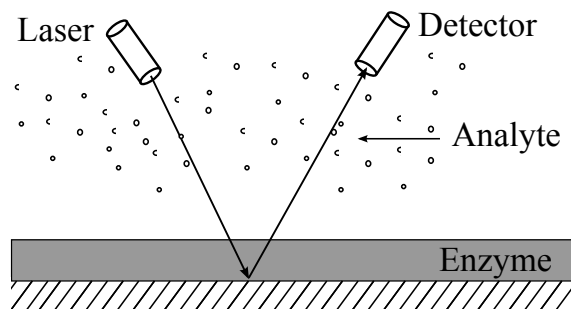

Figure 2.1: Schematic representation of peroxidase-based optical biosensor.

We consider the reaction scheme of the optical biosensor involving hydrogen peroxide (H_2O_2) reaction with peroxidase (E) to form compound I (cmpI) and

water (H_2O) with the constant reaction rate k_1 [3A, 4A, 7A]. The compound I interacts with the substrate (S) to form product (P) and free enzyme (E) assuming the constant reaction rate k_2 (see Fig. 2.2),
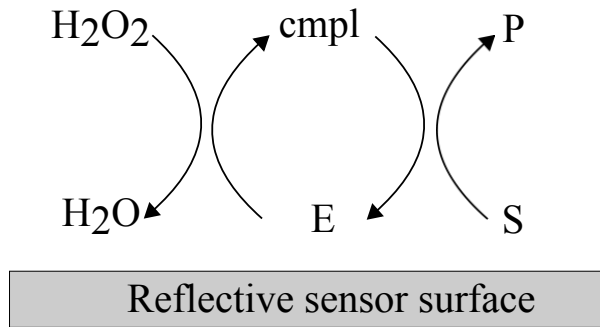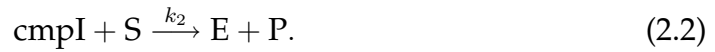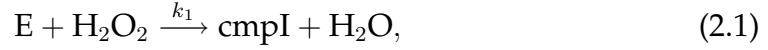
$$E + H_2O_2 \xrightarrow{k_1} \text{cmpI} + H_2O, \tag{2.1}$$

$$\text{cmpI} + S \xrightarrow{k_2} E + P. \tag{2.2}$$

Figure 2.2: Reaction scheme of peroxidase-based optical biosensor.

The product (P) absorbs light and therefore the response of the biosensor increases during the reaction as the product forms. The concentration of the analyte (S) can be directly determined from the absorbance of the product (P) [145].

2.1.2 Mathematical model

Governing equations

Assuming the symmetrical geometry of the biosensor and homogeneous distribution of immobilized enzyme, the mass transport and the reaction kinetics in the enzyme layer can be described by the following system of the reaction-diffusion equations ($0 < x < d, t > 0$),

$$\frac{\partial S_e}{\partial t} = D_{Se} \frac{\partial^2 S_e}{\partial x^2} - k_2 C S_e, \tag{2.3}$$

$$\frac{\partial P_e}{\partial t} = D_{Pe}\frac{\partial^2 P_e}{\partial x^2} + k_2 C S_e, \tag{2.4}$$

$$\frac{\partial H_e}{\partial t} = D_{He}\frac{\partial^2 H_e}{\partial x^2} - k_1 E H_e, \tag{2.5}$$

$$\frac{\partial E}{\partial t} = -k_1 E H_e + k_2 C S_e, \tag{2.6}$$

$$\frac{\partial C}{\partial t} = k_1 E H_e - k_2 C S_e, \tag{2.7}$$

where x and t stand for space and time, $S_e(x,t)$, $P_e(x,t)$, $H_e(x,t)$, $E(x,t)$, $C(x,t)$ are the substrate, product, hydrogen peroxide, peroxidase and compound I concentrations in the enzyme layer, d is the thickness of the enzyme layer, and D_{Se}, D_{Pe}, D_{He} are the diffusion coefficients. The enzyme and the formed compound I are immobilized and therefore there are no diffusion terms in the enzyme and compound I equations.

Outside the enzyme layer only mass transport by diffusion of the substrate, product and hydrogen peroxide takes place. We assume that the external mass transport obeys a finite diffusion regime ($d < x < d + \delta, t > 0$),

$$\frac{\partial S_b}{\partial t} = D_{Sb}\frac{\partial^2 S_b}{\partial x^2}, \tag{2.8}$$

$$\frac{\partial P_b}{\partial t} = D_{Pb}\frac{\partial^2 P_b}{\partial x^2}, \tag{2.9}$$

$$\frac{\partial H_b}{\partial t} = D_{Hb}\frac{\partial^2 H_b}{\partial x^2}, \tag{2.10}$$

where δ is the thickness of the diffusion layer, $S_b(x,t)$, $P_b(x,t)$, $H_b(x,t)$ are the substrate, product and hydrogen peroxide concentrations in the diffusion layer, and D_{Sb}, D_{Pb}, D_{Hb} are the diffusion coefficients.

The diffusion layer ($d < x < d + \delta$) may be treated as the Nernst diffusion layer [146]. According to the Nernst approach a layer of thickness δ remains unchanged with time. It was assumed that away from it the solution is uniform in concentration.

Initial conditions

Let $x = 0$ represents the plate surface, while $x = d$ is the boundary between the enzyme layer and the buffer solution. The biosensor operation starts when some substrate appears in the bulk solution. This is used in the initial conditions ($t = 0$)

$$
\begin{aligned}
&S_e(x, 0) = P_e(x, 0) = C(x, 0) = 0, \ H_e(x, 0) = H_0, \\
&E(x, 0) = E_0, \quad 0 \le x \le d, \\
&P_b(x, 0) = 0, \ H_b(x, 0) = H_0, \quad d \le x \le d + \delta, \\
&S_b(x, 0) = 0, \quad d \le x < d + \delta, \\
&S_b(d + \delta, 0) = S_0,
\end{aligned}
\tag{2.11}
$$

where E_0 stands for the initial concentration of the enzyme in the enzyme layer, H_0 is the hydrogen peroxide concentration in the bulk solution as well as in the enzyme layer, and S_0 is the substrate concentration in the bulk solution.

Boundary conditions

In the bulk solution the concentrations of the substrate, product and hydrogen peroxide remain constant ($t > 0$),

$$
S_b(d + \delta, t) = S_0, \quad P_b(d + \delta, t) = 0, \quad H_b(d + \delta, t) = H_0.
\tag{2.12}
$$

Assuming the impenetrable and unreactive plate surface, the mass flux of the species must vanish at this boundary,

$$
\left.\frac{\partial S_e}{\partial x}\right|_{x=0} = \left.\frac{\partial P_e}{\partial x}\right|_{x=0} = \left.\frac{\partial H_e}{\partial x}\right|_{x=0} = 0.
\tag{2.13}
$$

On the boundary between two regions having different diffusivities, we define

the matching conditions ($t > 0$)

$$
\begin{aligned}
D_{Se}\frac{\partial S_e}{\partial x}\bigg|_{x=d} &= D_{Sb}\frac{\partial S_b}{\partial x}\bigg|_{x=d}, & S_e(d,t) &= S_b(d,t), \\
D_{Pe}\frac{\partial P_e}{\partial x}\bigg|_{x=d} &= D_{Pb}\frac{\partial P_b}{\partial x}\bigg|_{x=d}, & P_e(d,t) &= P_b(d,t), \\
D_{He}\frac{\partial H_e}{\partial x}\bigg|_{x=d} &= D_{Hb}\frac{\partial H_b}{\partial x}\bigg|_{x=d}, & H_e(d,t) &= H_b(d,t).
\end{aligned}
\tag{2.14}
$$

These conditions mean that fluxes of the substrate, product and hydrogen peroxide through the stagnant external diffusion layer equals to the corresponding fluxes entering the surface of the enzyme layer. The partitions of the substrate, product and hydrogen peroxide in the enzyme layer versus bulk are assumed to be equal [9, 80].

Response of the biosensor

The light absorbance was assumed as the response of the optical biosensor. The optical signal is due to the product absorbance in the enzyme and diffusion layers. The optical biosensor was assumed to be placed in the flow or inside of a very high volume of mixed solution. The product molecules which escape the enzyme and diffusion layers do not contribute to the signal. The absorbance $A(t)$ at time t may be obtained as follows:

$$
A(t) = \varepsilon_P l_{ef} \bar{P}, \quad l_{ef} = d + \delta,
\tag{2.15}
$$

where ε_P is molar extinction coefficient of the product, $\bar{P}$ - the concentration of the product averaged through the enzyme and diffusion layers, l_{ef} - the effective thickness of the enzyme layer and Nernst layer [145]. For organic compounds ε_P varies between 10^4 and $10^2\,\mathrm{m^2 mol^{-1}}$.

For the further representation of averaged concentrations of substrate, product and hydrogen peroxide through the enzyme and diffusion layers, we introduce

the following designations:

$$\bar{U} = \frac{1}{d+\delta} \left(\int\limits_0^d U_e(x,t)dx + \int\limits_d^{d+\delta} U_b(x,t)dx \right), \quad U \in \{S, P, H\}. \tag{2.16}$$

The concentrations of the substrate, product, hydrogen peroxide, enzyme and compound I averaged only through the enzyme layer are given by

$$\bar{V} = \frac{1}{d} \int\limits_0^d U_e(x,t)dx, \quad U_e \in \{S_e, P_e, H_e, E, C\}. \tag{2.17}$$

We assume that the system (2.3)-(2.14) approaches a steady state as $t \to \infty$,

$$A_\infty = \lim_{t \to \infty} A(t), \tag{2.18}$$

where A_∞ is the steady state absorbance.

The sensitivity is another very important characteristic of biosensors [124, 139]. It is defined as a gradient of the steady state absorbance with respect to the substrate concentration. The absorbance varies in orders of magnitude with the concentration of the substrate to be analyzed [92]. Therefore dimensionless expression of the sensitivity is preferable,

$$B_S(S_0) = \frac{S_0}{A_\infty(S_0)} \times \frac{d\,A_\infty(S_0)}{d\,S_0}, \tag{2.19}$$

where B_S stands for the dimensionless sensitivity of the biosensor, $A_\infty(S_0)$ is the steady state absorbance calculated at the substrate concentration S_0 in bulk solution.

We consider the dimensionless Biot number Bi to express the ratio of internal mass transfer resistance to the external one [4, 74],

$$Bi = \frac{d/D_{Se}}{\delta/D_{Sb}} = \frac{dD_{Sb}}{\delta D_{Se}}. \tag{2.20}$$

The reaction product may be fluorescent and it may be the fluorescence which is measured [7A]. Optical biosensors based on the fluorescence detection generate a photoluminescent signal indicative of target analyte binding [30, 92]. Fluorescence emission is then detected and converted into an analytical signal [77]. They have been used for the analysis of many chemical and biological substances, especially in cases limited by low analyte concentrations [5].

By an extension of the Beer-Lambert law, the response of a fluorescent biosensor describing the intensity of fluorescence $F_I(t)$ at time t may be obtained as follows [7, 77]:

$$F_I(t) = I_0 \varphi \left(1 - 10^{-\varepsilon_P l_{ef} \bar{P}} \right), \tag{2.21}$$

where I_0 stands for the intensity of excitation light, φ is a quantum yield of fluorophore, $\bar{P}$ - the concentration of the product averaged through the entire diffusion layer. The quantum yield of the product fluorescence φ, defined as the ratio of the number of photons emitted to the number of photons absorbed, practically varies between 0.001 and 1.

The fluorescence $F_I(t)$ is almost linearly proportional to the averaged concentration of the product $\bar{P}$,

$$F_I(t) \approx 2.303 I_0 \varphi \varepsilon_P l_{ef} \bar{P}, \tag{2.22}$$

when the absorbance expressed as $\varepsilon_P l_{ef} \bar{P}$ is less than 0.1 [145]. Since the fluorescence intensity $F_I(t)$ is directly proportional to the intensity I_0 of the excitation light, the measured fluorescence $F(t)$ is usually reported in relative fluorescent units (RFU),

$$F(t) = F_I(t)/I_0. \tag{2.23}$$

We also assume that the system approaches a steady state as $t \to \infty$,

$$F_\infty = \lim_{t \to \infty} F(t), \tag{2.24}$$

where F_∞ is the steady state fluorescence.

2.2   Laccase-based Synergistic Biosensor

There are many different schemes of enzymatic catalysis apart from the simplest Michaelis-Menten case that might be exploited for the bioelectrocatalysis and the construction of biosensors [34, 42]. Synergistic scheme of substrates conversion is of particular interest due to the fact that this scheme allows producing highly sensitive bioelectrodes and powerful biofuel cells [18, 40, 55, 107, 128]. In the synergistic scheme, an enzyme catalyses the parallel conversion of substrates into the products, with the concomitant cross-reaction of the substrates and the products. Moreover, in this case, the average rate of substrates conversion exceeds the rate of individual reaction steps [82, 84, 136].

Recently, the laccase-based bioelectrode utilising synergistic N-substituted phenothiazines and phenoxazines oxidation in the presence of hexacyanoferrate(II) was built and investigated [83]. The synergistic process was analytically investigated assuming the steady state conditions, ignoring the mass transport and applying many other simplifications. The action of bioelectrodes includes not only biocatalytical conversion but also the mass transport of substrates as well as products [95, 124, 139, 152]. The diffusion limitations causes bioelectrode sensitivity changes. For the accurate prediction of the bioelectrode response, the mass transport by diffusion has to be considered together with the biocatalytical conversion [10, 20, 94]. The modeling of these processes by an analytical solution of the system of differential equations is practically impossible [32, 99].

This section presents a mathematical model of a laccase-based biosensor utilizing simultaneous substrates conversion. The developed model is based on non-stationary non-linear reaction-diffusion equations [17, 32]. The modeling biosensor comprises three compartments, an enzyme layer, a dialysis membrane and an outer diffusion layer. By changing input parameters the biosensor action was analysed with a special emphasis to the influence of the species concentrations on the synergy of the simultaneous substrates conversion. The digital simulation was carried out using the finite difference technique [17, 32, 120].

2.2.1 Modeling biosensor

We assume that a laccase-based biosensor is composed of a graphite electrode covered with the net (mesh = 160, thickness of the thread 100 μm) and the enzyme solution [83]. The enzyme layer is separated from the bulk solution by means of the dialysis membrane. The diffusion layer where the flux of the substances takes place is also considered. The schematic view of the modeled biosensor is presented in the Fig. 2.3.
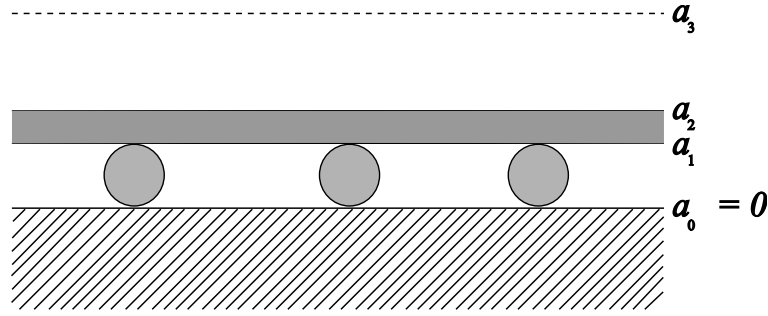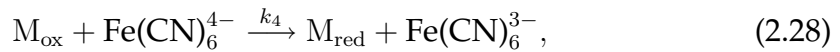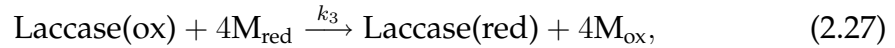

Figure 2.3: The schematic view of the laccase-based amperometric biosensor.

The scheme of the laccase action (see Fig. 2.4) comprises the stadium of oxidized laccase interaction with two substrates as well as a cross reaction of the oxidized mediator and ferrocyanide [83]. The laccase is activated with oxygen,

$$\text{Laccase(red)} + \text{O} + 4\text{H}^+ \xrightarrow{k_1} \text{Laccase(ox)} + 2\text{H}_2\text{O}, \tag{2.25}$$

$$\text{Laccase(ox)} + 4\text{Fe(CN)}_6^{4-} \xrightarrow{k_2} \text{Laccase(red)} + 4\text{Fe(CN)}_6^{3-}, \tag{2.26}$$

$$\text{Laccase(ox)} + 4\text{M}_{\text{red}} \xrightarrow{k_3} \text{Laccase(red)} + 4\text{M}_{\text{ox}}, \tag{2.27}$$

$$\text{M}_{\text{ox}} + \text{Fe(CN)}_6^{4-} \xrightarrow{k_4} \text{M}_{\text{red}} + \text{Fe(CN)}_6^{3-}, \tag{2.28}$$

where Laccase(red) and Laccase(ox) are the reduced and oxidized forms of laccase, O - oxygen (O_2), H_2O - water, H^+ stands for the hydrogen ion, Fe(CN)_6^{4-} is the hexacyanoferrate(II) (ferrocyanide), Fe(CN)_6^{3-} is the hexacyanoferrate(III)

(ferricyanide), M_{red}, M_{ox} - stand for the reduced and oxidized mediators respectively, k_1, k_2, k_3, k_4 are the reaction rate constants.

On the electrode surface the ferricyanide is reduced to ferrocyanide whereas oxidized mediator is converted to its reduced form,
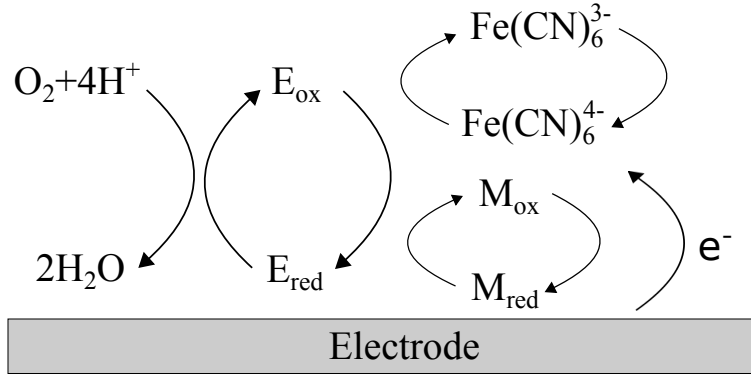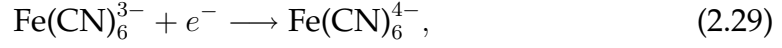
$$Fe(CN)_6^{3-} + e^- \longrightarrow Fe(CN)_6^{4-}, \tag{2.29}$$
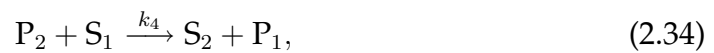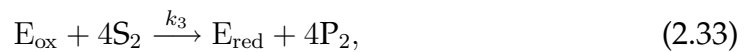
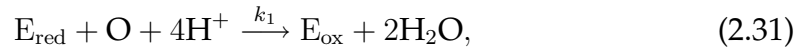$$M_{ox} + e^- \longrightarrow M_{red}. \tag{2.30}$$

Figure 2.4: Scheme of electron transfer in laccase biosensor.

In the terms of substrates and products the reaction scheme (2.25)-(2.30) can be written as follows:

$$E_{red} + O + 4H^+ \xrightarrow{k_1} E_{ox} + 2H_2O, \tag{2.31}$$

$$E_{ox} + 4S_1 \xrightarrow{k_2} E_{red} + 4P_1, \tag{2.32}$$

$$E_{ox} + 4S_2 \xrightarrow{k_3} E_{red} + 4P_2, \tag{2.33}$$

$$P_2 + S_1 \xrightarrow{k_4} S_2 + P_1, \tag{2.34}$$

$$P_1 + e^- \longrightarrow S_1, \tag{2.35}$$

$$P_2 + e^- \longrightarrow S_2, \tag{2.36}$$
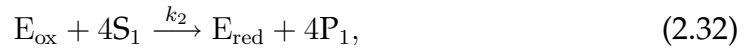
where E_{red} and E_{ox} correspond to the reduced and the oxidized laccase enzyme, respectively, S_1 and S_2 are the substrates, P_1, P_2 - stand for the products of the reactions. S_2 and P_2 are called the reduced and the oxidized mediators, respectively. The products P_1 and P_2 are the electrochemically active substances.

2.2.2 Mathematical model

The biosensor model involves the following regions: an enzyme-loaded nylon net, a dialysis membrane, an outer diffusion limiting region, and a convective region where the analyte concentration is maintained constant. Due to the relatively small volume of the nylon net in comparison with the volume of the enzyme, the enzyme-loaded mesh can be assumed as a periodic media, and the homogenisation process can be applied to the enzyme-loaded mesh [150]. These assumptions lead to a three compartment model. The homogenised enzyme layer corresponds to the first compartment. The dialysis membrane and the outer diffusion are the next two compartments.

Governing equations

Assuming the homogeneous distribution of immobilised enzyme, the mass transport and the reaction kinetics in the enzyme layer of the uniform thickness can be described by the following system of the reaction-diffusion equa-

tions ($0 < x < a_1$, $t > 0$):

$$\frac{\partial E_{red,1}}{\partial t} = D_{E_{red,1}} \frac{\partial^2 E_{red,1}}{\partial x^2} + 4k_2 E_{ox,1} S_{1,1} - k_1 E_{red,1} O_1 + 4k_3 E_{ox,1} S_{2,1}, \quad \text{(2.37a)}$$

$$\frac{\partial E_{ox,1}}{\partial t} = D_{E_{ox,1}} \frac{\partial^2 E_{ox,1}}{\partial x^2} + k_1 E_{red,1} O_1 - 4k_2 E_{ox,1} S_{1,1} - 4k_3 E_{ox,1} S_{2,1}, \quad \text{(2.37b)}$$

$$\frac{\partial S_{1,1}}{\partial t} = D_{S_{1,1}} \frac{\partial^2 S_{1,1}}{\partial x^2} - 4k_2 E_{ox,1} S_{1,1} - k_4 P_{2,1} S_{1,1}, \quad \text{(2.37c)}$$

$$\frac{\partial S_{2,1}}{\partial t} = D_{S_{2,1}} \frac{\partial^2 S_{2,1}}{\partial x^2} - 4k_3 E_{ox,1} S_{2,1} + k_4 P_{2,1} S_{1,1}, \quad \text{(2.37d)}$$

$$\frac{\partial P_{1,1}}{\partial t} = D_{P_{1,1}} \frac{\partial^2 P_{1,1}}{\partial x^2} + 4k_2 E_{ox,1} S_{1,1} + k_4 P_{2,1} S_{1,1}, \quad \text{(2.37e)}$$

$$\frac{\partial P_{2,1}}{\partial t} = D_{P_{2,1}} \frac{\partial^2 P_{2,1}}{\partial x^2} + 4k_3 E_{ox,1} S_{2,1} - k_4 P_{2,1} S_{1,1}, \quad \text{(2.37f)}$$

$$\frac{\partial O_1}{\partial t} = D_{O_1} \frac{\partial^2 O_1}{\partial x^2} - k_1 E_{red,1} O_1, \quad \text{(2.37g)}$$

where $E_{red,1}$, $E_{ox,1}$, $S_{i,1}$, $P_{i,1}$ and O_1 stand for the concentrations of the reduced and oxidized forms of the enzyme, i-th substrate, i-th product and oxygen, respectively, a_1 is the thickness of the enzyme layer, $D_{E_{red,1}}$, $D_{E_{ox,1}}$, $D_{S_{i,1}}$, $D_{P_{i,1}}$ and D_{O_1} are the diffusion coefficients, $i = 1, 2$.

In the dialysis membrane as well as in the outer diffusion layer no enzymatic reaction occurs. Hence, only the mass transport by diffusion and the electrochemical reaction (2.34) are modeled ($a_{j-1} < x < a_j$, $t > 0$),

$$\frac{\partial S_{1,j}}{\partial t} = D_{S_{1,j}} \frac{\partial^2 S_{1,j}}{\partial x^2} - k_4 P_{2,j} S_{1,j}, \quad \text{(2.38a)}$$

$$\frac{\partial S_{2,j}}{\partial t} = D_{S_{2,j}} \frac{\partial^2 S_{2,j}}{\partial x^2} + k_4 P_{2,j} S_{1,j}, \quad \text{(2.38b)}$$

$$\frac{\partial P_{1,j}}{\partial t} = D_{P_{1,j}} \frac{\partial^2 P_{1,j}}{\partial x^2} + k_4 P_{2,j} S_{1,j}, \quad \text{(2.38c)}$$

$$\frac{\partial P_{2,j}}{\partial t} = D_{P_{2,j}} \frac{\partial^2 P_{2,j}}{\partial x^2} - k_4 P_{2,j} S_{1,j}, \quad \text{(2.38d)}$$

$$\frac{\partial O_j}{\partial t} = D_{O_j} \frac{\partial^2 O_j}{\partial x^2}, \quad \text{(2.38e)}$$

where $S_{i,j}$, $P_{i,j}$ and O_j stand for the concentrations of the i-th substrate, i-th product and oxygen in the dialysis membrane ($j = 2$) and the diffusion layer ($j = 3$), respectively, a_1 is the thickness of the enzyme layer, $a_2 - a_1$ and $a_3 - a_2$ are the thicknesses of the membrane and the diffusion layer, respectively, $D_{S_{i,j}}$,

$D_{P_{i,j}}$ and D_{O_j} are the diffusion coefficients, $i = 1, 2$, $j = 2, 3$.

Initial conditions

The biosensor operation starts when the substrates appear on the boundary of the diffusion layer ($t = 0$),

$$S_{i,j} = 0, \quad x \in [a_{j-1}, a_j], \quad j = 1, 2, \tag{2.39a}$$

$$S_{i,3} = 0, \quad x \in [a_2, a_3), \tag{2.39b}$$

$$S_{i,3} = S_{i,0}, \quad x = a_3, \tag{2.39c}$$

where $S_{i,0}$ is the concentration of the i-th substrate in the buffer solution, $a_0 = 0$, $i = 1, 2$.

Initially, the oxygen is assumed to be of uniform concentration, while the products are assumed of zero concentration ($t = 0$),

$$P_{i,j} = 0, \quad O_j = O_0, \quad x \in [a_{j-1}, a_j], \quad j = 1, 2, 3, \tag{2.40}$$

where O_0 is the initial concentration of the oxygen.

The whole enzyme is initially in the reduced form ($t = 0$),

$$E_{red,1} + E_{ox,1} = E_0, \quad E_{red,1} = E_0, \quad E_{ox,1} = 0, \quad x \in [0, a_1], \tag{2.41}$$

where E_0 stands for the initial as well as the total concentration of the enzyme.

Boundary conditions

On the electrode surface the products are consumed and the substrates are re-generated by reactions (2.35) and (2.36) ($t > 0$),

$$P_{i,1} = 0, \quad x = 0, \tag{2.42a}$$

$$D_{S_{i,1}} \frac{\partial S_{i,1}}{\partial x}\bigg|_{x=0} = -D_{P_{i,1}} \frac{\partial P_{i,1}}{\partial x}\bigg|_{x=0}, \quad i = 1, 2. \tag{2.42b}$$

Assuming the impenetrable plate surface, the mass flux of the electro-inactive substance vanishes at this boundary ($t > 0$),

$$\frac{\partial O_1}{\partial x}\bigg|_{x=0} = 0. \tag{2.43}$$

During the biosensor operation the enzyme remains locked in the enzyme layer ($t > 0$),

$$\frac{\partial E_{ox}}{\partial x}\bigg|_{x=0} = \frac{\partial E_{ox}}{\partial x}\bigg|_{x=a_1} = \frac{\partial E_{red}}{\partial x}\bigg|_{x=0} = \frac{\partial E_{red}}{\partial x}\bigg|_{x=a_1} = 0. \tag{2.44}$$

The outer diffusion layer ($a_2 < x < a_3$) can be treated as the Nernst diffusion layer [32]. According to the Nernst approach the layer of the thickness ($a_3 - a_2$) remains constant. In the bulk solution the concentrations of the substances remain constant ($t > 0$),

$$S_{1,3} = S_{1,0}, \quad S_{2,3} = S_{2,0}, \quad P_{1,3} = 0, \quad P_{2,3} = 0, \quad O_3 = O_0, \quad x = a_3. \tag{2.45}$$

On the boundary between the adjacent regions having different diffusivities,

we define the matching conditions ($t > 0$),

$$D_{S_{i,j}} \frac{\partial S_{i,j}}{\partial x}\bigg|_{x=a_j} = D_{S_{i,j+1}} \frac{\partial S_{i,j+1}}{\partial x}\bigg|_{x=a_j}, \quad S_{i,j} = S_{i,j+1}, \quad x = a_j, \qquad (2.46a)$$

$$D_{P_{i,j}} \frac{\partial P_{i,j}}{\partial x}\bigg|_{x=a_j} = D_{P_{i,j+1}} \frac{\partial P_{i,j+1}}{\partial x}\bigg|_{x=a_j}, \quad P_{i,j} = P_{i,j+1}, \quad x = a_j, \qquad (2.46b)$$

$$D_{O_j} \frac{\partial O_j}{\partial x}\bigg|_{x=a_j} = D_{O_{j+1}} \frac{\partial O_{j+1}}{\partial x}\bigg|_{x=a_j}, \quad O_j = O_{j+1}, \quad x = a_j, \qquad (2.46c)$$

where $i = 1, 2, \quad j = 1, 2$.

Response of the biosensor

The measured current is accepted as a response of an amperometric biosensor in a physical experiment. The current $I(t)$ depends upon the fluxes of the hexacyanoferrate(III) and mediator at the electrode surface,

$$I(t) = n_e F \mathrm{A}\left(D_{P_{1,1}} \frac{\partial P_{1,1}}{\partial x}\bigg|_{x=0} + D_{P_{2,1}} \frac{\partial P_{2,1}}{\partial x}\bigg|_{x=0}\right), \qquad (2.47)$$

where n_e is a number of electrons involved in the electrochemical reaction, F is Faraday's constant and A stands for the geometrical surface of the electrode.

We assume that the system (2.37)-(2.46) approaches a steady state as $t \to \infty$,

$$I_\infty = \lim_{t \to \infty} I(t), \qquad (2.48)$$

where I_∞ is the steady state current.

2.3   Conclussions

The mathematical models for the optical and synergistic multi-step biosensors were introduced in this chapter. The models include the governing reaction-diffusion equations, initial as well as boundary conditions. The expressions for the calculation of the biosensor response were also formulated, taking into

account the practically significant steady state case. The results of this chapter were published in six journal articles (see [1A, 3A, 4A, 7A, 9A, 10A]).

Chapter 3

Automated Modeling of Multi-step Biosensors

Computational modeling of multi-step biosensors is a complex process and generally requires a huge amount of CPU time [2, 32]. There is a number of the standard computational tools available for the numerical computations [57, 134]. However, numerical methods presented in these tools are not adequate for the solution of the reaction-diffusion diffusion equations. Moreover, these tools are generally not convenient for the great number of biochemists and bioengineers. In this chapter a new tool for the automated and user-friendly modeling of multi-step biosensor will be presented. In order to optimize the numerical solution a detail analysis of the finite difference schemes was produced.

3.1 Computational Schemes for Modeling of Biosensors

Analytical solutions for mathematical models of the biosensors are obtainable exclusively in special cases [33, 79]. In common case the models have to be

solved numerically [32, 125]. Finite difference method is one of the most popular approximation techniques [120]. Numerous types of finite difference schemes can be considered for the solution of non-linear reaction-diffusion systems [4, 120]. Three major factors must be taken into account when choosing the technique for simulation: the accuracy of the solution, computation time needed to solve the problem and ease of use of the technique. This chapter is focused on the analysis of several most commonly known finite difference schemes using computer simulation [5A].

3.1.1 Mathematical model

An amperometric biosensor can be considered as an amperometric electrode, having a layer of enzyme immobilized onto the surface of the electrode. We assume the symmetrical geometry of the electrode and homogeneous distribution of the immobilized enzyme in the enzyme membrane.

In this section, we consider the following enzyme-catalysed reaction

$$S + E \rightleftarrows ES \rightarrow E + P. \tag{3.1}$$

In this scheme the substrate (S) combines reversibly with an enzyme (E) to form a complex (ES). The complex then dissociates into a product (P) and the enzyme is regenerated. Assuming the quasi steady state approximation, the concentration of the intermediate complex (ES) do not change and may be neglected when simulating the biochemical behaviour of biosensors [124, 139]. The scheme (3.1) reduces to a simplified model of enzyme-catalyzed reaction where the enzyme (E) binds to the substrate (S) producing the product (P) is considered,

$$S \xrightarrow{E} P. \tag{3.2}$$

Coupling the enzyme-catalyzed reaction with the one-dimensional-in-space diffusion, described by Fick's second law, leads to the following system of equa-

tions [79, 125]:

$$\frac{\partial S}{\partial t} = D_S \frac{\partial^2 S}{\partial x^2} - \frac{V_{max}S}{K_M + S},$$
$$\frac{\partial P}{\partial t} = D_P \frac{\partial^2 P}{\partial x^2} + \frac{V_{max}S}{K_M + S}, \quad 0 < x < d,\ t > 0, \tag{3.3}$$

where $S(x,t)$ and $P(x,t)$ are the substrate and product concentrations, respectively, t stands for time and x - for space, D_S and D_P are the diffusion coefficients of the substrate and product, respectively, K_M is the Michaelis-Menten constant, V_{max} is the maximal enzymatic rate attainable when the enzyme is fully saturated with substrate, d is the thickness of the enzyme membrane.

Let $x = 0$ represents the electrode surface, while $x = d$ represents the bulk solution-membrane interface. The biosensor operation starts when some substrate appears on the surface of the enzyme layer,

$$S(x,0) = 0, \quad 0 \le x < d,$$
$$S(d,0) = S_0, \tag{3.4}$$
$$P(x,0) = 0, \quad 0 \le x \le d,$$

where S_0 stands for the concentration of substrate in the bulk solution.

In the case of amperometric biosensors, due to the electrode polarization, the concentration of the reaction product at the electrode surface is being permanently reduced to zero. The substrate does not react at the electrode surface. If the substrate is well-stirred and in powerful motion, then the diffusion layer $(0 < x < d)$ remains at a constant thickness of d during the biosensor operation. This is used in the boundary conditions given by:

$$\frac{\partial S}{\partial x}\Big|_{x=0} = 0,$$
$$S(d,t) = S_0, \tag{3.5}$$
$$P(0,t) = P(d,t) = 0.$$

The measured current is accepted as a response of an amperometric biosensor in a physical experiment. The current depends upon the flux of the reaction product at the electrode surface, i.e. at the border $x = 0$. Consequently, the density $J(t)$ of the anodic current at a time t can be obtained explicitly from Faraday's and second Fick's laws using the flux of the product concentration at the surface of the electrode,

$$J(t) = n_e F D_P \frac{\partial P}{\partial x}\bigg|_{x=0},\tag{3.6}$$

where n_e is a number of electrons, involved in charge transfer at the electrode surface, and F is the Faraday constant.

We assume that the system (3.3)-(3.5) approaches a steady state as $t \to \infty$,

$$J_p = \lim_{t\to\infty} J(t),\tag{3.7}$$

where J_p is the density of the steady state current.

3.1.2 Solution of the problem

The analytical solutions for nonlinear partial differential equations generally do not exist. Equations (3.3)-(3.5) describing the action of an amperometric biosensor do not have ones either, so numerical approximation must be used. We applied finite difference technique to solve (3.3)-(3.5) the boundary value problem numerically [32, 120].

3.1.2.1 Analytical solutions

In a special, low-concentration case $S_0 \ll K_M$, the reaction rate is directly proportional to the substrate concentration. Therefore, the analytical solutions are known for the boundary value problem at a steady-state (3.3)-(3.5),

$$S(x) = S_0 \frac{\cosh(Q(d-x))}{\cosh(Qd)},\tag{3.8}$$

$$P\left(x\right) = \frac{S_0 D_S}{D_P} \left[\left(\frac{1}{\cosh(Qd)} - 1 \right) \frac{x}{d} - \frac{\cosh(Q(d-x))}{\cosh(Qd)} + 1 \right],$$ (3.9)

where $S(x)$ and $P(x)$ are the stationary functions,

$$Q = \sqrt{\frac{V_{max}}{K_M D_S}}.$$ (3.10)

Applying these analytical solutions to the equation (3.6) the biosensor steady state current can be calculated as follows [79]:

$$J_l = n_e F D_P S_0 \frac{1}{d} \left(1 - \frac{1}{\cosh(\sigma)} \right),$$ (3.11)

where σ^2 is a dimensionless diffusion modulus, Damköhler number,

$$\sigma^2 = \frac{V_{max} d^2}{D_S K_M}.$$ (3.12)

The biosensor response is known to be under mass transport control if the enzymatic reaction in the enzyme layer is faster than the mass transport process [4, 79, 125]. The diffusion modulus essentially compares the rate of enzymatic reaction (V_{max}/K_M) with the diffusion through the enzyme layer (D_S/d^2), If $\sigma^2 \ll 1$ then the enzyme kinetics controls the biosensor response. The response is under diffusion control when $\sigma^2 \gg 1$.

At the high concentration of the substrate ($S_0 \gg K_M$), the biosensor steady state current does not depend on the concentration S_0 of the analyte [33],

$$J_g = \frac{n_e F V_{max} d}{2}.$$ (3.13)

However, in the intermediate concentration cases, i.e. if $S_0 \approx K_M$, the analytical solutions are unknown and numerical methods are used to solve the problem [4, 32, 125].

3.1.2.2   Finite Difference schemes

We introduce an uniform discrete grid $\Omega_{h\tau}$ to simulate the biosensor using finite difference method,

$$\Omega_{h\tau} = \{(x_i, t_j) : x_i = ih; t_j = j\tau; hN = d; \tau M = T; i = 0, ..., N; j = 0, ..., M\},$$

(3.14)

where T stands for the duration of the process analysis.

The differential equations are discretized in that domain assuming the following definitions:

$$S_i^j = S(x_i, t_j), \quad P_i^j = P(x_i, t_j), \quad J_j = J(t_j),$$
$$i = 0, \dots, N; \quad j = 0, \dots, M.$$

(3.15)

3.1.2.3   Explicit Finite Difference scheme

Using explicit finite difference scheme for the substrate and product concentrations (3.3) we obtain the following finite difference equations [32, 120, 125]:

$$\frac{S_i^{j+1} - S_i^j}{\tau} = D_S \left(\frac{S_{i+1}^j - 2S_i^j + S_{i-1}^j}{h^2} \right) - \frac{V_{max}S_i^j}{K_M + S_i^j},$$
$$\frac{P_i^{j+1} - P_i^j}{\tau} = D_P \left(\frac{P_{i+1}^j - 2P_i^j + P_{i-1}^j}{h^2} \right) + \frac{V_{max}S_i^j}{K_M + S_i^j},$$
$$i = 1, \dots, N-1; \quad j = 1, \dots, M.$$

(3.16)

The initial conditions (3.4) in numerical model has the following form

$$S_i^0 = 0, \quad 0 \le i < N,$$
$$S_N^0 = S_0,$$
$$P_i^0 = 0, \quad 0 \le i \le N.$$

(3.17)

For the boundary conditions (3.5) we obtain:

$$
\begin{aligned}
S_0^j &= S_1^j, \\
S_N^j &= S_0, \\
P_0^j &= P_N^j = 0, \quad 1 \le j \le M.
\end{aligned}
\tag{3.18}
$$

The formulae for calculation of current density (3.6) becomes thus ($0 < j \le M$):

$$
J_j = n_e F D_P \frac{P_1^j}{h}.
\tag{3.19}
$$

We consider the density J_R of the steady state current calculated at the moment T_R

$$
J_R = J(T_R) \approx J_p, \quad T_R = \min_{j>0,\, J_j>0} \left\{ \tau_j : \frac{J_j - J_{j-1}}{J_j} < \varepsilon \right\}, \quad \tau_j = \tau j, \quad T \approx T_R.
\tag{3.20}
$$

We used $\varepsilon = 10^{-5}$ for the calculations.

One of the most important features of the scheme is the stability [120]. The prerequisite for the stability of the explicit finite difference scheme (3.16)-(3.18) is the following condition:

$$
\tau \le \min \left\{ \frac{h^2}{2D_S}, \frac{h^2}{2D_P} \right\}.
\tag{3.21}
$$

Because of these stability conditions, a number of the time steps must be magnified strongly as the number of the space steps is increased. This leads to the inefficient calculations.

3.1.2.4 Implicit 1 Finite Difference scheme

Mathematical model of a biosensor can be solved using several implicit finite difference schemes [32, 120, 125]. Let us name first of them "Implicit 1 Finite

Difference Scheme" and compose its equations.

The model governing equation for the substrate concentration in (3.3) is re-placed by the following finite difference equation:

$$\frac{S_i^j - S_i^{j-1}}{\tau} = D_S \left(\frac{S_{i+1}^j - 2S_i^j + S_{i-1}^j}{h^2} \right) - \frac{V_{max} S_i^{j-1}}{K_M + S_i^{j-1}}. \tag{3.22}$$

Known concentration values of the substrate at the upper layer can be used for calculation of the product concentration. Hence, governing equation for the product concentration can be approximated with:

$$\frac{P_i^j - P_i^{j-1}}{\tau} = D_P \left(\frac{P_{i+1}^j - 2P_i^j + P_{i-1}^j}{h^2} \right) + \frac{V_{max} S_i^j}{K_M + S_i^j}. \tag{3.23}$$

The rest equations (3.4)-(3.6) take the same form as those of the explicit scheme.

3.1.2.5 Implicit 2 Finite Difference scheme

The model equation for the substrate concentration in (3.3) may be approx-imated with a more implicit scheme than equation (3.22). At a numerator of reaction term the concentration of substrate can be used in a upper level,

$$\frac{S_i^j - S_i^{j-1}}{\tau} = D_S \left(\frac{S_{i+1}^j - 2S_i^j + S_{i-1}^j}{h^2} \right) - \frac{V_{max} S_i^j}{K_M + S_i^{j-1}}. \tag{3.24}$$

Present numerical equation is linear, same as (3.22). The other equations match those obtained using the explicit scheme.

3.1.2.6 Crank-Nicolson scheme

Using Crank-Nicolson [43, 120] method the reaction-diffusion equations (3.3) are approximated by linear finite difference equations,

$$
\begin{aligned}
\frac{S_i^j - S_i^{j-1}}{\tau} = \frac{D_S}{2h^2}\Big(& S_{i+1}^j - 2S_i^j + S_{i-1}^j + \\
& S_{i+1}^{j-1} - 2S_i^{j-1} + S_{i-1}^{j-1}\Big) - \frac{V_{max}S_i^{j-1}}{K_M + S_i^{j-1}}, \\
\frac{P_i^j - P_i^{j-1}}{\tau} = \frac{D_P}{2h^2}\Big(& P_{i+1}^j - 2P_i^j + P_{i-1}^j + \\
& P_{i+1}^{j-1} - 2P_i^{j-1} + P_{i-1}^{j-1}\Big) + \frac{V_{max}S_i^j}{K_M + S_i^j}.
\end{aligned}
\tag{3.25}
$$

The rest equations (3.4)-(3.6) are approximated like in the explicit scheme.

3.1.2.7 Hopscotch scheme

Using Hopscotch scheme unknown grid points are obtained at two phases [120]. On the first phase, even grid points ($S[e]_i^{j+1}$, $P[e]_i^{j+1}$) are calculated explicitly using known lower layer values (S_i^j, P_i^j),

$$
\begin{aligned}
\frac{S[e]_i^{j+1} - S_i^j}{\tau} &= D_S\left(\frac{S_{i+1}^j - 2S_i^j + S_{i-1}^j}{h^2}\right) - \frac{V_{max}S_i^j}{K_M + S_i^j}, \\
\frac{P[e]_i^{j+1} - P_i^j}{\tau} &= D_P\left(\frac{P_{i+1}^j - 2P_i^j + P_{i-1}^j}{h^2}\right) + \frac{V_{max}S_i^j}{K_M + S_i^j}.
\end{aligned}
\tag{3.26}
$$

On the second phase, odd grid points ($S[o]_i^{j+1}$, $P[o]_i^{j+1}$) are calculated using odd values of the lower level and already known even values of the upper layer,

$$
\begin{aligned}
\frac{S[o]_i^{j+1} - S_i^j}{\tau} &= D_S\left(\frac{S[e]_{i+1}^{j+1} - 2S[o]_i^{j+1} + S[e]_{i-1}^{j+1}}{h^2}\right) - \frac{V_{max}S_i^j}{K_M + S_i^j}, \\
\frac{P[o]_i^{j+1} - P_i^j}{\tau} &= D_P\left(\frac{P[e]_{i+1}^{j+1} - 2P[o]_i^{j+1} + P[e]_{i-1}^{j+1}}{h^2}\right) + \frac{V_{max}S_i^{j+1}}{K_M + S_i^{j+1}}.
\end{aligned}
\tag{3.27}
$$

Computation continues alternating the calculation order of the odd and even points.

Hopscotch scheme is fully explicit yet unconditionally stable for $V_{max} = 0$ and therefore it can operate with any size of time and space steps.

3.1.2.8 Mathematical software packages

The major mathematical software packages provide tools for solving systems of the partial differential equations. However, a greater ease of use and wider range of solvable problems often comes at the expense of lower precision or less efficiency.

We used Maple (Maplesoft, Inc.) version 10 general-purpose solver "*pdsolve*" to find numerical solution for the system of the partial differential equations [57]. This solver uses finite difference method and can be configured with eleven classical schemes, calculation step size and other parameters.

The biosensor action was also simulated with MATLAB (The MathWorks, Inc.) software package [114, 154]. The problem was solved using built-in solver "*pdepe*", which provides a numerical solution for systems of differential equations in single spatial dimension and time.

3.1.3 Results and discussion

Computer simulation was used to compare accuracy and performance of the solution techniques. Since the system of linear algebraic equations is tridiagonal it can be solved efficiently [120]. Calculation results are compared in terms of precision and computation time. We define the relative error E_r as the absolute difference of the steady state current density estimated by analytical and numerical solutions divided by the steady state current density of analytical solution.

$$E_r = \frac{|J_R - J_a|}{J_a}, \quad J_a = \begin{cases} J_l, & S_0 \ll K_M, \\ J_g, & S_0 \gg K_M, \end{cases} \tag{3.28}$$

where J_R is the numerical solution defined by (3.20) while J_l and J_g are analytical solutions defined by (3.11) and (3.13), respectively.

The following values of the model parameters were employed:

$$K_M = 100\mu M, \ S_0 \in \{10^{-3}K_M; 10^3 K_M\}, \ V_{max} = 100\mu M/s,$$
$$D_S = D_P = 300\mu m^2/s, \ n_e = 2, \ T = 10s, \ d = 100\mu m. \tag{3.29}$$

The routines of the finite difference method were implemented in Java programming language [105]. For performance reasons, we executed programs of the mathematical software packages using command-line approach. The experiments were performed on the 2 GHz Intel Core 2 Duo Processor with 1GB of RAM.

As a first test problem, relative errors of the finite difference schemes and mathematical software packages were examined using two known analytical solutions (3.11) and (3.13). We applied $M = 10^2$ for the calculations using implicit 1, implicit 2 and Crank-Nicolson schemes and $M = 10^5$ using explicit and Hopscotch schemes because of the stability constraints on the time step. All the considered finite difference schemes yield very similar precision, therefore only explicit scheme results are presented in Figure 3.1 as the example. The smallest relative errors are obtained using finite difference schemes. Maple package calculates the steady state biosensor current more accurately than MATLAB. In cases of high substrate concentration (3.13) Maple's results are as precise as those obtained by explicit scheme. The numbers of steps used in calculations do not influence the accuracy of the MATLAB solution.

In Figure 3.2 the finite difference schemes are compared to the explicit scheme. The Hopscotch scheme differs very slightly from the explicit scheme in both analytical solution cases, whereas the implicit schemes showed the maximal difference of approximately 0.8 % when the number of space steps N equals to 160 (Figure 3.2). The relative errors computed using the analytical solution (3.13) at $S_0 \gg K_M$ are by a few orders of magnitude larger than the corresponding errors at $S_0 \ll K_M$ calculated using (3.11). This could be explained by less accuracy of the analytical solution (3.13) compared to the solution (3.11) [33, 79]. Considered schemes yield more similar results using analytical solu-
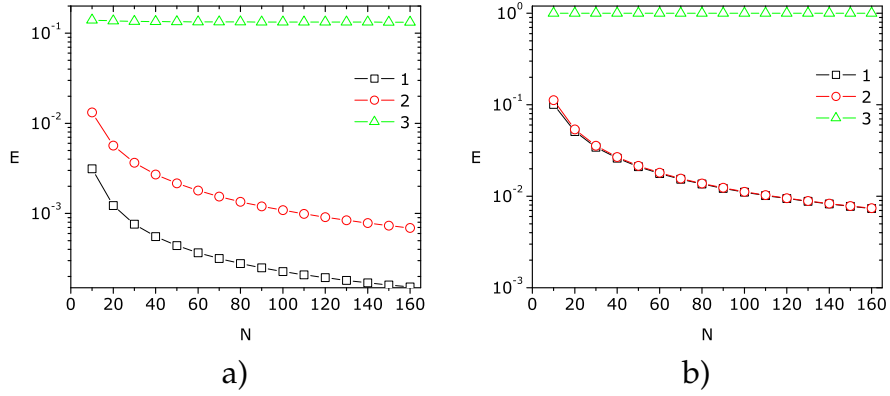
Figure 3.1: Dependence of relative error E_r on the number of space steps N for two values of S_0: $10^{-3}K_M$ (a) and $10^3 K_M$ (b). 1 - explicit scheme ($M = 10^5$), 2 - Maple ($M = 10^2$), 3 - MATLAB ($M = 10^2$).
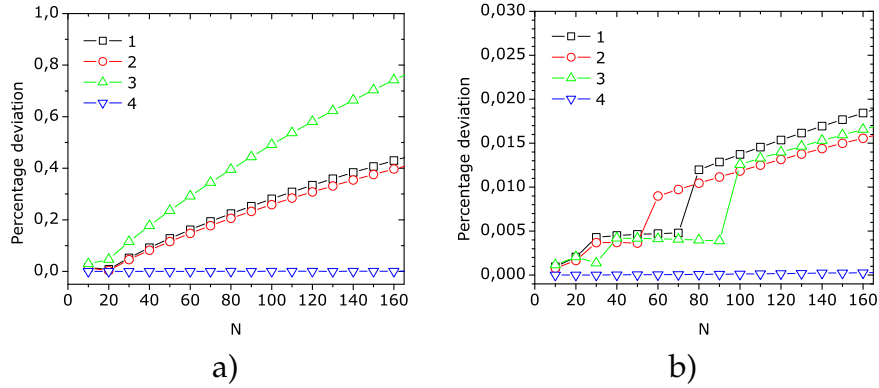
tion (3.13).

Figure 3.2: The percentage ratio of the relative error E_r of the finite difference schemes to the error E_r of the explicit scheme for two values of S_0: $10^{-3}K_M$ (a) and $10^3 K_M$ (b). 1 - implicit 1 scheme, 2 - implicit 2 scheme, 3 - Crank-Nicolson scheme, 4 - Hopscotch scheme.

In the next test problem, we consider the computation time as a function of the relative error (Figure 3.3). Introducing different limits ϵ for the relative error E_r, the computation time $T_E(\epsilon)$ is given by:

$$T_E(\epsilon) = \min_{N,M} \left\{ T_{N,M} : \ E_r \leq \epsilon \right\}, \tag{3.30}$$

where $T_{N,M}$ is the time of calculation at given numbers of grid steps N and M. $T_E(\epsilon)$ is the minimal time of computation needed to achieve the relative

error E_r not greater than ϵ. The calculations were performed for very different values of space and time steps, $N, \; M \; \in \{20, 40, 80, 160, 320, 640, 1280, 2560, 5120, 10240\}$.
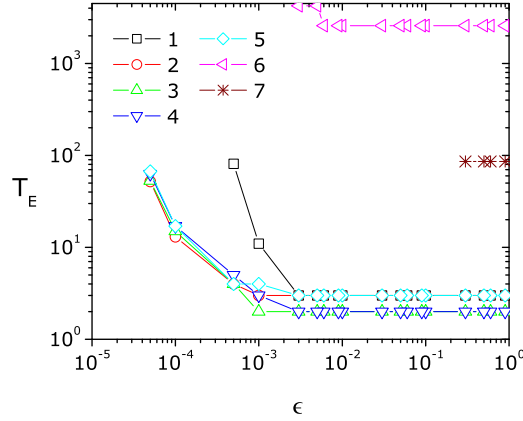
Figure 3.3: The computation time T_E versus the relative error ϵ, $N, M \in \{20, 40, 80, 160, 320, 640, 1280, 2560, 5120, 10240\}$. 1 - explicit scheme, 2 - implicit 1 scheme, 3 - implicit 2 scheme, 4 - Crank-Nicolson scheme, 5 - Hopscotch scheme, 6 - Maple, 7 - MATLAB.

As one can see in Figure 3.3, the implicit and Hopscotch are the fastest schemes to achieve the required relative error. Despite being very computationally intensive, partial differential equation solvers in mathematical software packages cannot accurately calculate the results. The MATLAB solver does not obtain higher precision than 0.1.

Finally, the computation times for different grid steps are reported in Tables 3.1 and 3.2. The Table 3.1 shows that there is a very small difference between schemes implicit 2 and Crank-Nicolson and they are the most computationally intensive schemes. Explicit scheme is the fastest computation technique. Mathematical software packages are significantly more computationally intensive, particularly Maple, see Table 3.2.

Table 3.1: Computation time (ms) by the finite difference schemes, $N = 100$.

M	Explicit	Implicit 1	Implicit 2	Crank-Nicolson	Hopscotch
10000	284	555	996	1064	659
20000	398	1108	1967	2090	1356
40000	755	2232	3974	4205	3062
80000	1480	4450	8080	8853	5563
160000	2957	8866	16542	16829	10623

Table 3.2: Computation time (s) by the mathematical software packages, $N = 100$.

M	Maple	MATLAB
100	695	0.64
200	2480	0.74
400	9379	0.85

3.2   Tool for Automated Model Development

The new types of biosensors are being introduced constantly. In order to simulate the action of those biosensors a new mathematical and numerical models must be developed every time. This process becomes cumbersome if biosensor involves multi-step reaction scheme. Considering a deterministic nature of model development this process can be automated. To make this process less work intensive we developed a computer software for the simulation of chemical reactions and diffusion.

3.2.1   Model representation language

SBML is a powerful language to describe the reaction scheme of the model. Although it does not provide all the features needed for the biosensor model, it can be readily extended.

With the introduction of SBML level 2 version 3, all model entities can now be

annotated using ontological terms. The *Annotation* element, which is encoded using the resource description framework (RDF), allows to specify additional information. According to the SBML specification, kinds of data that may be appropriately stored in annotation include information about the model that cannot be readily encoded in existing SBML elements [68]. Therefore, for the input of our software we chose SBML, supplementing additional information in form of SBML annotations.

We use XML Schema (XSD) trees to define new elements introduced for biosensor modeling (see Figures 3.4, 3.5, 3.6, 3.7) [144]. The structure of SBML document can be validated against this specification. The new schema uses a different XML namespaces to identify which elements are associated with it and covers the parameters that are not included in the SBML model definitions.
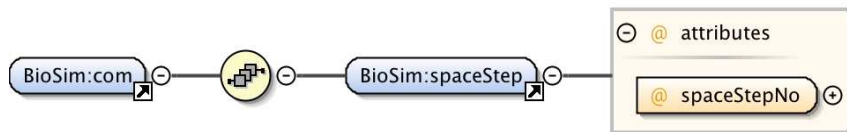
Figure 3.4: Extract of SBML schema for *Compartment* annotation element.

Using annotation we can add new properties to various model elements. As Figure 3.4 shows, *Compartment* element in SBML can now also define attribute *spaceStepNo* to specify the number of space steps for numerical simulation.

The *Species* element can be supplemented with two additional elements: *BioSim:diffCoef* and *BioSim:speciesType* (see Figure 3.5). Species occur in a single compartment only with corresponding diffusion coefficient. *BioSim:diffCoef* element defines the identifier *id* and the value *value* of the diffusion coefficient. Additional attributes of the species defined in *BioSim:speciesType* element are also important to our automated solver. The *enzymatic* attribute marks the substances that are of enzymatic nature. Considering various types of biosensors' responses, different physical characteristics are noted by the attribute *respons-*
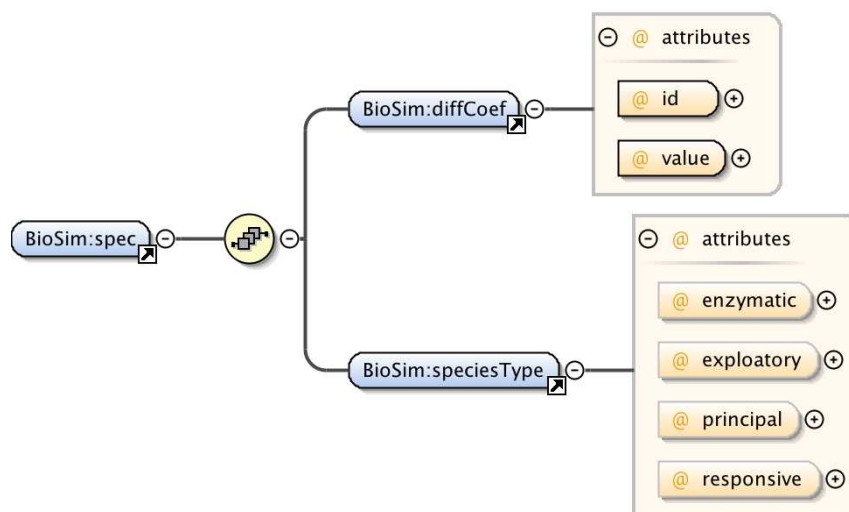
Figure 3.5: Extract of SBML schema for *Species* annotation element.

ive. In case of amperometric biosensors electrochemically active species are marked with that attribute. For biosensors that are based on optical principals, absorbing or light emitting species must be indicated. The attribute *exploratory* refers to the substance that is being measured (analyte). The value of this attribute is used for the initial conditions. Since substances are expected to diffuse to several compartments, species are named differently in each of them. The attribute *principal* is used to distinguish the same species, which denotes the name of species in the first compartment.
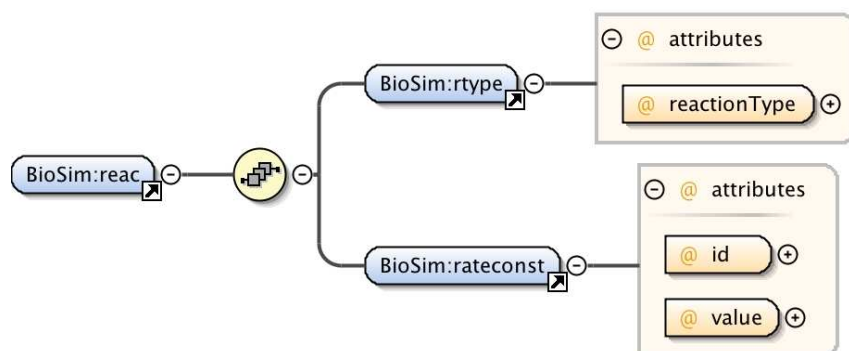
Figure 3.6: Extract of SBML schema for *Reaction* annotation element.

In the annotation of *Reaction* element we introduce *reactionType* attribute (see Figure 3.6). The values of this attribute (either *chemical* or *electrochemical*) define the type of reaction being annotated. Also, the *BioSim:rateconst* element with attributes for identifier (*id*) and value (*value*) of reaction rate constant must be entered.
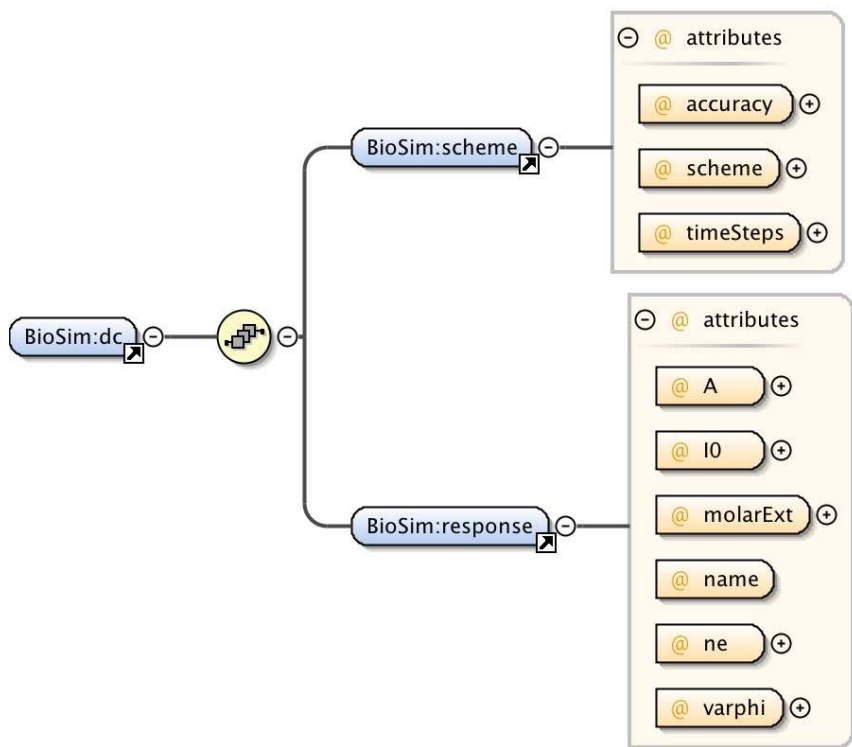
Figure 3.7: Extract of SBML schema for *Model* annotation element.

To the annotation of the *model* element we introduce parameters of numerical modeling and biosensor response (see Figure 3.7). The element *BioSim:scheme* defines finite difference scheme to be used for the simulation (*scheme*), solution stationarity parameter (*accuracy*) and number of time steps (*timeSteps*). For the calculation of the response of amperometric biosensor values of the number of the electrons involved in charge transfer (*ne*) and the geometrical surface of the electrode (*A*) must be defined. While for the response of the optical biosensor values of the molar extinction coefficient (*molarExt*), intensity of excitation light

(*I0*) and quantum yield of fluorophore (*varphi*) are entered.

Not all of the features provided in standard SBML are used by our tool. The tool takes into account all the above mentioned elements: *species*, *reaction*, *compartment*. Though it does not use other elements of SBML, like *rule*, *constraint* and *unitDefinition*. The quantities of corresponding units of measurement must be used in the modeling. Preserving original structure of SBML document will allow integration with other SBML supporting tools.

3.2.2 Generation of simulator

The developing of the computer models is based on the algorithm that generates mathematical and numerical models. SBML document containing the model description serves as an input for the algorithm. The overall process of simulator generation is shown in Fig. 3.8.
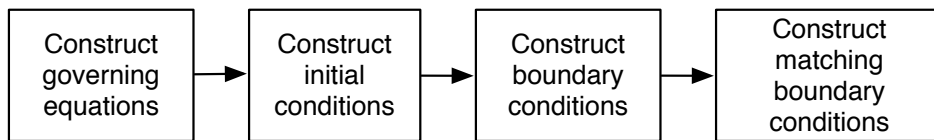
Figure 3.8: Process of the simulator generation.

The Figure 3.9 shows the algorithm for construction of governing equations. The main parts of the routine are to form diffusion equation (i.e. equation (1.14)) for every species in the model and supplement it with reaction terms (i.e. equation (1.8)) if necessary.

Initial conditions are expressed by the external concentrations of the species, except for the exploratory species, which initial conditions are set to be equal to zero (see Figure 3.10). On the boundary of the last compartment the substances
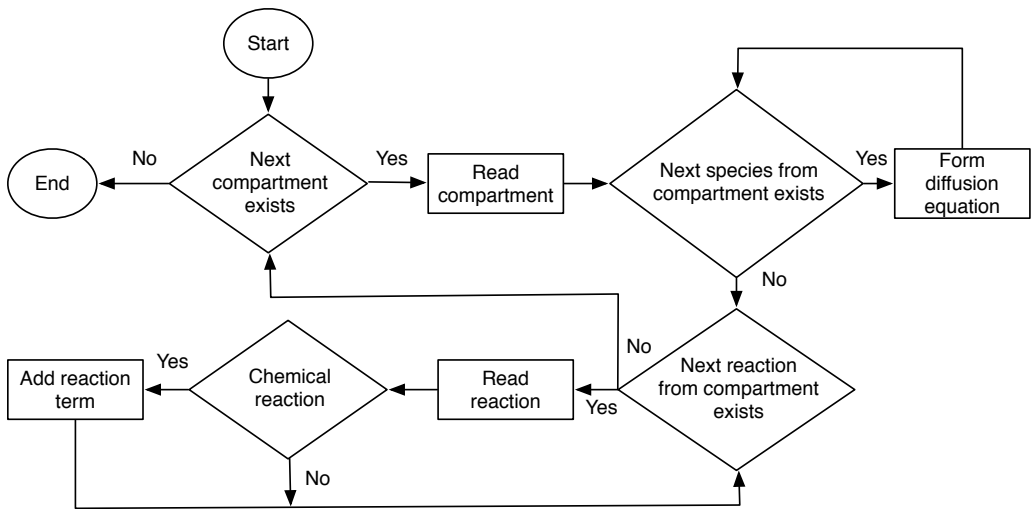
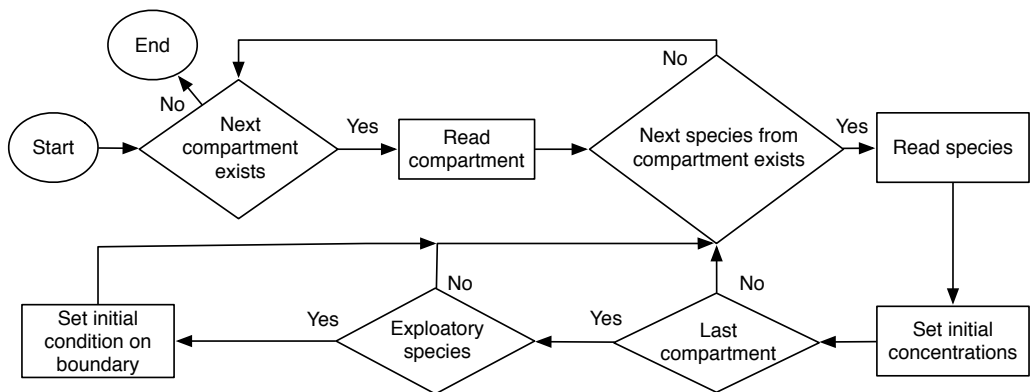Figure 3.9: Algorithm for the construction of governing equations.

Figure 3.10: Algorithm for the construction of initial conditions.

that are marked as a exploratory species are set to their initial concentration. This denotes the start of the operation action.

As Figure 3.11 shows, the procedure of boundary conditions generation depends on the compartment that is being modeled. On the boundary of the first compartment usually the Neumann boundary condition is defined (i.e. equation (2.13)). In case of amperometric biosensor the Dirichlet boundary condi-
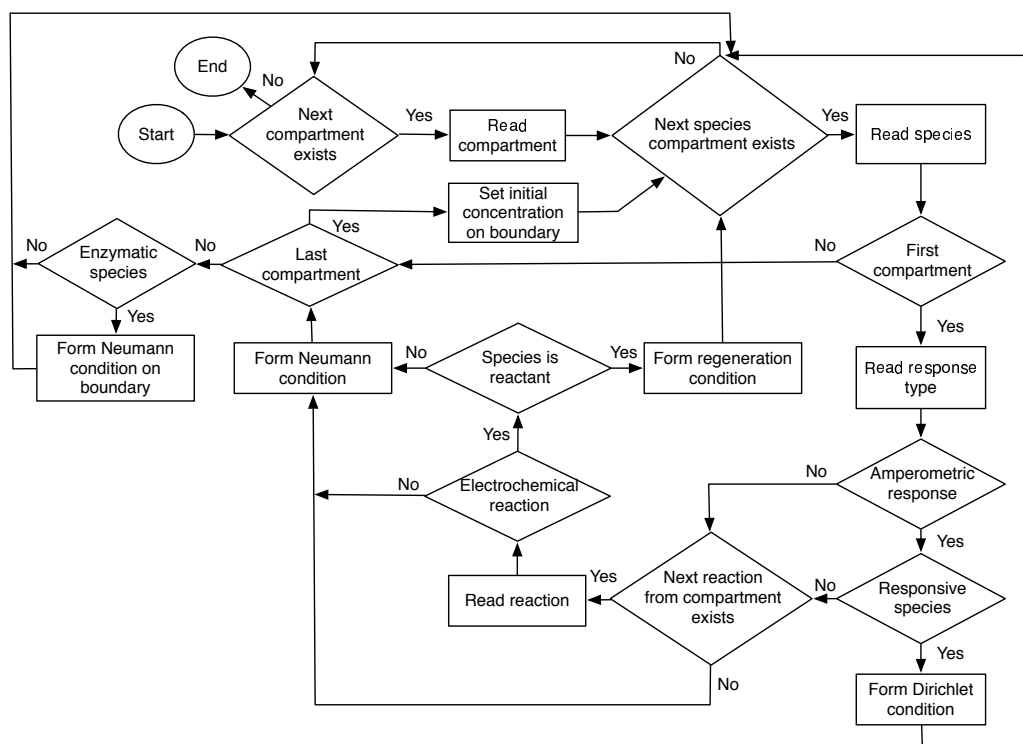
Figure 3.11: Algorithm for the construction of boundary conditions.

tion (i.e. equation (2.42a)) is defined for the responsive species. Responsive species are the substances which must be included in the response calculation. For the substance that reacts in a electrochemical reaction a regenerating boundary condition (i.e. equation (2.42b)) is created. On the boundary of the last compartment the concentrations of the substances remain constant. Generally enzymatic species are not diffusing substances and therefore boundary conditions for such species must be defined in some inner compartment.

A matching boundary conditions between compartments must be defined in case of multiple compartments (see Figure 3.12). These conditions involve species from two adjacent compartments (e.g. equation (2.14)). The similar species can be identified by the attribute *principal*.

The routine for the response equation generation is straightforward.

69
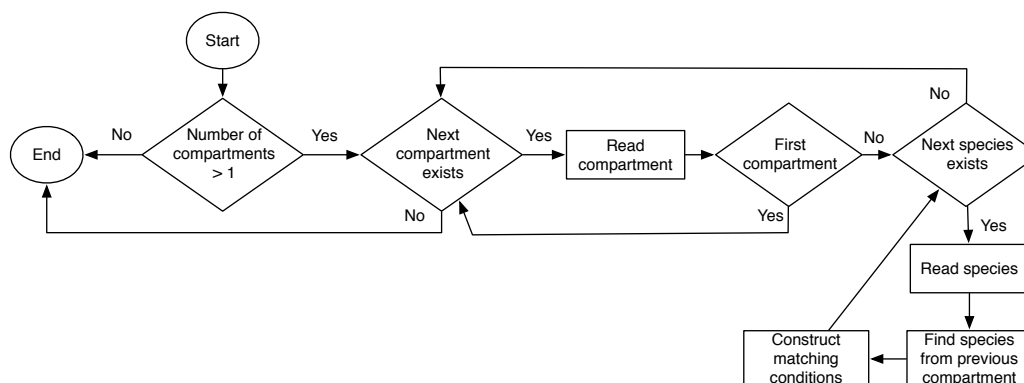
Figure 3.12: Algorithm for the construction of boundary matching conditions.

3.2.3 Graphical user interface

Tedious task of model specification can be mitigated by the handy graphical user interface (GUI). The GUI provides three tabs to enter model description: Model, Species and Reactions tabs. The Species tab provides fields to specify species that take part in the reaction scheme of biosensor. Species have to be defined in every compartment they appear separately. The reactions themselves ought to be entered in the Reactions tab. Complex multi-step reactions must be divided into simple reactions. The biosensor response and simulation parameters are entered in the Model tab. A full list of model parameters is given in Table 3.3.

The developed tool is aimed to do the following:

- Import predefined model in SBML document. The biological model can be defined by any tool that supports SBML and then imported into developed software program for additional specification of biosensor parameters.

- Export SBML model with additional annotations. The resulting document can be later reimported into software program or used with other

Table 3.3: Input fields of graphical user interface. $[L]$ - length, $[T]$ - time and $[n]$ - amount of substance dimensions.

Field name	Description	Unit
Reactions tab		
Reagent 1 - 4	Name of the species that is a reactant in the a reaction	
Product 1 - 4	Name of the species that is a product in the a reaction	
Reaction type	Type of the reaction. Possible values of this attribute are "Chemical" and "Electrochemical"	
Rate constant	Name of the reaction rate constant	
Rate value	Value of the reaction rate constant	$[n]^{-1}[L]^3[T]^{-1}$
Species tab		
Name	Unique name of the species	
Responsive	Checkbox denotes electrochemically active, absorbing or light emitting species	
Enzyme species	Checkbox denotes species that are of enzymatic nature	
Exploatory	Checkbox refers to the substance that is being measured	
Initial conc.	Value of the initial concentration	$[n][L]^{-3}$
Diffusion coef.	Name of the diffusion coefficient	
Diff. coef. value	Value of the diffusion coefficient	$[L]^2[T]^{-1}$
Compartment	Name of the compartment that species belongs to	
Principal species	Name of the same species in the first compartment	
Model tab		
Model name	Name of the model	
Response	Type of the biosensor response. Possible values include "Amperometric biosensor", "Absorbance biosensor" and "Fluorescent biosensor"	
Name	Unique name of the compartment	
Size	Size of the compartment	$[L]$
Number of space step (N)	Number of space steps to be used in numerical simulation	
Scheme	Name of the finite difference scheme to be used for simulation. Possible values include "Explicit" and "Implicit"	
Accuracy	Accuracy of the relative response difference	
Number of time step (M)	Number of time steps to be used in numerical simulation	
Molar ext. coef.	Value of the molar extinction coefficient. This value is used only for optical biosensors	$[L]^2[n]^{-1}$
Intensity of excit. light	Value of the intensity of excitation light. This value is used only for fluorescent biosensors	
Quantum yield	Value of the quantum yield of fluorophore. This value is used only for fluorescent biosensors	
Number of electrons	Number of electrons involved in the electrochemical reaction. This value is used only for amperometric biosensors	
Surface of electrode	Geometrical surface of the electrode	$[L]^2$

SBML tools.

- Generate LATEX document containing a full description of mathematical model. This mathematical model is presented in terms of governing reaction - diffusion equations, initial and boundary conditions.

- Generate representation of numerical solution of the mathematical model by finite difference explicit and implicit schemes in LATEX.

- Generate computer model code in JAVA. The numerical solution of the mathematical model is represented in output file *model.java*. A hosting application *starter.java* to run a simulation is also generated. These files can be compiled in a Java IDE or from command line to create class files that can then be run using the Java virtual Machine (JVM). To create the class files from command line use:

```
javac starter.java model.java
```

The following command will then run the simulation:

```
java starter
```

3.2.4   Software architecture

The software program is based on factory pattern to handle various results (SBML, LATEXdocuments and Java code) generation (see Fig. 3.13). In enables system to handle new products in a generic manner.

The software program is written in Java, an object-oriented language [27, 105]. It uses SWING library to implement the Graphical User Interface (GUI) and libSBML library to manipulate SBML documents [29]. The tool can be deployed on all platforms that support Java.
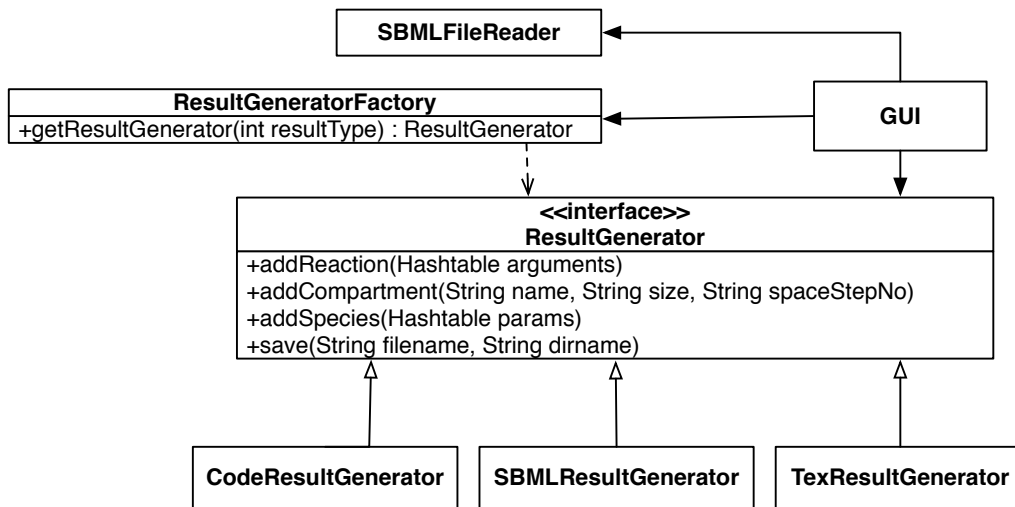
Figure 3.13: Class diagram of the system.

3.3 Conclusions

In this chapter, several finite difference schemes were applied for modeling an amperometric biosensor. Using all the considered schemes quite satisfactory results were obtained when sufficient number of steps of the discrete grid is employed.

The best accuracy is achieved using implicit calculation and Hopscotch approaches. For the problems where accuracy is not a significant factor but the speed is, the simplest explicit scheme should be used.

General-purpose solvers of Maple and MATLAB are less precise to simulate the biosensor action and need more computation time. Those solvers can be applied for basic problems while taking advantage of the simplicity.

An additional advanced investigation of the accuracy of the finite difference computational schemes were presented in the recent publication [2A]. The finite difference equations were solved explicitly taking into account the nonlin-

earities. The results of this research indicated that linearisation of the nonlinear chemical term reduces both the accuracy and, in the case of the second-order methods such as Crank-Nicolson, reduces the global order.

The deterministic nature of model construction allows to automate this process. The multi-step biosensors can be encoded in existing SBML elements, supplementing additional information in form of SBML annotations. The proposed algorithm enables model description to be converted into mathematical and numerical models in terms of reaction - diffusion equations, initial and boundary conditions. The process of biosensor modeling can be greatly facilitated by graphical user interface.

The results of this chapter are the subject of three articles published ([2A, 5A, 11A]).

Chapter 4

Computational Modeling of Multi-step Biosensors

The computer simulation enables to investigate the influence of the physical and kinetic parameters on the biosensor response. This chapter presents a results of the computational modeling of the multi-step biosensors: peroxidase-based optical and laccase-based synergetic biosensors. These investigations indicated applicability of our approach for the complex biosensors. A detail modeling at transition and steady state conditions revealed the dependence of the biosensor response on the different parameters. Moreover, the results of the research can be also applied for the creation of the new biosensors as well as for the control of the action of the functional biosensors.

4.1 Computational Modeling of Peroxidase-based Optical Biosensor

4.1.1 Digital simulation

Because of non-linearity of the problem, no analytical solutions are possible [4, 32]. Hence numerical simulation is employed. We applied a uniform discrete grid to simulate the biosensor using implicit finite difference method [9, 15, 120].

We assume the biosensor response A_R calculated at the moment T_R as the steady state response,

$$A_R = A(T_R) \approx A_\infty, \quad T_R = \min_{j>0, \, A_j>0} \left\{ \tau j : \frac{A_j - A_{j-1}}{A_j \tau} < \varepsilon \right\}, \qquad (4.1)$$

where τ stands for the size of time step. We used $\varepsilon = 10^{-3}$ for the calculations. The response time T_R as an approximate steady state time is highly sensitive to the decay rate ε, i.e. $T_R \to \infty$ when $\varepsilon \to 0$. We introduce less sensitive part of the steady state time function $A^*(t)$,

$$A^*(t) = \frac{A_R - A(t)}{A_R}, \quad A^*(0) = 1, \quad A^*(T_R) = 0, \quad 0 \leq A^*(t) \leq 1. \qquad (4.2)$$

$T_{0.5}$ is defined as the time at which a half of the steady state absorbance is reached, i.e., $A^*(T_{0.5}) = 0.5$. $T_{0.5}$ is usually called the half time of the steady state.

The following values of the model parameters were employed in all the numer-

ical experiments:

$$D_{Se} = D_{Pe} = D_{He} = 300\mu\text{m}^2\text{s}^{-1}, \quad D_{Sb} = D_{Pb} = D_{Hb} = 600\mu\text{m}^2\text{s}^{-1},$$
$$k_1 = 7.1 \times 10^6 \text{s}^{-1}\text{M}^{-1}, \quad k_2 = 2 \times 10^7 \text{s}^{-1}\text{M}^{-1}, \quad \varepsilon_P = 10^3 \text{m}^2\text{mol}^{-1}. \tag{4.3}$$

The following constant-concentration conditions can be derived from equations (2.3)-(2.14):

$$E(x,t) + C(x,t) = E_0, \quad 0 \leq x \leq d, \quad t > 0, \tag{4.4}$$

$$S_e(x,t) + P_e(x,t) = S_0, \quad 0 \leq x \leq d, \quad t \to \infty,$$
$$S_b(x,t) + P_b(x,t) = S_0, \quad d \leq x \leq d+\delta, \quad t \to \infty, \tag{4.5}$$

$$H_e(x,t) + P_e(x,t) = H_0, \quad 0 \leq x \leq d, \quad t \to \infty,$$
$$H_b(x,t) + P_b(x,t) = H_0, \quad d \leq x \leq d+\delta, \quad t \to \infty. \tag{4.6}$$

These conditions were employed in testing the numerical solution of the model.

We define the steady state fluorescence F_R of the biosensor as the fluorescence intensity calculated at the time T_R,

$$F_R = F(T_R) \approx F_\infty,$$
$$T_R = \min_{j>0,\,F_j>0} \left\{ \tau_j : \frac{F_j - F_{j-1}}{F_j \tau} < \varepsilon \right\}, \tag{4.7}$$

where τ is the size of time step. We used $\varepsilon = 10^{-5}$ for the calculations.

Unless otherwise stated, the model used the following values of the paramet-

ers:

$$D_S = D_P = D_H = 300 \ \mu\text{m}^2\text{s}^{-1},$$

$$k_1 = 7.1 \times 10^6 \ \text{s}^{-1}\text{M}^{-1}, \ k_2 = 2 \times 10^7 \ \text{s}^{-1}\text{M}^{-1},$$

$$\varepsilon_P = 10^3 \ \text{m}^2\text{mol}^{-1}, \ \varphi = 0.01, \ d = 1 \ \mu\text{m}. \tag{4.8}$$

Figure 4.1: The *Reactions* tab describing reactions of peroxidase-based optical biosensor.

Figure 4.2: The *Species* tab describing species of peroxidase-based optical biosensor.

The computer simulation was performed using the new software program presented in Chapter 3. The user interface of this tool is divided into three screens: Reactions tab (Fig. 4.1), Species tab (Fig. 4.2) and the Model tab (Fig. 4.3). The Reactions (Fig. 4.1) tab contains reaction scheme of the peroxidase-based optical biosensor (2.1, 2.2). All the chemical species that participate in the reactions are listed in the Species tab (Fig. 4.2) as well as their properties. Other model parameters are inputed in the Model tab (Fig. 4.3). In case of fluorescent biosensor the program input is very similar. What differs though is the
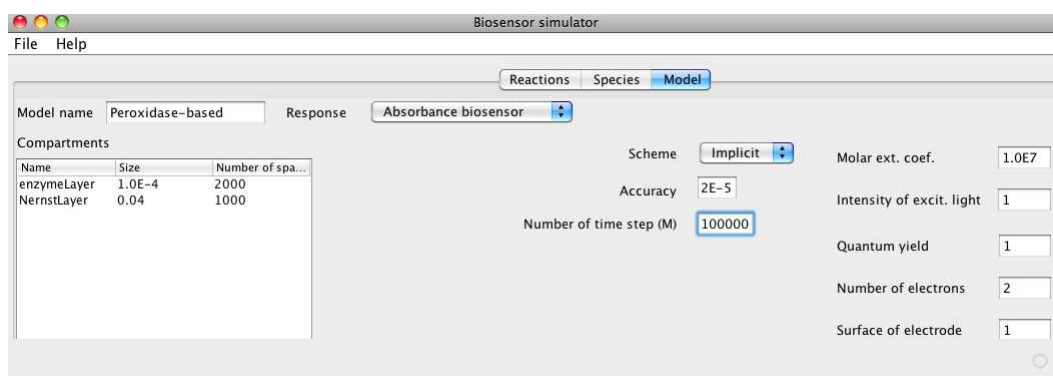
Figure 4.3: The *Model* tab describing model parameters of peroxidase-based optical biosensor.

response type and the response parameters in the Model tab. This example demonstrates intuitive user interface of the developed program.

4.1.2 Results and discussion: Absorbance biosensor

By changing input parameters the output results were numerically analyzed with special emphasis to the influence of the biosensor geometry and of the catalytical parameters on the biosensor response at transition and steady state conditions.

The dynamics of the concentrations of the compounds

Figs. 4.4 and 4.5 show the concentration profiles of substrate, product, hydrogen peroxide, compound I and enzyme peroxidase in the enzyme and diffusion layers. These concentration profiles were obtained when the steady state and the half of it was reached.

As one can see in Figs. 4.4 and 4.5, constraints (4.6) on the concentrations are ensured. When the biosensor operation starts, the initial ($t = 0$) concentration
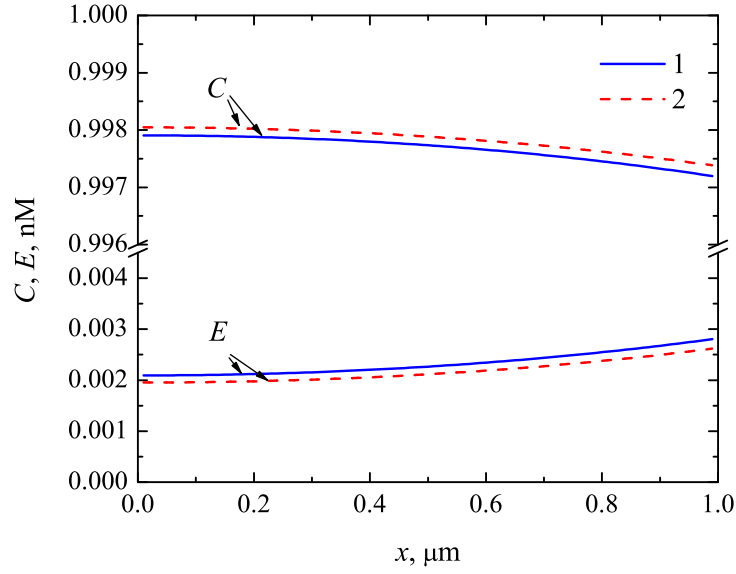
Figure 4.4: The steady state ($T_R = 305\,\text{s}$, 1) and the half of it ($T_{0.5} = 116\,\text{s}$, 2) concentration profiles of compound I (C) and peroxidase (E) in the enzyme layer ($d = 1\mu\text{m}$) at $S_0 = 100\,\mu\text{M}$, $E_0 = 1\,\text{nM}$, $H_0 = 1\,\text{mM}$, $\delta = 400\,\mu\text{m}$.
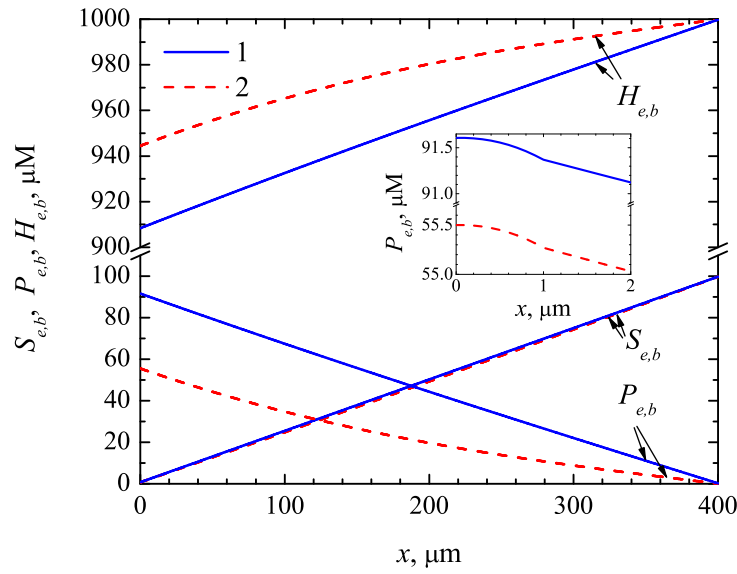

Figure 4.5: The concentration profiles of the substrate ($S_{e,b}$), product ($P_{e,b}$) and hydrogen peroxide ($H_{e,b}$) in the enzyme layer and diffusion layers. The parameters and notation are the same as in Fig. 4.4.

of the enzyme (E) equals E_0 and the compound I (C) starts at zero concentration. Fig. 4.4 shows, that the final (at steady state conditions) concentration E

80

of the enzyme is less than 0.3% of the initial concentration E_0 while the concentration C of the compound I is equal approximately to the initial concentration E_0 of the enzyme. These concentrations quickly become invariable. The dynamics of the substrate concentration is also quit fast. The final (steady state) concentrations of these three compounds differ only slightly from the concentrations obtained at the half time of the steady state. The concentrations of the hydrogen peroxide (H_e, H_b) and of the product (P_e, P_b) change notably slower.

Although the dependence of the product concentration is linear as seen in Fig. 4.5, the linear dependence is not followed in the enzyme layer (1 μm). This is highlighted in the inset of Fig. 4.5. The non-linear dependence could be explained by the enzymatic reaction occurring in the enzyme layer.

The dynamics of the concentrations of the compounds is also presented in Figs. 4.6 and 4.7. Fig. 4.6 shows the concentrations averaged through the enzyme layer while Fig. 4.7 shows the concentrations averaged through both compartments, the enzyme layer and the diffusion layer. The thickness d of the enzyme layer equals 1 μm. The thickness δ of the external diffusion layer is in two orders of magnitude higher, $\delta = 400\mu$m = 400d. After a certain time the equilibrium approaches and the concentrations become invariable.

During the biosensor action the substrate diffuses into the enzyme layer and this results in a decrease of the enzyme as well as of the hydrogen peroxide and in an increase of the compound I as well as of the product concentrations. The inset in Fig. 4.6 shows very high concentration dynamics of the enzyme ($\bar{E}$) as well as of the compound I ($\bar{C}$) in the beginning of the reacting process. In about 1 ms these concentrations become approximately constant. The concentration dynamics of all other compounds is significantly lower.

Figs. 4.8 and 4.9 present the averaged concentrations for tenfold thinner enzyme layer ($d = 0.1\mu$m). One can observe similar concentration evolution as

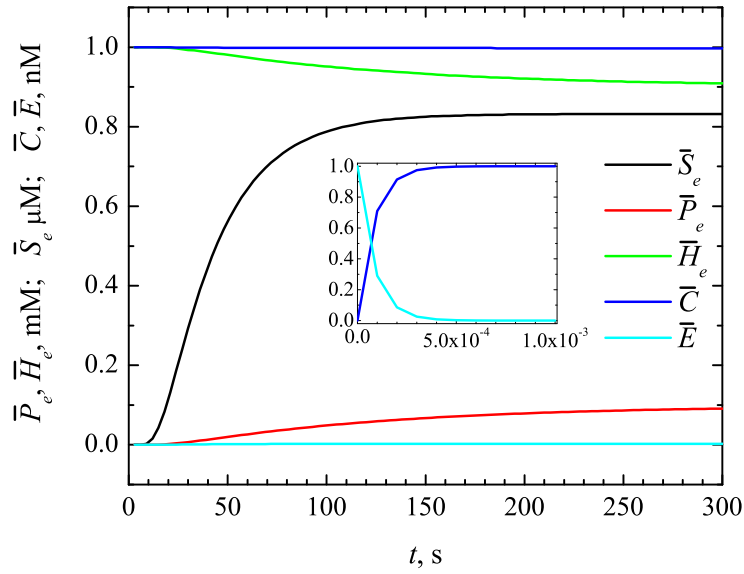Figure 4.6: The concentrations of the substrate ($\bar{S}_e$), product ($\bar{P}_e$), hydrogen peroxide ($\bar{H}_e$), compound I ($\bar{C}$) and enzyme ($\bar{E}$) averaged through the enzyme layer ($d = 1\mu$m). The parameters are the same as in Fig. 4.4.

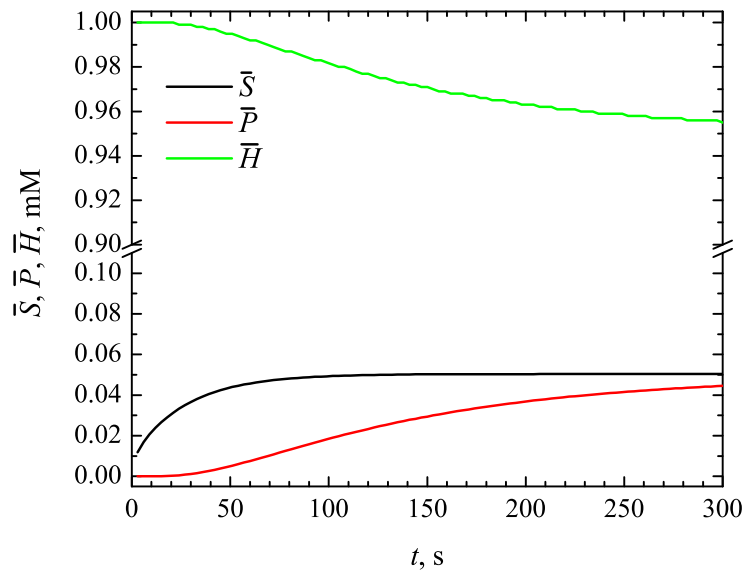Figure 4.7: The concentrations of the substrate ($\bar{S}$), product ($\bar{P}$) and hydrogen peroxide ($\bar{H}$) averaged through the enzyme and diffusion layers. The parameters are the same as in Fig. 4.4.

in the previous case, with some differences from a quantitative point of view. The shortage of compound I results to larger amounts of unreacted hydrogen
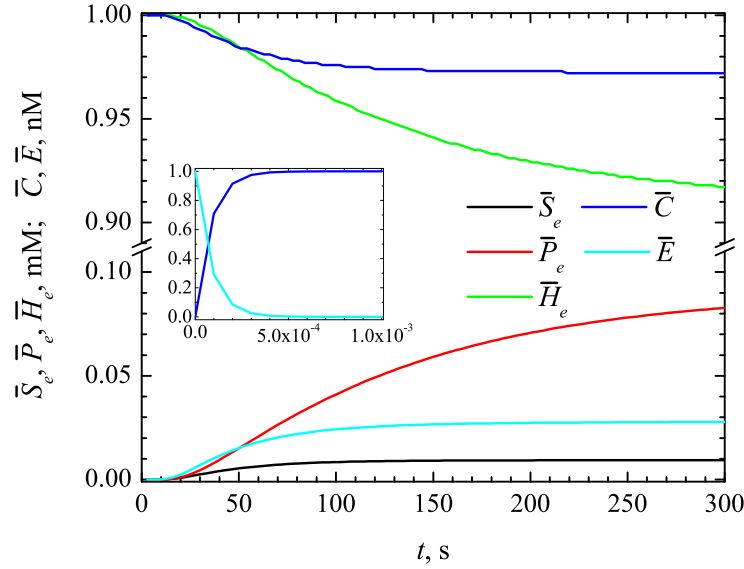
peroxide and substrate.

Figure 4.8: The concentrations of substrate ($\bar{S}_e$), product ($\bar{P}_e$), hydrogen peroxide ($\bar{H}_e$), compound I ($\bar{C}$) and enzyme ($\bar{E}$) averaged through the enzyme layer of the thickness $d = 0.1\mu$m. Other parameters are the same as in Fig. 4.4.

Fig. 4.8 also shows non-monotony of $\bar{E}$ and $\bar{C}$ as functions of time t. The inset in Fig. 4.8 shows very fast reduction of the enzyme ($\bar{E}$) and so fast growth of the compound I ($\bar{C}$). In about 0.5 ms practically whole enzyme peroxidase converts to compound I. In about 10 s some substrate reaches the enzyme layer and the reaction (2.2) starts. Because of this, the enzyme ($\bar{E}$) is regenerated from the compound I ($\bar{C}$). Fig. 4.8 expressly shows that biosensor action starts very quickly with the reaction (2.1) while the reaction (2.2) starts with notable delay. Certainly, the delay term depends on the thickness δ of the external diffusion layer.

The impact of the thickness of the diffusion layer

The dependence of the absorbance on the thickness of the diffusion layer is shown in the Fig. 4.10. The Biot number Bi was calculated assuming a constant
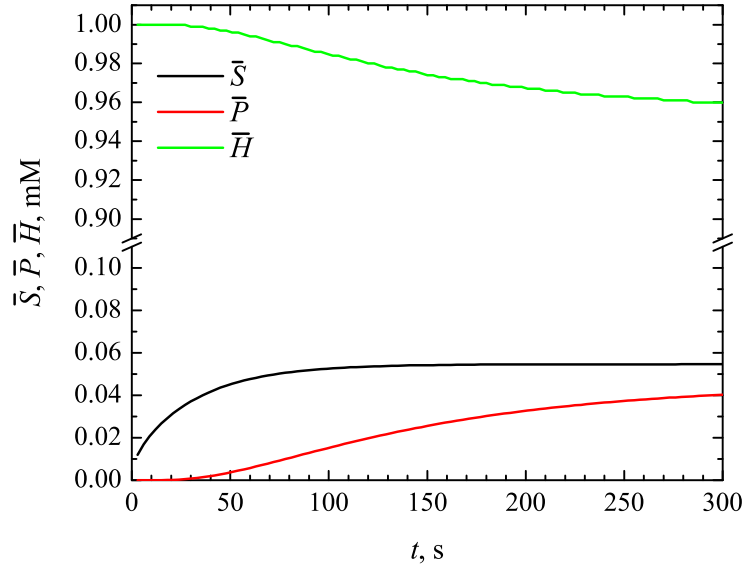
Figure 4.9: The concentrations of substrate ($\bar{S}$), product ($\bar{P}$) and hydrogen peroxide ($\bar{H}$) averaged through the enzyme and diffusion layers at the thickness $d = 0.1\mu$m of the enzyme layer. Other parameters are the same as in Fig. 4.4.

thickness of the enzyme layer. The absorbance increases with an increase in the substrate concentration. The absorbance strongly depends on the outer concentration S_0 of the substrate whereas the effect of other parameters is notably less important. In cases of a thick diffusion layer ($Bi <\approx 0.02$ or $\delta >\approx 100\mu$m) only the substrate concentration effects the absorbance. The concentration of the product (which absorbs light) directly depends on the concentration of the substrate, thus the absorbance changes in relation to the concentration of the substrate.

The approximately linear decrease of the steady state absorbance A_R with the Biot number Bi can be explained by a linear distancing the border ($x = d + \delta$) where the product concentration is permanently reduced to zero (see the boundary condition (2.12)). Consequently, the exact evaluation of the thickness of the external (Nernst) diffusion layer is of crucial importance to predict the biosensor response accurately.
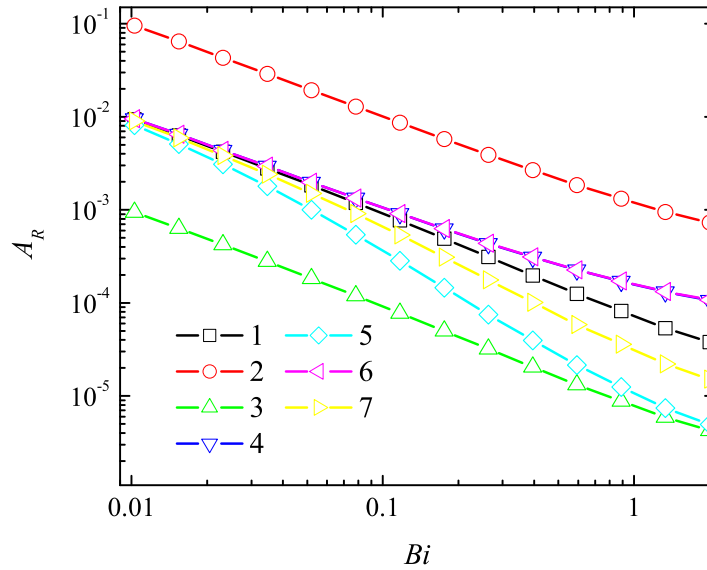
Figure 4.10: Dependence of the absorbance A_R on the Biot number Bi at a constant thickness $d = 1\mu m$ of the enzyme layer, three substrate concentrations S_0: 10 (3), 100 (1, 4, 5, 6, 7), 1000 (2) μM, three initial concentrations of the enzyme E_0: 0.1 (5), 1 (1, 2, 3, 6, 7), 10 (4) nM and three initial concentrations of the hydrogen peroxide H_0: 0.1 (7), 1 (1, 2, 3, 4, 5), 10 (6) mM.

As one can see in Fig. 4.10, the gradient of the steady state absorbance A_R as a function of the Biot number Bi is notably higher at lower initial concentrations of the enzyme (E_0, curve 5) as well as of the hydrogen peroxide (H_0, curve 7) rather than at higher ones (corresponding curves 4 and 6). Thus, the absorbance is less sensitive to changes in the thickness δ of the external diffusion layer (which is reversally proportional to the Biot number Bi) at higher values of E_0 and H_0 than at lower ones.

The response time increases with thickening the diffusion layer due to the time delay needed for substrate to appear in the enzyme layer (Fig. 4.11). A tenfold increase in the thickness δ increases the response time approximately hundredfold. All other considered parameters affect the biosensor response time slightly. The half time $T_{0.5}$ of the steady state response is approximately a linear function of the Biot number Bi as well as of the thickness δ of the diffusion

layer. Slight variations in the linear behaviour of $T_{0.5}$ can be explained by a non-linearity of the reaction process in the enzyme layer (see the inset in Fig. 4.5).
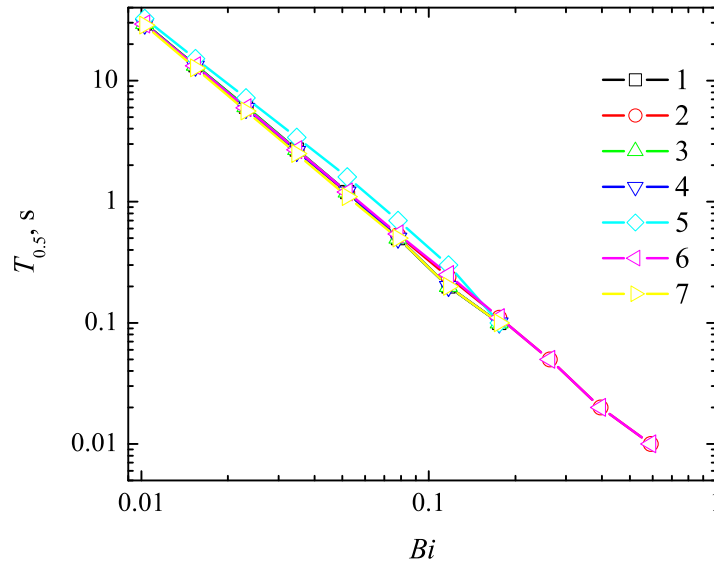

Figure 4.11: Dependence of the half time $T_{0.5}$ of the steady state response on the Biot number Bi at a constant thickness $d = 1\mu m$ of the enzyme layer. The parameters and notation are the same as in Fig. 4.10.

Observed values of the biosensor sensitivity are fairly high except two cases (see Fig. 4.12). At high outer substrate concentration S_0 the enzyme becomes saturated and cannot respond effectively to the change of the substrate concentration (see curve 2). Very similar results were obtained at low concentration H_0 of the hydrogen peroxide (curve 7). The decrease in the initial enzyme concentration E_0 (curve 5) also determines a decrease in the sensitivity of the biosensor response. However, in all the cases increase in the thickness of the diffusion layer (i.e. decrease of the Biot number) positively effects the biosensor sensitivity.

A relatively short linear range of the calibration curve is one of serious drawbacks restricting wider use of the biosensor [124, 139, 152]. This problem can be partially solved by an application of an additional inert outer membrane
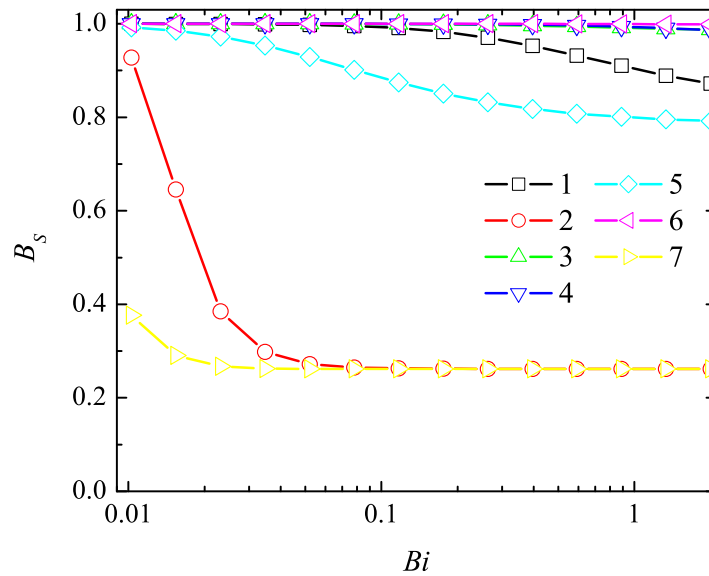
Figure 4.12: Dependence of dimensionless sensitivity B_S on the Biot number Bi at a constant thickness $d = 1\mu m$ of the enzyme layer. Calculation parameters and notation are the same as in Fig. 4.10.

on the surface of the enzyme layer [124, 139, 152]. In the case of optical biosensors, outer membranes are of limited applicability [30, 37]. Therefore, an opportunity to increase the biosensor sensitivity as well as the linear range of the calibration curve by increasing the thickness of the external diffusion layer is especially important.

The impact of the thickness of the enzyme layer

The effect of enzyme layer thickness on the absorption, response time and sensitivity was analyzed. In this test problem the Biot number was calculated assuming a constant thickness of the diffusion layer.

In general, the importance of the enzyme layer (membrane) thickness to the biosensor response is rather well known [8, 16, 41, 79, 95, 124, 139]. Usually, the effect of the enzyme layer thickness decreases with an increase in the layer

thickness. Fig. 4.13 shows that in the case of the peroxidase-based optical biosensor, the enzyme layer thickness d effects the absorbance A_R slightly only. This can be explained by relatively thick external diffusion layer [8, 95]. The analyzed thickness δ of the external diffusion layer was in several orders of magnitude greater than the enzyme layer thickness d. The biosensor response is highly stable to changes in the enzyme layer thickness when the Biot number Bi varies from 0.02 to 0.2 (the thickness d varies from 0.01δ up to 0.1δ). The high stability of the biosensor response to changes in the enzyme layer thickness is a useful characteristic for the biosensor developers [30, 37].

In addition, Fig. 4.13 shows that the absorbance strongly depends on the bulk concentration S_0 of the substrate. Below this property is discussed in detail.

Figure 4.13: Dependence of the absorbance A_R on the Biot number Bi at a constant thickness $\delta = 100\,\mu\mathrm{m}$ of the diffusion layer. Other parameters and notation are the same as in Fig. 4.10.

Fig. 4.14 shows the effect of the Biot number, which is directly proportional to the enzyme layer thickness d, on the half time $T_{0.5}$ of the steady state response of the optical biosensor. In most cases the half time $T_{0.5}$ is a non-monotonous

function of the thickness d. This is especially notable in the case of low concentration of enzyme compared to the concentrations of substrate and hydrogen peroxide (curve 5). The behaviour of the half time $T_{0.5}$ when changing the enzyme layer thickness d at high substrate concentration S_0 as compared to the concentrations of enzyme and hydrogen peroxide (curve 2) is very similar to that at low (see the parameters in Fig. 4.10) concentration H_0 of the hydrogen peroxide (curve 7). Only in both these cases (curves 2 and 7) the half time $T_{0.5}$ is a monotonous function of d. However, in all the cases when the enzyme layer is relatively thick ($Bi >\approx 0.2$ or $d >\approx 10\,\mu\mathrm{m}$) $T_{0.5}$ is a monotonous increasing function of d at all values of the parameters.
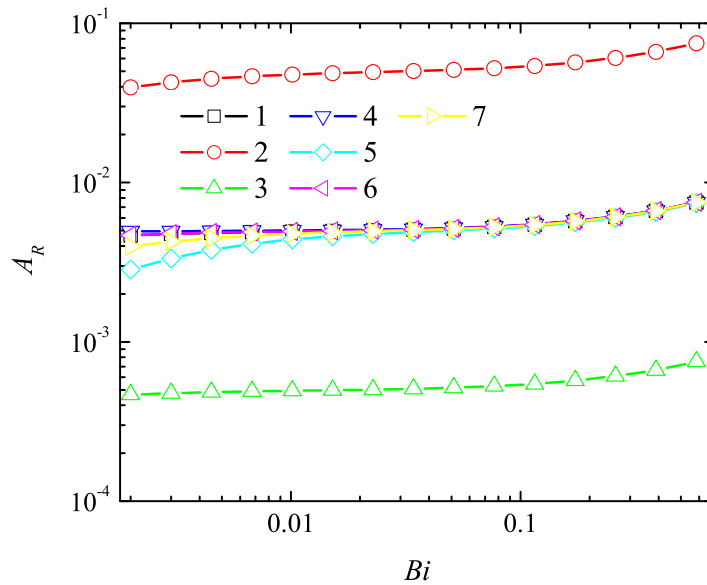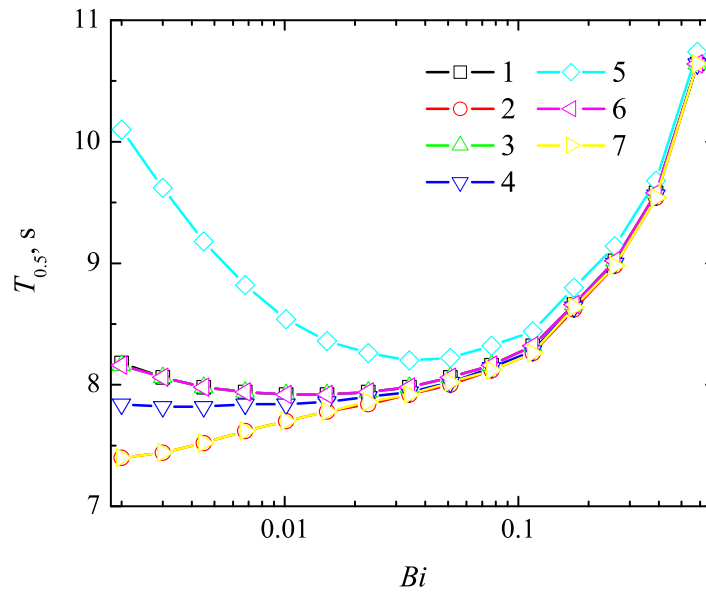

Figure 4.14: Dependence of the response time on the Biot number Bi at a constant thickness $\delta = 100\,\mu\mathrm{m}$ of the diffusion layer. Other parameters and notation are the same as in Fig. 4.10.

The effect of the Biot number Bi on the biosensor sensitivity B_S is depicted Fig. 4.15. The effect of the layer thickness is rather similar to that of the external diffusion layer. The sensitivity of the biosensor increases extending the enzyme layer (Fig. 4.15). The observed values of the sensitivity are very high except two cases (curves 2 and 7). The sensitivity is notable lower at a high

concentration S_0 of the substrate (curve 2) and at a low concentration H_0 of the hydrogen peroxide (curve 7) as compared to the values of other concentrations. In both these cases the biosensor sensitivity B_S is rather sensitive to changes in the enzyme layer thickness d. At a high concentration S_0 as well as at a low concentration H_0 (see the parameters in Fig. 4.10) the biosensor sensitivity B_S can be notably increased by increasing the thickness d of the enzyme layer.
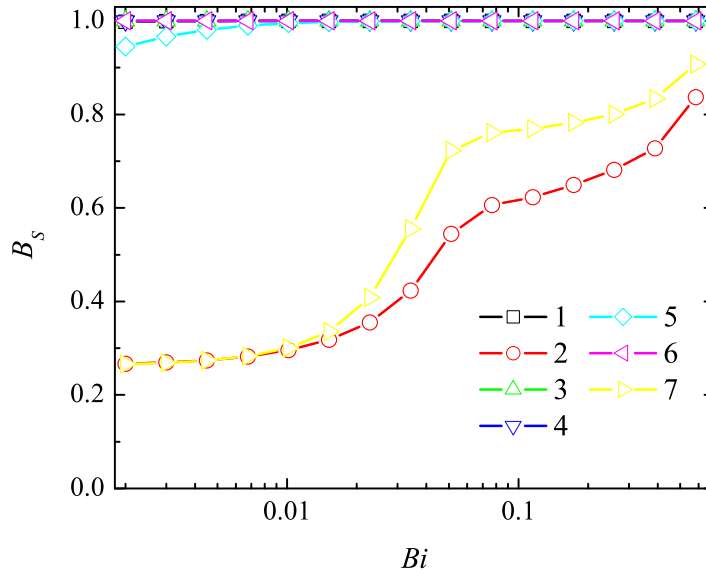
Figure 4.15: Dependence of the dimensionless sensitivity B_S on the Biot number Bi at a constant thickness $\delta = 100\,\mu\mathrm{m}$ of the diffusion layer. Other parameters and notation are the same as in Fig. 4.10.

The impact of the outer substrate concentration

In this test problem the outer substrate concentration is expressed as the ratio of the substrate and hydrogen peroxide concentrations combining with the rates of the corresponding reactions (1) and (2)

$$\Sigma = \frac{k_2 S_0}{k_1 H_0}. \tag{4.9}$$

The dependence of the absorbance and sensitivity of the biosensor on the dimensionless ratio Σ of the reactions (2) and (1) is depicted in the Figs. 4.16 and 4.17, respectively.

Figure 4.16: Dependence of the absorbance A_R on the dimensionless ratio Σ of the reactions (2) and (1) changing the substrate concentration S_0 at three initial concentrations H_0 of the hydrogen peroxide: 0.1 (5), 1 (1, 2, 3), 10 (4) mM and three initial concentrations E_0 of the enzyme: 0.1 (3), 1 (1, 4, 5), 10 (2) nM; $d = 1\mu$m, $\delta = 400\mu$m.

One can see in Fig. 4.16 a linear range of the calibration curve up to $\Sigma \approx 5 \times 10^3$ ($S_0 \approx 200\,\mu M$). The dependence of the absorbance A_R on the ratio Σ is noticeably affected by the hydrogen peroxide (H_0). The absorbance is directly proportional to the concentration H_0 of the hydrogen peroxide. A tenfold increase in the concentration H_0 increases the absorbance approximately tenfold (curve 4). The corresponding decrease in H_0 decreases the A_R tenfold (curve 5). A variation in the initial concentration E_0 of enzyme effects the absorbance slightly (curves 2 and 3).

Fig. 4.17 shows, that the biosensor sensitivity notably decreases with a decrease in the concentrations E_0 on the enzyme (curve 3). The concentrations
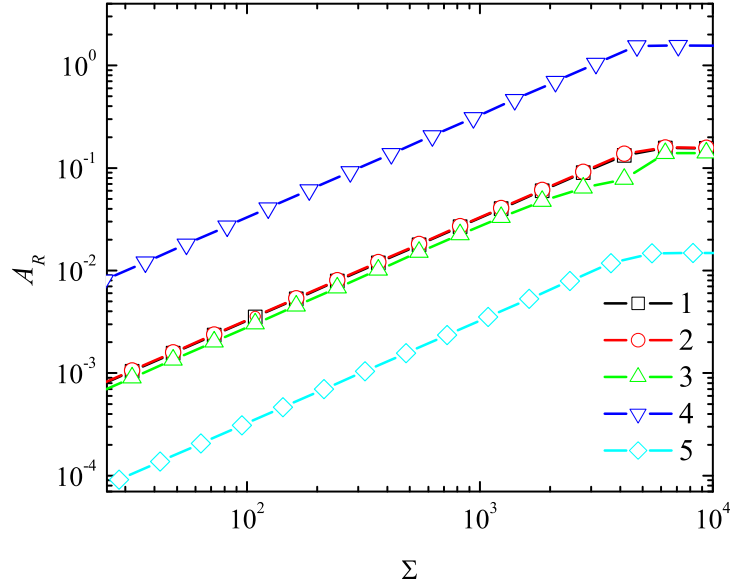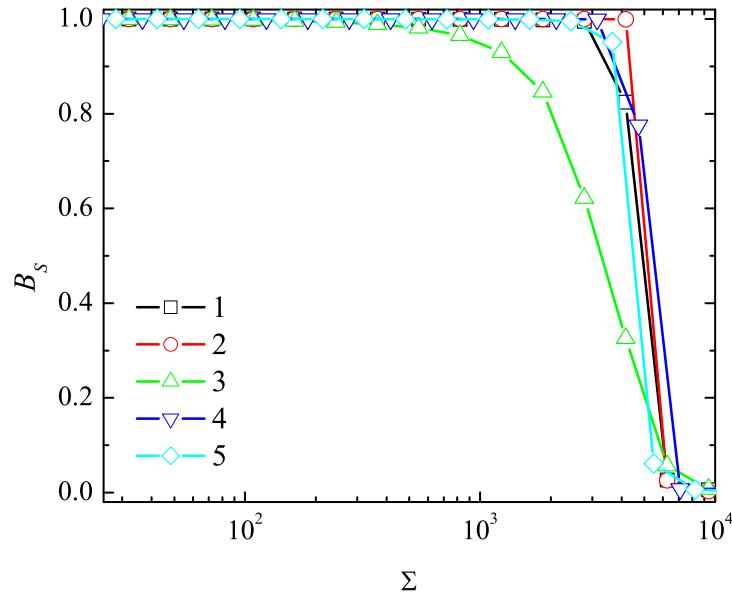
Figure 4.17: Dependence of the dimensionless sensitivity B_S on the dimensionless ratio Σ of the reactions (2) and (1). The parameters and notation are the same as in Fig. 4.16.

of the enzyme and of the hydrogen peroxide determine the concentration of the compound I (reaction (2.1)), which interacts with the substrate to form the product (reaction (2.2)). A decrease in enzyme concentration E_0 decreases the rate of product formation, while an increase in substrate concentration S_0 increases the reaction rate up to saturation [124, 139]. A lower concentration E_0 of the enzyme corresponds to a lower substrate concentration S_0 at which the enzyme is saturated with the substrate. Fig. 4.17 show this effect as a decreasing sensitivity of the biosensor with a decrease in the enzyme concentration E_0.

4.1.3 Results and discussion: Fluorescent biosensor

Distributions of the concentrations of substrate, product, hydrogen peroxide, compound I and enzyme peroxidase in time and space were given in previous section. By changing input parameters we analyze the behavior of the bio-

sensor response and sensitivity.

The Effect of the Thickness of the Enzyme Layer

The effect of the thickness of the enzyme layer on the response of amperometric as well as potentiometric biosensors has been studied recently [8, 16, 124, 139]. Fig. 4.18 shows the dependence of the dimensionless steady state fluorescence F_R on the thickness of enzyme membrane.

In the case of fluorescent biosensors, thickening the enzyme membrane causes the increase of the product concentration and therefore light is emitted to a greater extent. The response of the biosensor mostly depends on the outer concentration S_0 of the substrate (see curves 2 and 3 in Fig. 4.18). When the enzyme layer is relatively thick ($d > 1\mu$m), the used variations of enzyme and hydrogen peroxide have similar effect on the fluorescence (see curves 1, 4, 5, 6 and 7). This can be explained by production of the same amount of the compound I, limited by the equation (2.1).

The effect of the enzyme layer thickness on the biosensor dimensionless sensitivity B_S is shown in Fig. 4.19. The sensitivity of the biosensor increases extending the enzyme layer. With exception of curves 2 and 7, the high values of sensitivity ($B_S > 0.8$) are observed within specified interval. At higher outer substrate concentration S_0 the enzyme becomes saturated and cannot respond effectively to the change of the substrate concentration (curve 2). The almost similar results were obtained at lower concentration of hydrogen peroxide H_0 (curve 7). The sensitivity is significantly reduced because of the lower concentration of the formed compound I in comparison with the concentration of the substrate. In both cases, the sensitivity B_S of the biosensor can be greatly enhanced by increasing the thickness of the enzyme layer.
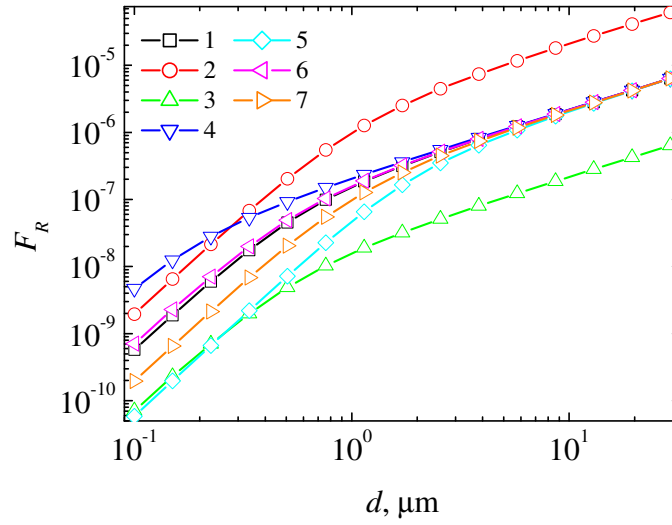
Figure 4.18: Dependence of the dimensionless steady state fluorescence F_R on the thickness d of the enzyme membrane at three substrate concentrations S_0: 10 (3), 100 (1, 4, 5, 6, 7), 1000 (2) μM, three enzyme concentrations E_0: 0.1 (5), 1 (1, 2, 3, 6, 7), 10 (4) nM and three hydrogen peroxide concentrations H_0: 0.1 (7), 1 (1, 2, 3, 4, 5), 10 (6) mM

The Effect of the Outer Substrate Concentration

The effect of outer substrate concentration S_0 on the dimensionless steady state fluorescence F_R is depicted in Fig. 4.20. The approximately linear curves of the fluorescence F_R increase asymptotically approaching the steady states. A variation in the initial concentration E_0 of the enzyme affects the fluorescence, but has no effect on the limit of linearity of the calibration curve (see curves 2 and 3). However, the initial concentration H_0 of hydrogen peroxide have an effect upon the dynamic range of the calibration curves (curves 4 and 5). An increase of the concentration H_0 expands the limit of linearity and wise versa.

The dimensionless sensitivity B_S is markedly reduced as the concentration of the substrate S_0 increases (see Fig. 4.21). The change of the initial enzyme concentration E_0 has slight effect on the biosensor sensitivity (curves 2 and 3). However, the lower concentration of enzyme (curve 3) causes an unacceptable

94
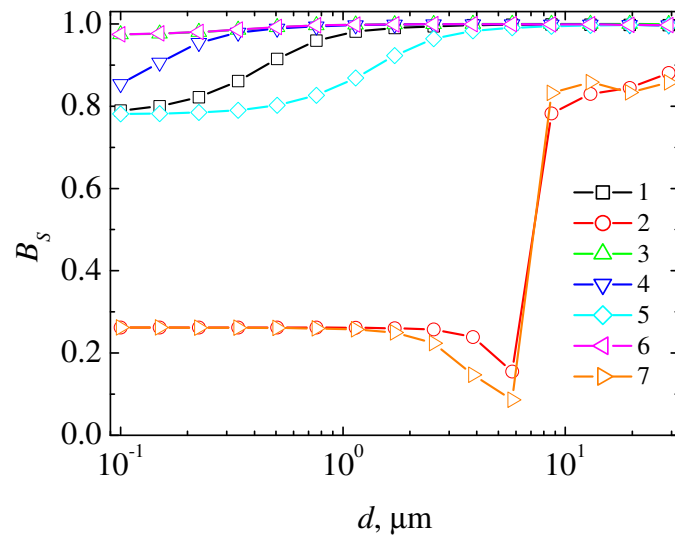
Figure 4.19: Dependence of the dimensionless sensitivity B_S on the thickness d of the enzyme membrane. The parameters and notation are the same as in Fig. 4.18
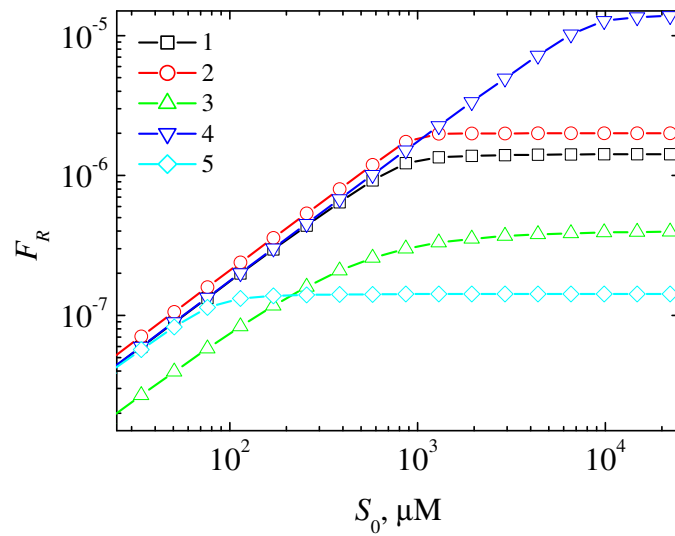
Figure 4.20: Dependence of the dimensionless steady state fluorescence F_R on the substrate concentration in the bulk solution S_0 at three concentrations E_0 of the enzyme: 0.1 (3), 1 (1, 4, 5), 10 (2) nM and three concentrations H_0 of the hydrogen peroxide: 0.1 (5), 1 (1, 2, 3), 10 (4) mM

sensitivity at $S_0 \approx> 1.1 \times 10^2 \mu$M. The high values of the sensitivity up to $S_0 \approx 10^4 \mu$M can be observed with the increased initial concentration H_0 of hydrogen peroxide (curve 4).
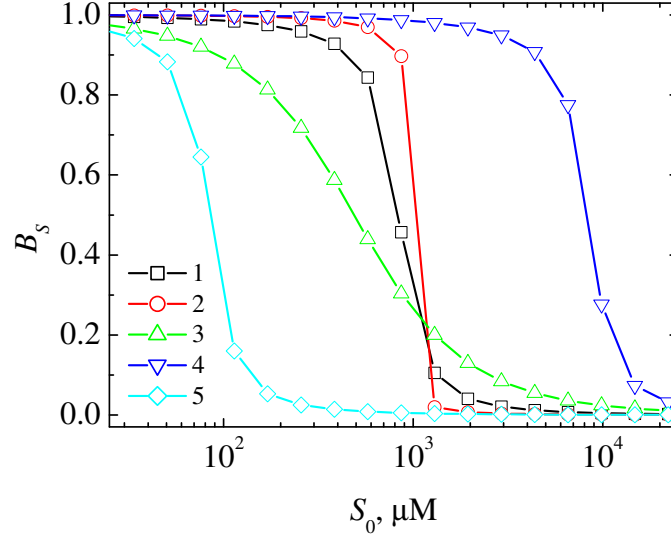
Figure 4.21: Dependence of the dimensionless sensitivity B_S on the substrate concentration S_0 in the bulk solution. The parameters and notation are the same as in Fig. 4.20

4.2 Computational Modeling of Laccase-based Synergetic Biosensor

4.2.1 Digital simulation

In our computational modeling we assume the biosensor response I_R calculated at the moment T_R as the steady state response,

$$I_R = I(T_R) \approx I_\infty, \quad T_R = \min_{j>0, I_j>0} \left\{ \tau_j : \frac{I_j - I_{j-1}}{I_j} < \varepsilon \right\}, \quad \tau_j = \tau j, \qquad (4.10)$$

96

where τ stands for the size of time step, $I_j = I(\tau_j)$. We used $\varepsilon = 10^{-3}$ for the calculations.

The values and references of the model parameters employed in the numerical experiments are summarized in Table 4.1.

Table 4.1: Simulation parameters.

Parameter	Value	Reference
a_1	100μm	[83]
a_2	18.7μm	[83]
a_3	64.2μm	[81]
k_1	2.44μM^{-1}s^{-1}	[136]
k_2	0.26μM^{-1}s^{-1}	[83]
k_3	18μM^{-1}s^{-1}	[83]
k_4	330μM^{-1}s^{-1}	[85]
E_0	2.76μM	[83]
$S_{1,0}$	28μM	[83]
$S_{2,0}$	11μM	[83]
O_0	253μM	[83]
$D_{S_{1,1}}, D_{S_{2,1}}, D_{P_{1,1}}, D_{P_{2,1}}$	3.2×10^{-10}m^{2}s^{-1}	[59]
$D_{S_{1,2}}, D_{S_{2,2}}, D_{P_{1,2}}, D_{P_{2,2}}$	5.6×10^{-11}m^{2}s^{-1}	[59]
$D_{S_{1,3}}, D_{S_{2,3}}, D_{P_{1,3}}, D_{P_{2,3}}$	6.3×10^{-10}m^{2}s^{-1}	[59]
D_{O_1}	2.01×10^{-9}m^{2}s^{-1}	[25]
D_{O_2}	2.01×10^{-9}m^{2}s^{-1}	[25]
D_{O_3}	2.01×10^{-9}m^{2}s^{-1}	[25]
$D_{E_{red,1}}, D_{E_{ox,1}}$	3.6×10^{-11}m^{2}s^{-1}	[130]
n_e	1	[83]
A	7×10^{-6}m^2	[83]

Similarly to peroxidase-based optical biosensor (section 4.1), the computer simulation was performed using the developed software program (see Chapter 3).

4.2.2 Results and discussion

The behaviour of the laccase-based biosensor response was investigated by using computer simulation. By changing input parameters the biosensor action

was analysed with a special emphasis to the influence of the species concentrations on the synergy of the simultaneous substrates conversion. The simulation was performed at wide ranges of the parameter values.

Fig. 4.22 shows the steady-state profiles of the concentrations simulated at values given in Table 4.1. As expected, the concentrations of S_1 and S_2 are lower than the concentrations of P_1 and P_2 due to the enzymatic conversion of the substrates to the products. In the outer part of the enzyme layer, the concentrations are constant and they change gradually in the dialysis membrane and the diffusion layer. In the close proximity to the electrode, the increase of S_1 and the concomitant decrease of P_1 are observed due to the electrochemical reaction (2.35). A similar but relatively smaller change is followed by S_2 and P_2 which was probably caused by the reaction (2.36) .
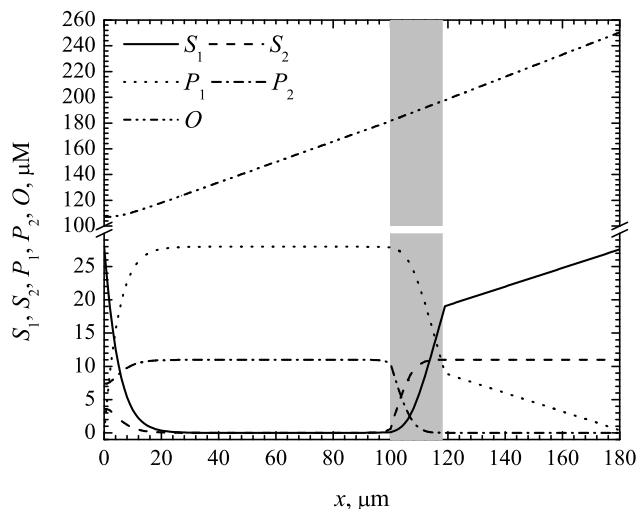
Figure 4.22: The steady state concentration profiles of the ferrocyanide (S_1), mediator (S_2), ferricyanide (P_1), oxidased mediator (P_2) and oxygen (O) in the enzyme layer ($0 < x < 100\mu$m), dialysis membrane ($100 < x < 118.7\mu$m) and the diffusion layer ($118.7 < x < 182.9\mu$m). The grey zone represents the dialysis membrane. Values of the model parameters are given in Table 4.1.

To see the effect of the mediator (substrate S_2) on the biosensor response, two

different experiments were simulated. The simulated biosensor currents are depicted in Fig. 4.23. In the initial stage of both simulated experiments, only the first substrate S_1 ($S_{1,0} = 28\mu M$) was infused into the buffer solution. When the system has reached the steady state ($t = 800\,$s), an additional substrate was infused. In the first case of the biosensor operation (curve 1), the mediator (second substrate, $S_{2,0} = 11\mu M$) was infused keeping the concentration of S_1 unchanged, while in the second case (curve 2) an additional amount of S_1 was infused keeping the zero concentration of S_2. Finally, the total concentration of the substrates was the same ($S_{1,0} + S_{2,0} = 39\mu$M) in both cases. As one case see in Fig. 4.23 that the addition of the hexacyanoferrate(II) (substrate S_1, curve 2) increases the bioelectrode current, which after ca. $200\,$s reaches the steady-state. However, the addition of the mediator (substrate S_2, curve 1) causes a supplementary increase of the bioelectrode response over that which is attained with equal amount of S_1.

The addition of the mediator cases additional increase of the bioelectrode response (Fig. 4.23). To investigate this effect in details, the bioelectrode responses were simulated at a wide range of the mediator concentrations. Fig. 4.24 shows the dependence of the steady state bioelectrode response I_R on the concentration $S_{2,0}$ of the mediator at three enzyme concentrations E_0. The increase of the current notably depends on the mediator concentration. The dependence of I_R on $S_{2,0}$ is practically linear up to 10μM. At higher concentrations of the mediator, the dependence of the current on the mediator concentration shows a saturation character. Very similar dependence of the response on the mediator concentration was observed in real experiments [83]. In [83] the observation was made that the bioelectrode sensitivity was dependent on immobilized laccase concentration. Contradictory results were obtained by using the modeling as sensitivity was nearly unchanged in the range of E_0 from 0.69 to 2.76 μM.
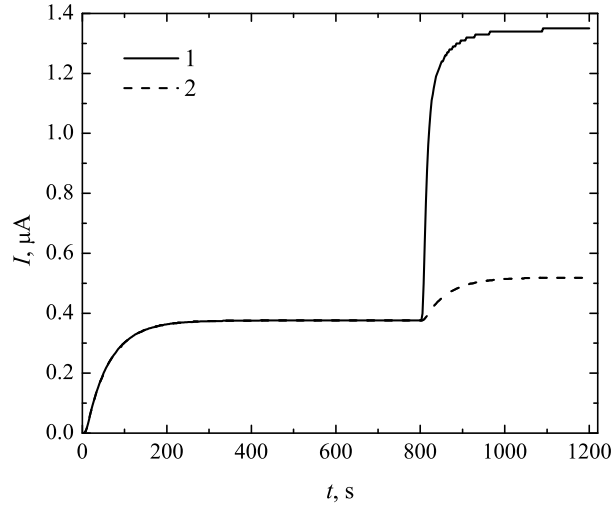
Figure 4.23: The change of the laccase-based biosensor current $I(t)$ in two operation cases: (1) the concentration $S_{2,0}$ of the mediator was set to $11\mu M$ at time $t = 800s$, (2) in absence of mediator ($S_{2,0} = 0$) the concentration $S_{1,0}$ of the ferrocyanide was increased to 39μM at time $t = 800s$. The other parameters are the same as in Fig. 4.22.

Fig. 4.25 presents the dependence of the bioelectrode response on the concentration $S_{1,0}$ of ferrocyanide (S_1) and time (t). As it is apparent from Fig. 4.25, the increase of the current upon the addition of the mediator also depends on the concentration $S_{1,0}$ of ferrocyanide. With the higher amount of $S_{1,0}$, a relatively smaller increase of the current is obtained. This can be explained by the competitive action of S_1 and S_2. S_1 competes with S_2 for the binding to the active site of laccase, and, at the high concentrations $S_{1,0}$ of ferrocyanide, there is almost none of P_2, which participates in the synergistic reaction, produced.

In order to estimate the limits of synergistic effect it is useful to introduce the difference I_S,

$$I_S = I_R - I_{0R}, \qquad (4.11)$$

where I_{0R} stands for the steady state current before the addition of the me-

100

Figure 4.24: The dependence of steady state bioelectrode response I_R on the concentration $S_{2,0}$ of the mediator at three enzyme concentrations E_0: 2.76 (1), 1.38 (2), 0.69 (3) μM. The other parameters are listed in Table 4.1.

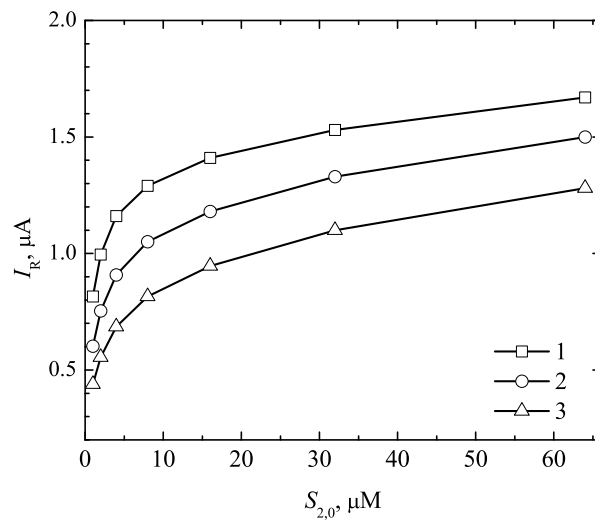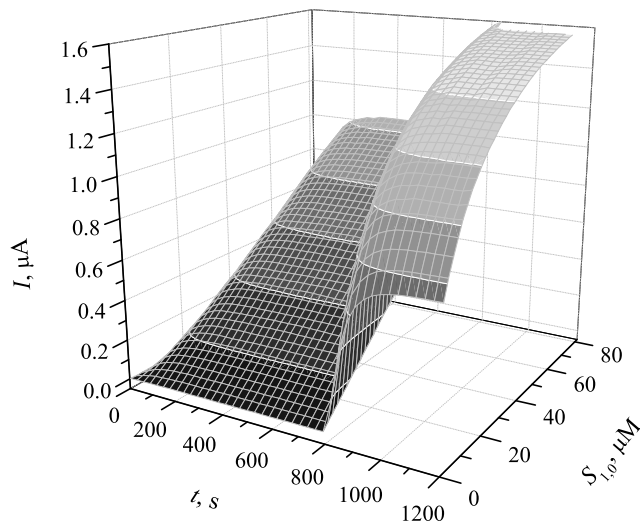Figure 4.25: The dynamics of the bioelectrode response at different concentrations $S_{1,0}$ of ferrocyanide. The other parameters are listed in Table 4.1.

diator [83]. I_S is the the current calculated by withdrawing from the overall bioelectrode current the bioelectrode current in the presence of ferrocyanide at zero mediator concentration. The difference I_S between the steady state currents I_R and I_{0R} can be called as the synergistic current [83].

Fig. 4.26 shows the dependence of the synergistic current I_S on the enzyme concentration E_0. The source currents I_R and I_{0R} are also depicted in Fig. 4.26. As one can see in Fig. 4.26 the synergistic current I_S is a non-monotonous function of E_0. It shows that the synergistic current reaches a maximum at $E_0 = 5\mu M$. Below that value, small amount of product P_2 is produced for the synergetic reaction to occur. Above the peak value, most of S_1 is consumed in reaction (2.32) hindering the synergetic reaction.
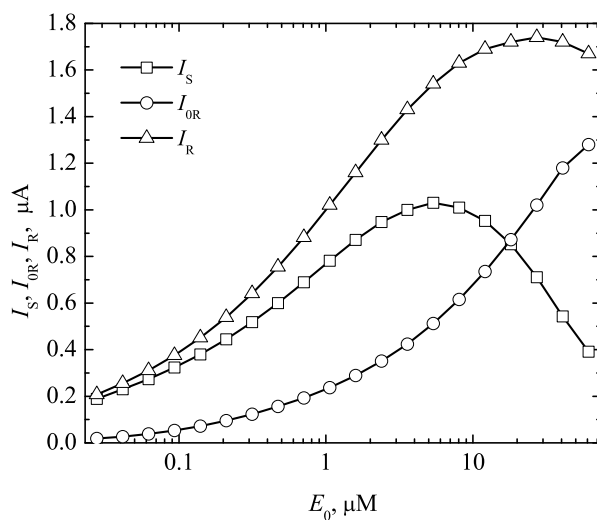
Figure 4.26: The steady state bioelectrode responses I_R and I_{0R} as well as the synergistic current I_S vs. the enzyme concentration E_0. The other parameters are listed in Table 4.1.

Fig. 4.27 shows the dependence of the synergistic current I_S on the concentration $S_{1,0}$ of the ferrocyanide (substrate S_1). This dependence can be explained similarly as the dependence of I_S on the enzyme concentration E_0. At very

high concentrations $S_{1,0}$ of the substrate S_1, the enzyme is mostly involved in reaction (2.32) and this slows down the production of the product P_2 which is necessary for the synergetic reaction.
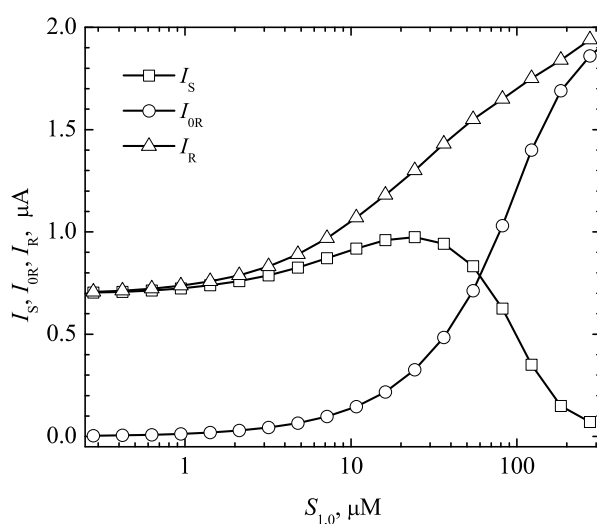
Figure 4.27: The dependences of the steady state bioelectrode responses I_R and I_{0R} as well as the synergistic current I_S on the substrate concentration $S_{1,0}$ at values of the model parameters given in Table 4.1.

4.3 Conclusions

The mathematical models of peroxidase-based optical and laccase-based synergetic biosensors can be specified in SBML together with the annotations.

The computational modeling of the peroxidase-based optical biosensor were produced. The results indicated that the sensitivity of the optical biosensor increases with an increase in the thickness δ of the external diffusion layer (Fig. 4.12). The light absorbance is less sensitive to changes in the thickness δ at higher concentrations of the enzyme and of the hydrogen peroxide than at lower concentrations of those species.

Assuming the relatively thick external diffusion layer, the biosensor response is highly stabile to changes in the enzyme layer thickness d when d varies from one hundredth to one tenth of the thickness δ of the diffusion layer ($0.01\delta < d < 0.1\delta$, Fig. 4.13). The response stability to changes in d reduces at low concentrations of the hydrogen peroxide and at high concentrations of the substrate (Fig. 4.15).

The sensitivity of the optical biosensor decreases with a decrease in the concentration of the enzyme (Fig. 4.17).

The developed mathematical model of a peroxidase-based fluorescent biosensor can be also used for biosensors digital simulations and research.

By providing a relatively thick enzyme layer d a high sensitivity and fluorescence values can be obtained. However, a great care must be taken in cases of high outer substrate and low initial hydrogen peroxide concentrations (Fig. 4.19).

The higher sensitivity of fluorescent biosensor can be achieved at increased values of hydrogen peroxide (Fig. 4.21).

The properties of the laccase-based synergetic biosensor were also investigated. According to the results the synergistic current I_S is a non-monotonous function of the enzyme concentration E_0 (Fig. 4.26) as well as of the substrate concentration $S_{1,0}$ (Fig. 4.27). The limits of synergistic effect were estimated with the maximum synergistic current I_S obtained at E_0=5μM and $S_{1,0}$=12μM. Taken together, these results confirm the synergistic effect in the laccase biosensor [83].

The synergistic effect of the laccase-based biosensors can be increased by selecting an appropriate concentration of the enzyme as well as values of some other model parameters. The computational simulation of the biosensor re-

sponse can be used as a tool in design of novel highly sensitive laccase-based biosensors.

To prove conclusions made the experiments are running using peroxidase-based optical biosensors and laccase-based biosensors with different geometry and catalytical parameters.

Conclusions

1. The detail applicability analysis of various finite difference schemes for the computational solution of reaction-diffusion problem with Michaelis-Menten kinetics showed that the fastest schemes to achieve the required relative error are implicit calculation and Hopscotch approaches. For the problems where accuracy is not a significant factor but the speed is, the simplest explicit scheme should be used.

2. The multi-step character of chemical processes in complex biosensors can be specified extending SBML language. The developed tool can be applied for the computational modeling of the various multi-step biosensors.

3. A synergistic mathematical model with new regeneration boundary conditions can be used for the computational simulations of the synergistic multi-step biosensors action. The computational modeling of the laccase-based biosensor qualitatively explained and confirmed the experimentally observed synergistic effect of the mediator on the biosensor response [83].

4. The mathematical model of a peroxidase-based optical biosensor can be successfully used to investigate the kinetic peculiarities of the biosensor response. The results of the computational modeling indicated that biosensor response is highly stable at the relatively thick external diffusion

layer, which has little effect on the response at high enzyme concentrations.

Publications by the Author

Periodic

[1A] E. Gaidamauskaitė, R. Baronas, and J. Kulys. Modelling Synergistic Action of Laccase-based Biosensor Utilizing Simultaneous Substrates Conversion. *Journal of Mathematical Chemistry*, 49:1573-1586, 2011 [ISI Web of Science].

[2A] D. Britz, R. Baronas, E. Gaidamauskaitė, and F. Ivanauskas. Futher Comparisons of Finite Difference Schemes for Computational Modelling of Biosensors. *Nonlinear Analysis: Modelling and Control*, 14(4):419–433, 2009 [ISI Web of Science].

[3A] E. Gaidamauskaitė, R. Baronas. A Computational Investigation of the Optical Biosensor by a Dimensionless Model. *Informacijos mokslai (Information Sciences)*, 50:306–310, 2009 [LISA].

[4A] R. Baronas, E. Gaidamauskaitė, and J. Kulys. Modelling a Peroxidase-based Optical Biosensor. *Sensors*, 7(11):2723–2740, 2007 [ISI Web of Science].

[5A] E. Gaidamauskaitė, R. Baronas. A Comparison of Finite Difference Schemes for Computational Modelling of Biosensors. *Nonlinear Analysis: Modelling and Control*, 12(3):359-369, 2007 [INSPEC].

Reviewed Conference Publications

[6A] E. Gaidamauskaitė, R. Baronas. Influence of Spontaneous Convection on Amperometric Biosensor Response. In *Proceedings of the 23rd Nordic Seminar on Computational Mechanics*, ISSN 0348-467X, 330–333, 2010.

[7A] E. Gaidamauskaitė, R. Baronas. Modelling a Peroxidase-based Fluorescent Biosensor. In *Proceedings of the 22nd European Conference on Modelling and Simulation ECMS 2008*, ISBN 978-0-9553018-5-8, 152–156, 2008 [ISI Proceedings].

[8A] E. Gaidamauskaitė, R. Baronas. Computational Modelling of Rotating Disc Enzyme Electrode. In *Proceedings of the 20th Nordic Seminar on Computational Mechanics*, ISSN 1652-8549, 2007.

[9A] E. Gaidamauskaitė, R. Baronas. Automatizuotas biojutiklių kompiuterinių modelių sudarymas (The development of computer models for amperometric biosensors). *Informacinės technologijos 2007*, Konferencijos pranešimų medžiaga, ISSN 1822-6337, 359–363, 2007.

[10A] E. Gaidamauskaitė. The Development of Computer Models for the Biosensors. In *Proceedings of the PhD Summer School "Formal Methods for System Analysis in Informatics"*, ISBN 978-9955-591-49-8, 15–18, 2007.

[11A] E. Gaidamauskaitė, R. Baronas. Baigtinių skirtumų metodo taikymas biojutiklio veiksmui modeliuoti. *Informacinės technologijos 2006*, Konferencijos pranešimų medžiaga, ISBN 9955-09-993-3, 527–531, 2006.

Bibliography

[1] P. Abad-Valle, M. T. Fernández-Abedul, and A. Costa-García. Genosensor on gold films with enzymatic electrochemical detection of a sars virus sequence. *Biosensors and Bioelectronics*, 20(11):2251–2260, 2005.

[2] P. Ahuja. *Introduction to Numerical Methods in Chemical Engineering*. PHI Learning Pvt. Ltd., 2010.

[3] C. Amatore, A. Oleinick, I. Svir, N. da Mota, and L. Thouin. Theoretical modeling and optimization of the detection performance: a new concept for electrochemical detection of proteins in microfluidic channels. *Nonlinear Analysis: Modelling and Control*, 11(4):345–365, 2006.

[4] R. Aris. *The Mathematical Theory of Diffusion and Reaction in Permeable Catalysts. The Theory of the Steady State*. Clarendon Press, 1975.

[5] J.L. Atwood and J.W. Steed. *Encyclopedia of Supramolecular Chemistry*. Taylor & Francis, 2004.

[6] B. R. Baker, R. Y. Lai, M. S. Wood, E. H. Doctor, A. J. Heeger, and K. W. Plaxco. An electronic, aptamer-based small-molecule sensor for the rapid, label-free detection of cocaine in adulterated samples and biological fluids. *Journal of American Chemical Society*, 128(10):3138–3139, 2006.

[7] F. Baldini and North Atlantic Treaty Organization. *Optical chemical sensors*. Springer, 2006.

[8] R. Baronas, F. Ivanauskas, and J. Kulys. The influence of enzyme membrane thickness on the response of amperometric biosensors. *Sensors*, 3 (7):248–262, 2003.

[9] R. Baronas, F. Ivanauskas, and J. Kulys. Computer simulation of the response of amperometric biosensors in stirred and non stirred solution. *Nonlinear Analysis: Modelling and Control*, 8(1):3–18, 2003.

[10] R. Baronas, F. Ivanauskas, and J. Kulys. The effect of diffusion limitations on the response of amperometric biosensors with substrate cyclic conversion. *Journal of Mathematical Chemistry*, 35(3):199–213, 2004.

[11] R. Baronas, F. Ivanauskas, J. Kulys, and M. Sapagovas. Computational modelling of a sensor based on an array of enzyme microreactors. *Nonlinear Analysis: Modelling and Control*, 9(3):203–218, 2004.

[12] R. Baronas, J. Kulys, and F. Ivanauskas. Modelling amperometric enzyme electrode with substrate cyclic conversion. *Biosensors and Bioelectronics*, 19 (8):915–922, 2004.

[13] R. Baronas, J. Kulys, and F. Ivanauskas. Mathematical model of the biosensors acting in a trigger mode. *Sensors*, 4(4):20–36, 2004.

[14] R. Baronas, F. Ivanauskas, I. Kaunietis, and V. Laurinavičius. Mathematical modeling of plate-gap biosensors with an outer porous membrane. *Sensors*, 6(7):727–745, 2006.

[15] R. Baronas, J. Kulys, and F. Ivanauskas. Computational modelling of biosensors with perforated and selective membranes. *Journal of Mathematical Chemistry*, 39(2):345–362, 2006.

[16] R. Baronas, F. Ivanauskas, and J. Kulys. Computational modelling of the behaviour of potentiometric membrane biosensors. *Journal of Mathematical Chemistry*, 42(3):321–336, 2007.

[17] R. Baronas, F. Ivanauskas, and J. Kulys. *Mathematical Modeling of Biosensors*. Springer-Verlag, 2009.

[18] F. Barriere, P. Kavanagh, and D. Leech. A laccase-glucose oxidase biofuel cell prototype operating in a physiological buffer. *Electrochimica Acta*, 51 (24):5187–5192, 2006.

[19] P. N. Bartlett and K. F. E. Pratt. Modelling of processes in enzyme elec-

trodes. *Biosensors and Bioelectronics*, 8(9-10):451–462, 1993.

[20] P. N. Bartlett and K. F. E. Pratt. Theoretical treatment of diffusion and kinetics in amperometric immobilized enzyme electrodes. part I: Redox mediator entrapped within the film. *Journal of Electroanalytical Chemistry*, 397(1-2):61–78, 1995.

[21] P. N. Bartlett and R. G. Whitaker. Electrochemical imobilisation of enzymes: Part 1. theory. *Journal of Electroanalytical Chemistry*, 224(1-2):27–35, 1987.

[22] M. S. Belluzo, M. É. Ribone, and C. M. Lagier. Assembling amperometric biosensors for clinical diagnostics. *Sensors*, 8(3):1366–1399, 2008.

[23] J. M. Berg, J. L. Tymoczko, and L. Stryer. *Biochemistry*. W. H. Freeman, 2002.

[24] M. Birbeck, J. Diamond, and J. Duckett et al. *Professional XML*. Wrox Press, 2000.

[25] R.B. Bird, W.E. Stewart, and E.N. Lightfoot. *Transport Phenomena*. John Wiley & Sons., 1960.

[26] H. Bisswanger. *Enzyme Kinetics. Principles and Methods*. WILEY-VCH Verlag GmbH & Co, 2008.

[27] J. Bloch. *Effective Java (2nd Edition) (The Java Series)*. Prentice Hall PTR, 2008.

[28] S. M. Borisov and O. S. Wolfbeis. Optical biosensors. *Chemical Reviews*, 108(2):423–461, 2008.

[29] B. J. Bornstein, S. M. Keating, A. Jouraku, and M. Hucka. LibSBML: an API Library for SBML. *Bioinformatics*, 24(6):880–881, 2008.

[30] M. E. Bosch, A. J. R. Sánchez, F. S. Rojas, and C. B. Ojeda. Recent development in optical fiber biosensors. *Sensors*, 7(6):797–859, 2007.

[31] G. E. Briggs and J. B. S. Haldane. A note on the kinetics of enzyme action. *Biochemical Journal*, 19(2):339–339, 1925.

[32] D. Britz. *Digital Simulation in Electrochemistry*. Springer-Verlag, 2005.

[33] P. W. Carr and L. D. Bower. *Immobilized Enzymes in Analytical and Clinical Chemistry: Fundamentals and Applications*. John Wiley, 1980.

[34] A. Chaubey and B. D. Malhotra. Mediated biosensors. *Biosensors and Bioelectronics*, 17(6-7):441–456, 2002.

[35] W. W. Chen, M. Niepel, and P. K. Sorger. Classic and contemporary approaches to modeling biochemical reactions. *Genes & Development*, 24(17): 1861–1875, 2010.

[36] E.W. Cheney and D.R. Kincaid. *Numerical mathematics and computing*. Brooks/Cole, 2007.

[37] M. M. F. Choi. Progress in enzyme-based biosensors using optical transducers. *Microchimica Acta*, 148(3-4):107–132, 2004.

[38] L. C. Clark and C. Lyons. Electrode systems for continuous monitoring in cardiovascular surgery. *Annals of the New York Academy of Sciences*, 102 (1):29–45, 1962.

[39] N. Conrath, B. Gründig, St. Hüwel, and K. Cammann. A novel enzyme sensor for the determination of inorganic phosphate. *Analytica Chimica Acta*, 309(1-3):47–52, 1995.

[40] M.J. Cooney, V. Svoboda, C. Lau, G. Martina, and S. D. Minteer. Enzyme catalysed biofuel cells. *Energy Environmental Science*, 1(3):320–337, 2008.

[41] J.I. Reyes De Corcuera, R.P. Cavalieri, J.R. Powers, and J. Tang. Amperometric enzyme biosensor optimization using mathematical modeling. In *Proceedings of the 2004 ASAE / Csae Annual International Meeting*, page Paper No. 047030, 2004.

[42] A. Cornish-Bowden. *Fundamentals of Enzyme Kinetics*. Portland Press, 2004.

[43] J. Crank and P. Nicolson. A practical method for numerical evaluation of solutions of partial differential equations of the heat conduction type. *Proceedings of the Cambridge Philosophical Society*, 43(1):50–64, 1947.

[44] E. L. Cussler. *Diffusion: Mass Transfer in Fluid Systems*. Cambridge Uni-

versity Press., 2009.

[45] P. Dhar, T. C. Meng, S. Somani, L. Ye, A. Sairam, M. Chitre, Z. Hao, and K. Sakharkar. Cellware - a multi-algorithmic software for computational systems biology. *Bioinformatics*, 20(8):1319–1321, 2004.

[46] A. Dräger, H. Planatscher, Motsou, A. Schröder, M. Hucka, L. Endler, M. Golebiewski, W. Müller, and A. Zell. SBML2LATEX: Conversion of SBML files into human-readable reports. *Bioinformatics*, 25(11):1455–1456, 2009.

[47] G. T. Drummond, M. G. Hill, and J. K. Barton. Electrochemical DNA sensors. *Nature Biotechnology*, 21(10):1192–1199, 2003.

[48] D. J. Duffy. *Finite Difference Methods in Financial Engineering - A Partial Differential Equation Approach*. John Wiley & Sons, 2006.

[49] R. Dutta. *Fundamentals of Biochemical Engineering*. Springer, 2008.

[50] V. I. Dybkov. *Reaction diffusion and solid state chemical kinetics*. The IPMS Publications, 2002.

[51] X. Fan, I. M. White, S. I. Shopova, H. Zhu, J. D. Suter, and Y. Sun. Sensitive optical biosensors for unlabeled targets: A review. *Analytica Chimica Acta*, 620(1-2):8–26, 2008.

[52] L. S. Ferreira, M. B. De Souza, J. O. Trierweiler, O. Broxtermann, R. O. M. Folly, and B. Hitzmann. Aspects concerning the use of biosensors for process control: experimental and simulation investigations. *Computers and Chemical Engineering*, 27(8):1165–1173, 2003.

[53] A. Fick. On liquid diffusion. *Philosophical Magazine Series 4*, 10(63):30–39, 1855.

[54] A. Finney and M. Hucka. Systems biology markup language: Level 2 and beyond. *Biochemical Society Transactions*, 31(6):1472–1473, 2003.

[55] R. S. Freire, C. A. Pessoa, L. D. Mello, and L. T. Kubota. Direct electron transfer: An approach for electrochemical biosensors with higher selectivity and sensitivity. *Journal of the Brazilian Chemical Society*, 14(2):

230–243, 2003.

[56] A. Funahashi, Y. Matsuoka, A. Jouraku, M. Morohashi, N. Kikuchi, and H. Kitano. CellDesigner 3.5: A versatile modeling tool for biochemical networks. *Proceedings of the IEEE*, 96(8):1254–1265, 2008.

[57] W. Gander and J. Hrebicek. *Solving Problems in Scientific Computing Using Maple and MATLAB$^{\circledR}$*. Springer-Verlag, 2004.

[58] A. Garny, D. P. Nickerson, J. Cooper, R. W. D. Santos, A. K. Miller, S. McKeever, P. M. F. Nielsen, and P. J. Hunter. CellML and associated tools and techniques. *Philosophical Transactions of the Royal Society A: Mathematical, Physical and Engineering Sciences*, 366(1878):3017–3043, 2008.

[59] D. A. Gough and J. K. Leypoldt. Membrane-covered, rotated disc electrode. *Analytical Chemistry*, 51(3):439–444, 1979.

[60] D. Grieshaber, R. MacKenzie, J. Vørøs, and E. Reimhult. Electrochemical biosensors - sensor principles and architectures. *Sensors*, 8(3):1400–1458, 2008.

[61] B. A. Grzybowski. *Chemistry in Motion: Reaction-Diffusion Systems for Micro- and Nanotechnology*. John Wiley & Sons, Inc., 2009.

[62] K. Habermüller, M. Mosbach, and W. Schuhmann. Electron-transfer mechanisms in amperometric biosensors. *Journal of Analytical Chemistry*, 366(6):560–568, 2000.

[63] W. J. Hedley, M. R. Nelson, D. P. Bullivant, and P. F. Nielsen. A short introduction to CellML. *Philosophical Transactions of the Royal Society A: Mathematical, Physical and Engineering Sciences*, 359(1783):1073–1089, 2001.

[64] Nicholas J. Higham. *Accuracy and Stability of Numerical Algorithms*. Society for Industrial and Applied Mathematics, 2002.

[65] J. E. House. *Principles of Chemical Kinetics*. Elsevier Inc., 2007.

[66] M. Hucka, A. Finney, H. Sauro, and H. Bolouri. Systems Biology Markup Language (SBML) Level 1: Structures and Facilities for Basic Model Definitions. 2003.

[67] M. Hucka, A. Finney, B. J. Bornstein, S. M. Keating, B. E. Shapiro, J. Matthews, B. L. Kovitz, M. J. Schilstra, A. Funahashi, J. C. Doyle, and H. Kitano. Evolving a lingua franca and associated software infrastructure for computational systems biology: the Systems Biology Markup Language (SBML) project. *Systems Biology*, 1(1):41–53, 2004.

[68] M. Hucka, S. Hoops, S. M. Keating, N. Le Novère, S. Sahle, and D. J. Wilkinson. Systems Biology Markup Language (SBML) Level 2: Structures and Facilities for Model Definitions. 2008.

[69] M. Hucka, F. Bergmann, S. Hoops, S. Keating, S. Sahle, J. C. Schaff, L. P. Smith, and D. J. Wilkinson. The Systems Biology Markup Language (SBML): Language Specification for Level 3 Version 1 Core. *Nature Precedings*, (713), 2010.

[70] M. Hucka et al. The systems biology markup language (SBML): a medium for representation and exchange of biochemical network models. *Bioinformatics*, 19(4):524–531, 2003.

[71] F. Ivanauskas, I. Kaunietis, V. Laurinavičius, J. Razumienė, and R. Šimkus. Computer simulation of the steady state currents at enzyme doped carbon paste electrodes. *Journal of Mathematical Chemistry*, 38:355–366, 2005.

[72] I. Kaunietis, R. Šimkus, V. Laurinavičius, and F. Ivanauskas. Apparent parameters of enzymatic plate-gap electrode. *Nonlinear Analysis: Modelling and Control*, 10(3):211–221, 2005.

[73] S. M. Keating, B. J. Bornstein, A. Finney, and M. Hucka. SBMLToolbox: an SBML toolbox for MATLAB users. *Bioinformatics*, 22(10):1275–1277, 2006.

[74] J. P. Kernevez. *Enzyme Mathematics. Studies in Mathematics and its Applications*. Elsevier Science, 1980.

[75] H. Kitano. Systems biology: a brief overview. *Science*, 295(5560):1662–1664, 2002.

[76] H. Kitano, A. Funahashi, Y. Matsuoka, and K. Oda. Using process diagrams for the graphical representation of biological networks. *Nature Biotechnology*, 23(8):961–966, 2005.

[77] G.K. Knopf and A.S. Bassi. *Smart biosensor technology*. CRC Press/Taylor & Francis, 2007.

[78] F. Kolpakov, M. Puzanov, and A. Koshukov. BioUML: Visual modeling, automated code generation and simulation of biological systems. In *Proceedings of the Fifth International Conference on Bioinformatics of Genome Regulation and Structure, Vol 3*, pages 281–284, 2006.

[79] J. Kulys. The development of new analytical systems based on biocatalysts. *Analytical Letters*, 14(6):377–397, 1981.

[80] J. Kulys and R. Baronas. Modelling of amperometric biosensors in the case of substrate inhibition. *Sensors*, 6(11):1513–1522, 2006.

[81] J. Kulys and V. Razumas. *Bioamperometry*. Mokslas, 1986.

[82] J. Kulys and R. Vidžiūnaitė. Amperometric biosensors based on recombinant laccases for phenols determination. *Biosensors and Bioelectronics*, 18(2-3):319–325, 2003.

[83] J. Kulys and R. Vidžiūnaitė. Laccase based synergistic electrocatalytical system. *Electroanalysis*, 21(20):2228–2233, 2009.

[84] J. Kulys and Ž. Dapkūnas. The effectiveness of synergistic enzymatic reaction with limited mediator stability. *Nonlinear Analysis: Modelling and Control*, 12(4):495–501, 2007.

[85] J. Kulys, L. Tetianec, and I. Bratkovskaja. Pyrroloquinoline quinone-dependent carbohydrate dehydrogenase: Activity enhancement and the role of artificial electron acceptors. *Biotechnology Journal*, 5(8):822–828, 2010.

[86] B. Kvedaras and M. Sapagovas. *Skaičiavimo metodai*. Mintis, 1974.

[87] N. Le Novére et al. The Systems Biology Graphical Notation. *Nature Biotechnology*, 27(8):735–741, 2009.

[88] R. J. Leatherbarrow and P. R. Edwards. Analysis of molecular recognition using optical biosensors. *Current Opinion in Chemical Biology*, 3(5):544–547, 1999.

[89] Y. Lei, W. Chen, and A. Mulchandani. Microbial biosensors. *Analytica Chimica Acta*, 568(1-2):200–210, 2006.

[90] V. Leskovac. *Comprehensive Enzyme Kinetics*. Kluwer Academic Publishers, 2004.

[91] J. C. Liao, M. Mastali, V. Gau, M. A. Suchard, A. K. Møller, D. A. Bruckner, J. T. Babbitt, Y. Li, J. Gornbein, E. M. Landaw, E. R. B. McCabe, B. M. Churchill, and D. A. Haake. Use of electrochemical dna biosensors for rapid molecular identification of uropathogens in clinical urine specimens. *Journal of Clinical Microbiology*, 44(2):561–570, 2006.

[92] F. S. Ligler and C. R. Taitt. *Optical Biosensors: Present and Future*. Elsevier Science, 2002.

[93] P. B. Luppa, L. J. Sokoll, and D. W. Chan. Immunosensors–principles and applications to clinical chemistry. *Clinica Chimica Acta*, 314(1-2):1–26, 2001.

[94] M. E. G. Lyons. Modelling the transport and kinetics of electroenzymes at the electrode/solution interface. *Sensors*, 6(12):1765–1790, 2006.

[95] M. E. G. Lyons, J. Murphy, and S. Rebouillat. Theoretical analysis of time dependent diffusion, reaction and electromigration in membranes. *Journal of Solid State Electrochemistry*, 4(8):458–472, 2000.

[96] T. Mairal, V. C. Ozalp, P. Lozano Sánchez, M. Mir, I. Katakis, and C. K. O'Sullivan. Aptamers: molecular tools for analytical applications. *Analytical and Bioanalytical Chemistry*, 390(4):989–1007, 2008.

[97] Bansi D. Malhotra and Asha Chaubey. Biosensors for clinical diagnostics industry. *Sensors and Actuators B: Chemical*, 91(1-3):117–127, 2003.

[98] A. Meena and L. Rajendran. Mathematical modeling of amperometric and potentiometric biosensors and system of non-linear equations - ho-

motopy perturbation approach. *Journal of Electroanalytical Chemistry*, 644 (1):50–59, 2010.

[99] A. Meena, A. Eswari, and L. Rajendran. Mathematical modelling of enzyme kinetics reaction mechanisms and analytical solutions of non-linear reaction equations. *Journal of Mathematical Chemistry*, 48(2):179–186, 2010.

[100] C.D. Mell and J. T. Maloy. A model for the amperometric enzyme electrode obtained through digital simulation and applied to the glucose oxidase system. *Analytical Chemistry*, 47(2):299–307, 1975.

[101] S. Merino, M. Grinfeld, and S. McKee. A degenerate reaction diffusion system modelling an optical biosensor. *Zeitschrift für angewandte Mathematik und Physik*, 49(1):46–85, 1998.

[102] L. Michaelis and M. Menten. Die kinetik der invertinwirkung. *Biochemische Zeitschrift*, 49(352):333–369, 1913.

[103] R. W. Missen, C. A. Mims, and B. A. Saville. *Introduction to Chemical Reaction Engineering and Kinetics*. John Wiley & Sons, Inc., 1999.

[104] W. E. Moerner. Single-molecule chemistry and biology special feature: New directions in single-molecule imaging and analysis. *Proceedings of the National Academy of Sciences of the United States of America*, 104(31): 12596–12602, 2007.

[105] J. E. Moreira, S. P. Midkiff, M. Gupta, P. V. Artigas, M. Snir, and R. D. Lawrence. Java programming for high-performance numerical computing. *IBM Systems Journal*, 39(6):21–56, 2000.

[106] C. L. Morgan, D. J. Newman, and C. P. Price. Immunosensors: technology and opportunities in laboratory medicine. *Clinical Chemistry*, 42(2):193–209, 1996.

[107] O.V. Morozova, G.P. Shumakovich, M. A. Gorbacheva, S. V. Shleev, and A. I. Yaropolov. "Blue" laccases. *Biochemistry (Moscow)*, 72(10):1136–1150, 2007.

[108] N. Nikolaus and B. Strehlitz. Amperometric lactate biosensors and their

application in (sports) medicine, for life quality and wellbeing. *Microchimica Acta*, 160(1-2):15–55, 2008.

[109] C. B. Ojeda and F. S. Rojas. Recent development in optical chemical sensors coupling with flow injection analysis. *Sensors*, 6(10):1245–1307, 2006.

[110] V. M. N. Passaro, F. Dell'olio, B. Casamassima, and F. De Leonardis. Guided-wave optical biosensors. *Sensors*, 7(4):508–536, 2007.

[111] M. Pohanka and P. Skládal. Electrochemical biosensors - principles and applications. *Journal of Applied Biomedicine*, 6(2):57–64, 2008.

[112] R. Popovtzer, A. Natan, and Y. Shacham-Diamand. Mathematical model of whole cell based bio-chip: an electrochemical biosensor for water toxicity detection. *Journal of Electroanalytical Chemistry*, 602(1):17–23, 2007.

[113] P. N. Prasad. *Introduction to Biophotonics*. John Wiley & Sons, Inc., 2003.

[114] M. Puida, F. Ivanauskas, I. Ignatjev, G. Valinčius, and V. Razumas. Computational modeling of the amperometric bioanalytical system for lipase activity assay: a time-dependent response. *Nonlinear Analysis: Modelling and Control*, 12(2):245–251, 2007.

[115] M. E. Ribone, M. S. Belluzo, D. Pagani, I. S. Macipar, and C. M. Lagier. Amperometric bioelectrode for specific human immunoglobulin G determination: Optimization of the method to diagnose American trypanosomiasis. *Analytical Biochemistry*, 350(1):61–70, 2006.

[116] R. L. Rich and D. G. Myszka. Survey of the year 2007 commercial optical biosensor literature. *Journal of Molecular Recognition*, 21(6):355–400, 2008.

[117] J. L. Rickus. Impact of coenzyme regeneration on the performance of an enzyme based optical biosensor: a computational study. *Biosensors and Bioelectronics*, 21(6):965–972, 2005.

[118] N. J. Ronkainen, H. B. Halsall, and W. R. Heineman. Electrochemical biosensors. *Chemical Society Reviews*, 39(5):1747–1763, 2010.

[119] O. A. Sadik, A. O. Aluoch, and A. Zhou. Status of biomolecular recogni-

tion using electrochemical techniques. *Biosensors and Bioelectronics*, 24(9): 2749–2765, 2009.

[120] A. A. Samarskii. *The Theory of Difference Schemes*. Marcel Dekker, 2001.

[121] V. Sanz, S. de Marcos, and J. Galbán. Direct glucose determination in blood using a reagentless optical biosensor. *Biosensors and Bioelectronics*, 22(12):2876–2883, 2007.

[122] A. K. Sarma, P. Vatsyayan, P. Goswami, and S. D. Minteer. Recent advances in material science for developing enzyme electrodes. *Biosensors and Bioelectronics*, 24(8):2313–2322, 2009.

[123] S. Sassolas, B. D. Leca-Bouvier, and L. J. Blum. DNA biosensors and microarrays. *Chemical Reviews*, 108(1):109–139, 2008.

[124] F. Scheller and F. Schubert. *Biosensors*. Elsevier, 1992.

[125] T. Schulmeister. Mathematical modelling of the dynamic behaviour of amperometric enzyme electrodes. *Selective Electrode Reviews*, 12(2):203–260, 1990.

[126] T. Schulmeister and D. Pfeiffer. Mathematical modelling of amperometric enzyme electrodes with perforated membranes. *Biosensors and Bioelectronics*, 8(2):75–79, 1993.

[127] V. Scognamiglio, G. Pezzotti, I. Pezzotti, J. Cano, K. Buonasera, D. Giannini, and M. Giardi. Biosensors for effective environmental and agrifood protection and commercialization: from research to market. *Microchimica Acta*, 170:215–225, 2010.

[128] K. Servat, S. Tingry, L. Brunel, S. Querelle, M. Cretin, C. Innocent, C. Jolivalt, and M. Rolland. Modification of porous carbon tubes with enzymes: Application for biofuel cells. *Journal of Applied Electrochemistry*, 37(1):121–127, 2007.

[129] B. E. Shapiro, M. Hucka, A. Finney, and J. Doyle. MathSBML: a package for manipulating SBML-based biological models. *Bioinformatics*, 20(16): 2829–2831, 2004.

[130] S. Shleev, A. Christenson, V. Serezhenkov, D. Burbaev, A. Yaropolov, L. Gorton, and T. Ruzgas. Electrochemical redox transformations of T1 and T2 copper sites in native trametes hirsuta laccase at gold electrode. *Biochemical Journal*, 385(3):745–754, 2005.

[131] A. Sorokin, K. Paliy, A. Selkov, O. V. Demin, S. Dronov, P. Ghazal, and I. Goryanin. The Pathway Editor: A tool for managing complex biological networks. *IBM Journal of Research and Development*, 50(6):561–573, 2006.

[132] Ioan Stamatin, C. Berlic, and A. Vaseashta. On the computer-aided modelling of analyte-receptor interactions for an efficient sensor design. *Thin Solid Films*, 495(1-2):312–315, 2006.

[133] L. De Stefano, P. Arcari, A. Lamberti, C. Sanges, L. Rotiroti, I. Rea, and I. Rendina. DNA optical detection based on porous silicon technology: from biosensors to biochips. *Sensors*, 7(2):214–221, 2007.

[134] L. Strömbäck, V. Jakonienė, H. Tan, and P. Lambrix. Representing, storing and accessing molecular interaction data: a review of models and tools. *Briefings in Bioinformatics*, 7(4):331–338, 2006.

[135] K. B. Taylor. *Enzyme Kinetics and Mechanisms*. Kluwer Academic Publishers, 2002.

[136] L. Tetianec and J. Kulys. Kinetics of N-substituted phenothiazines and n-substituted phenoxazines oxidation catalyzed by fungal laccases. *Central European Journal of Biology*, 4(1):62–67, 2009.

[137] D. R. Thévenot, R. P. Buck, K. Cammann, R. A. Durst, K. Toth, and G. S. Wilson. Electrochemical biosensors: recommended definitions and classification (technical report). *Pure and Applied Chemistry*, 71(12):2333–2348, 1999.

[138] C. S. Tsai. *An Introduction to Computational Biochemistry*. John Wiley & Sons, Inc., 2002.

[139] A. P. F. Turner, I. Karube, and G. S. Wilson. *Biosensors: Fundamentals and*

Applications. Oxford University Press, 1987.

[140] S. J. Updike and G. P. Hicks. The enzyme electrode. *Nature*, 214(5092): 986–988, 1967.

[141] M. A. Vannice. *Kinetics of Catalytic Reactions*. Springer, 2005.

[142] R. Čiegis. *Diferencialinių lygčių skaitiniai sprendimo metodai*. Technika, 2003.

[143] S. Viswanathan, H. Radecka, and J. Radecki. Electrochemical biosensors for food analysis. *Monatshefte fur Chemie*, 140(8):891–899, 2009.

[144] E. Van Der Vlist. *XML Schema*. O'Reilly Media, 2002.

[145] T. Vo-Dinh. *Biomedical Photonics Handbook*. CRC Press LLC, 2003.

[146] J. Wang. *Analytical Electrochemistry*. Springer - Verlag, 1988.

[147] J. Wang. Electrochemical glucose biosensors. *Chemical Reviews*, 108(2): 814–825, 2008.

[148] W. Wang. Electrochemical biosensors: Towards point-of-care cancer diagnostics. *Biosensors and Bioelectronics*, 21(10):1887–1892, 2006.

[149] Y. Wang, H. Xu, J. Zhang, and G. Li. Electrochemical sensors for clinic analysis. *Sensors*, 8(4):2043–2081, 2008.

[150] S. Whitaker. *The Method of Volume Averaging*. Kluwer Academic Publishers, 1999.

[151] I. Willner and M. Zayats. Electronic aptamer-based sensors. *Angewandte Chemie International Edition*, 46(34):6408–6418, 2007.

[152] U. Wollenberger, F. Lisdat, and F. W. Scheller. *Frontiers in Biosensorics 2. Practical Applications*. Birkhauser Verlag, 1997.

[153] B. Wu, Y. Wang, J. Li, Z. Song, J. Huang, X. Wang, and Q. Chen. An optical biosensor for kinetic analysis of soluble Interleukin-1 receptor I binding to immobilized Interleukin-1α. *Talanta*, 70(3):485–488, 2006.

[154] W. Y. Yang, W. Cao, T. S. Chung, and J. Morris. *Applied Numerical Methods Using MATLAB$^{\circledR}$*. John Willey & Sons, 2005.

[155] K. Yokoyama and Y. Kayanuma. Cyclic voltammetric simulation for electrochemically mediated enzyme reaction and determination of enzyme

kinetic constants. *Analytical Chemistry*, 70(16):3368–3376, 1998.

[156] D. Yu, B. Blankert, J. C. Virè, and J. M. Kauffmann. Biosensors in drug discovery and drug analysis. *Analytical Letters*, 38(11):1687–1701, 2005.

[157] M. Zayats, B. Willner, and I. Willner. Design of amperometric biosensors and biofuel cells by the reconstitution of electrically contacted enzyme electrodes. *Electroanalysis*, 20:583–601, 2008.

Curriculum Vitae

Evelina Gaidamauskaitė was born in Vilnius on 25th of July 1982. She graduated from Vilnius University receiving BSc degree in Informatics in 2004. In 2006 she received MSc degree Cum Laude in Informatics Vilnius University. From 2006 to 2010 she was enrolled into a PhD study program (Informatics) at Vilnius University.

During the 2008-2010 academic years she was assistant lecturer in the Faculty of Mathematics and Informatics for the Informatics and Database management systems courses. She also served as reviewer of master's theses. Since 2003, E. Gaidamauskaitė occupied the positions of IT consultant and analyst in financial institutions simultaneously.

The author was twice, in 2008 and 2010, awarded grants by the The State Studies Foundation to support her research activities. She also received PhD student scholarship by ECCOMAS to attend the 5th European Congress on Computational Methods in Applied Sciences and Engineering (ECCOMAS 2008).

In 2007, Evelina Gaidamauskaitė attended two PhD Summer Schools in Lithuania and Spain.